PID Control of Systems with Hysteresis

by

Alex Shum

A thesis
presented to the University of Waterloo
in fulfillment of the
thesis requirement for the degree of
Master of Mathematics
in
Applied Mathematics

Waterloo, Ontario, Canada, 2009

I hereby declare that I am the sole author of this thesis. This is a true copy of the thesis, including any required final revisions, as accepted by my examiners.

I understand that my thesis may be made electronically available to the public.

Abstract

Hysteresis is exhibited by many physical systems. Smart materials such as piezoelectrics, magnetostrictives and shape memory alloys possess useful properties, especially in the field of micropositioning, but the control of these systems is difficult due to the presence of hysteresis. An accurate model is required to predict the behaviour of these systems so that they can be controlled.

Several hysteresis models including the backlash, elastic-plastic and Preisach operators are discussed in detail. Several other models are mentioned. Other control methods for this problem are discussed in the form of a literature review.

The focus of this thesis is on the PID control of hysteretic systems. In particular, two systems experiencing hysteresis in their controllers are examined. The hysteresis in each system is described by different sets of assumptions. These assumptions are compared and found to be very similar. In the first system, a PI controller is used to track a reference signal. In the second, a PID controller is used to control a second-order system. The stability and tracking of both systems are discussed. An extension is made to the first system to include the dynamics of a first-order system. The results of the second system are verified to hold for a general first-order system.

Simulations were performed with the extension to a first-order system using different hysteresis models.

Acknowledgements

The completion of this thesis would not have been possible without the support from my family, friends, and co-workers.

Dr. Kirsten Morris has been of tremendous support throughout the entire project, offering not only support in mathematical aspects, but also in building confidence and character. Sina Valadkhan has taught me the basics and provided a solid working ground for this research topic. I'd like to also thank Dr. Brian Ingalls and Dr. Amir Khajepour for taking the time to read this work. Thanks to Helen Warren for taking care of all of the logistics. Thank you all.

I'd like to thank the wonderful community of applied mathematics graduate students and professors here at the University of Waterloo, who have been so helpful throughout courses and the research process. In particular: my officemate Dhanaraja Kasinathan who has had to endure all the aspects of my personality, my housemates Antonio Sánchez, Michael Dunphy, Ben Turnbull, my research group Amenda Chow, Rob Huneault, Matthew Cox, as well as Katie Ferguson, Greg Mayer, Dr. Marek Stasna, Killian Miller, Chad Wells, and Derek Steinmoeller.

To my closest friends: Inglebert Mui, Danny Li, Brandon Miles, Stephanie Kerrigan, Angela Gray, Lorna Yuen, Kitty Lau, Filgen Fung, Eric Hart and Mark Reitsma, who've been there and stood by me in all aspects of life be it math-related or not. Thank you.

To Colin Wallace and Elizabeth Yeung at Oasis: Ray of Hope, which has provided a welcome distraction to my work as well as the opportunity to serve the impoverished here in the Kitchener-Waterloo area. Thank you for opening my eyes.

Last but certainly not least, to my Lord and Saviour Jesus Christ, through which all things are made possible.

Contents

List of Figures

Chapter 1

Introduction

Hysteresis is a property experienced by many materials that is highly non-linear and difficult to model. Multiple outputs can be associated with the same input, so the system may exhibit path-dependence. Hysteresis can also be described as a delay in the reaction of a material when provided with actuation. Consider magnetic hysteresis: magnets may possess a range of magnetization values without the presence of an applied magnetic field. It is not possible to determine magnetization without knowledge of the input history.

Another example is the play behaviour exhibited by mechanical gears. In the operation of two mated gears, turning one gear causes the other to turn. Due to the tolerance between the teeth of each gear, the driving gear must move a certain distance before the mated gear will move. This hysteresis is known as backlash and will be discussed later. See Figure 1.1, obtained from [24].

An exciting group of hysteretic materials are smart materials. Relevant applications are easily found in the field of micropositoning. For example, a magnetostrictive material, Terfenol-D, can experience a change in length of 0.001m/m at a saturation magnetic field. Shape memory alloys are materials with multiple phases, in which deformed materials return to their original shape under appropriate temperature changes. Piezoelectric materials can convert strains into electrical signals. The issue however, is that all of these materials possess some sort of hysteresis. It is difficult to provide a model, and even harder to control a system that possesses hysteresis. For more information regarding smart materials, the reader is referred to [32].

An attempt in this thesis is made to study the mathematics behind certain hysteretic models and their control. The majority of the work presented in this thesis considers two closed-loop systems with hysteretic components. The control of a hysteretic system using a PI controller and of a second-order system with a

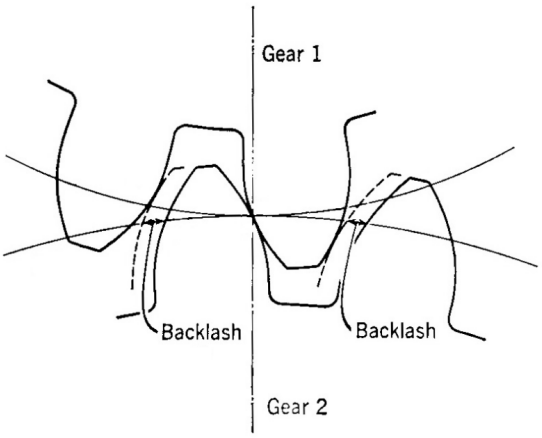

Figure 1.1: Backlash Hysteresis [24]

hysteretic actuator using a PID controller is studied.

The thesis is divided into five chapters. An introduction to several hysteretic models is provided in Chapter 2. The two aforementioned control systems are described and discussed in detail in Chapter 3. A review of other control methods used to control hysteretic systems is also provided in Chapter 3. Simulations are performed in Chapter 4. Some discussion is included with regard to future work.

Chapter 2

Hysteresis Models

As described previously, hysteresis is difficult to model due to its non-linearity, and the need for knowledge of previous states. Considering the generality of hysteresis, it is impossible to find one model that accurately describes all types of hysteresis. Several different models that describe hysteresis will be discussed in this chapter. This small selection is meant to provide an introduction to the models studied in the relevant research papers and theory to come.

A commonly-used mathematical definition of a hysteresis operator from [41] is first presented.

Let $\mathbb{R}_+ := \{t \in \mathbb{R} \mid t \geq 0\}$. Let $I \subseteq \mathbb{R}_+$. Let the set of all functions mapping I to the reals be denoted by $Map(I)$ (that is, $f \in Map(I) \Leftrightarrow f : I \to \mathbb{R}$). The next definition is the truncation property. For $T > 0$, let the truncation of $f \in Map(\mathbb{R}_+)$, be defined by

$$f_T(t) := \begin{cases} f(t), & t \in [0, T] \\ 0, & t > T. \end{cases}$$

Next, the two properties required to define a hysteresis operator are given. They are the causal and rate-independent properties. Note that in literature, the causal property may be also referred to as the Volterra property or the deterministic property.

Definition 2.0.1. *An operator $\Psi : Map(\mathbb{R}_+) \to Map(\mathbb{R}_+)$ is **causal**, if for every $v, w \in Map(\mathbb{R}_+)$, $T \geq 0$*

$$v_T = w_T \text{ implies } (\Psi v)_T = (\Psi w)_T.$$

That is, they must agree everywhere on $[0, T]$ for a given T.

From the definition of the causal property, the output $(\Psi(v))$ does not depend on future inputs, because the property must hold true for all $T \geq 0$.

In order to define rate-independence, another definition must first be introduced.

Definition 2.0.2. *A function $f : \mathbb{R}_+ \longrightarrow \mathbb{R}_+$ is a **time-transformation**, if f is continuous, nondecreasing, and $\lim_{t\to\infty} f(t) = \infty$.*

Definition 2.0.3. *An operator $\Psi : C(\mathbb{R}_+) \longrightarrow C(\mathbb{R}_+)$ is **rate-independent** if for all time transformations f,*

$$(\Psi(u \circ f))(t) = (\Psi(u))(f(t)), \text{ for all } u \in C(\mathbb{R}_+), \text{ for all } t \in \mathbb{R}_+. \tag{2.1}$$

That is, the order in which the operations are applied do not matter. The rate-independent operator can be applied before or after the time transformation. That is, a rate-independent operator cannot depend on derivatives of the input. To illustrate this, a graphical example is included. See Figure 2.1.

On the left of Figure 2.1(a), the input is a sinusoidal function with varying amplitude shown in blue, and the output of a rate-independent operator is shown in green. The input is plotted against the output. A piecewise linear function, constructed with the same local maximums and minimums is in Figure 2.1(b). Note that the input-output graphs are identical. The rate at which these local maximums and minimums are reached is irrelevant to the present value. Finally, the definition of a hysteresis operator is presented.

Definition 2.0.4. *An operator $\Phi : Map(\mathbb{R}_+) \to Map(\mathbb{R}_+)$ that is both causal and rate-independent is a **hysteresis operator**.*

2.1 Backlash Operator

Also known as play, the backlash operator is a hysteresis operator that is used in certain mechanical applications, especially to model the play between gear trains. In terms of application, backlash is the physical clearance between mated gear teeth. The gears will turn only after a certain amount of torque is provided. The following formulation can be found in [18]. An alternative definition can be found in [4]. A function will first be defined.

For all $h \in \mathbb{R}_+$, let the function $b_h : \mathbb{R}^2 \to \mathbb{R}$ be defined as:

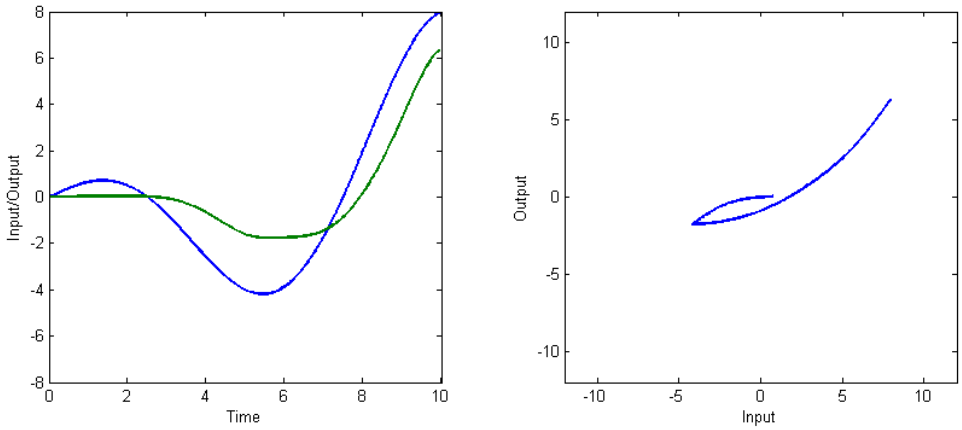

(a) Input Signal: $u(t) = 0.8t\cos(\pi t/5)$

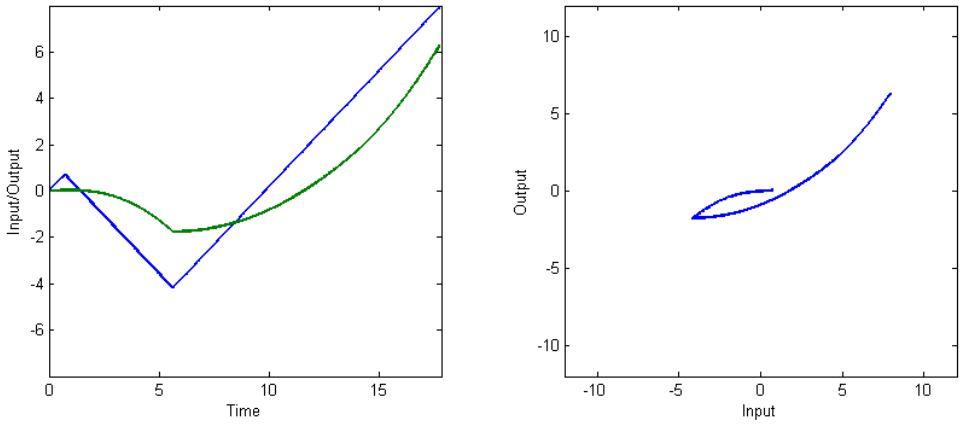

(b) Piecewise Linear Input Signal With Same Extrema

Figure 2.1: Rate-independence

$$b_h(v,w) = \max\{v-h, \min v + h, w\}$$

The backlash operator will be defined for every $h \in \mathbb{R}_+$ and $\xi \in \mathbb{R}$ as a function of b_h. For every piecewise monotone function $u \in C(\mathbb{R}_+)$,

$$(\mathcal{B}_{h,\xi}(u))(t) = \begin{cases} b_h(u(0),\xi), & \text{for } t = 0 \\ b_h(u(t),(\mathcal{B}_{h,\xi}(u))(t_i))), & \text{for } t_{i-1} < t \le t_i, i \in \mathbb{N} \end{cases}$$

where $0 < t_1 < t_2 < ...$ is a partition of $\mathbb{R}_+$ such that $u \in C(\mathbb{R}_+) \to \mathbb{R}$ is monotone (only non-decreasing or only non-increasing) on each of $[t_{i-1}, t_i], i \in \mathbb{N}$ and $t_0 = 0$. The parameter ξ represents the initial state of the operator. In the definition provided above, the parameter h can be thought of as the delay in the operator from the input function u. This is represented visually in Figure 2.2. Using MATLAB®, the continuous function $u(t) = \frac{1}{2}t\sin t$ is plotted against the backlash operator acting on this $u(t)$, with $h = 2,\ \xi = 1$.

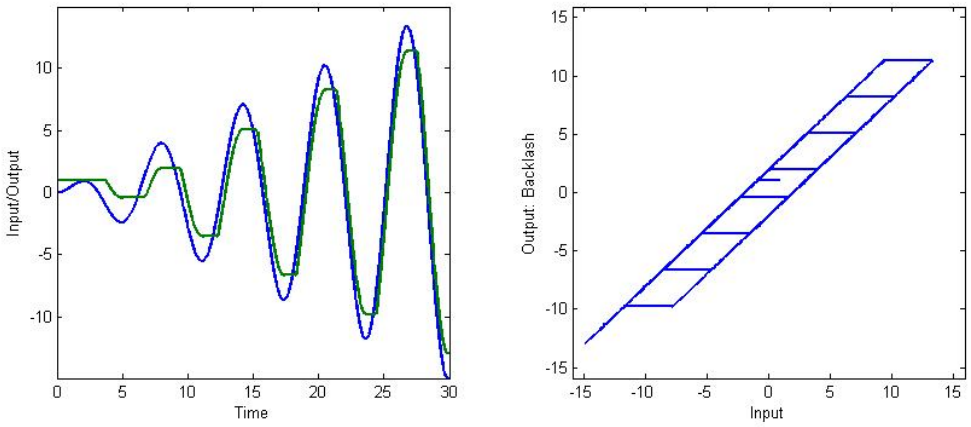

Figure 2.2: Backlash Operator acting on $u(t) = \frac{1}{2}t\sin t$ with $h = 2,\ \xi = 1$

The relationship between the input $u(t)$ and the backlash operator is shown on the right of Figure 2.2. The operator initially starts at $(1, 0)$. Following the plot of the $u(t)$ given on the left, it increases and decreases without any change in the operator. Then it proceeds to make successively larger counter-clockwise loops, closely following the shape of the input on the lines $(\mathcal{B}_{h,\xi}(u))(t) = u(t) + 2$ and $(\mathcal{B}_{h,\xi}(u))(t) = u(t) - 2$, which is representative of the delay of $h = 2$. At $t = 30$, the operator (in the right plot) reaches the point on the bottom left, $(-15, -13)$.

2.2 Elastic-Plastic Operator

The stress and strain relationship in a one-dimensional elastic-plastic element is modelled by this operator. If the stress applied is less than the yield stress, then the material's strain can be approximated by a linear relationship (Hooke's Law, $\sigma = E\epsilon$, where σ is the stress, E is Young's Modulus for the material and ϵ is the strain). If the stress acting on the element becomes greater than the yield stress, then the element deforms plastically (that is,t no additional strain is observed). This mathematical definition of the elastic-plastic operator is constructed much like the backlash operator and can be found in [18]. Let $e_h : \mathbb{R} \to \mathbb{R}$ be defined by

$$e_h(u) = \min\{h, \max\{-h, u\}\},$$

For all $h \in \mathbb{R}_+$, for all $\xi \in \mathbb{R}$, the elastic-plastic operator $\mathcal{E}_{h,\xi}$ is defined for piecewise monotone functions $u \in C(\mathbb{R}_+)$ by

$$(\mathcal{E}_{h,\xi}(u))(t) = \begin{cases} e_h(u(0) - \xi), & \text{for } t = 0 \\ e_h(u(t) - u(t_i) + (\mathcal{E}_{h,\xi}(u))(t_i))), & \text{for } t_{i-1} < t \leq t_i, i \in \mathbb{N} \end{cases}$$

where $0 < t_1 < t_2 < ...$ is a partition of $\mathbb{R}_+$ such that $u \in C(\mathbb{R}_+) \to \mathbb{R}$ is monotone (only non-decreasing or only non-increasing) on each of $[t_{i-1}, t_i], i \in \mathbb{N}$ and $t_0 = 0$. In Figure 2.3, the same function $u(t) = \frac{1}{2}t \sin t$ is plotted against the elastic-plastic operator acting on the same $u(t)$, with $h = 2,\ \xi = 1$. Here, h represents the strain observed once the yield stress is reached. So the operator is bounded by $-h$ and h. The variable $-\xi$ is the initial state of the operator.

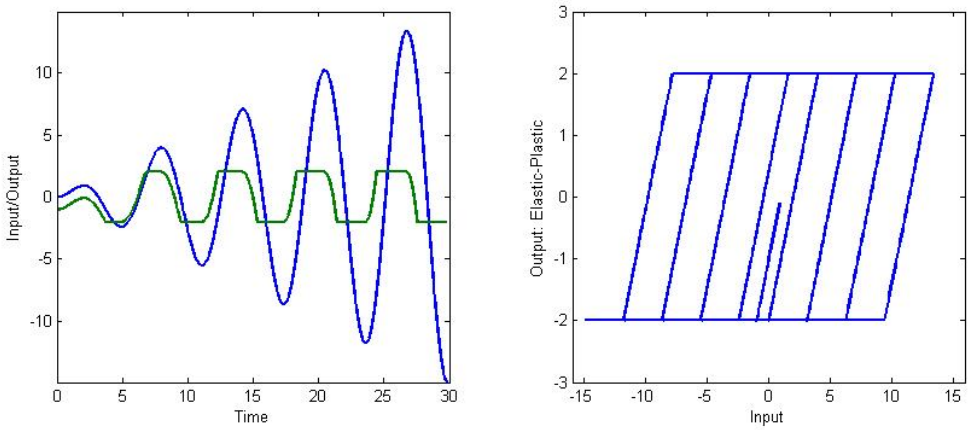

Figure 2.3: Elastic Operator acting on $u(t) = \frac{1}{2}t \sin t$ with $h = 2,\ \xi = 1$

The relationship between the operator and the input is shown on the right of Figure 2.3. As mentioned previously, the property $|(\mathcal{E}_{h,\xi}(u))(t)| \leq h$ is satisfied

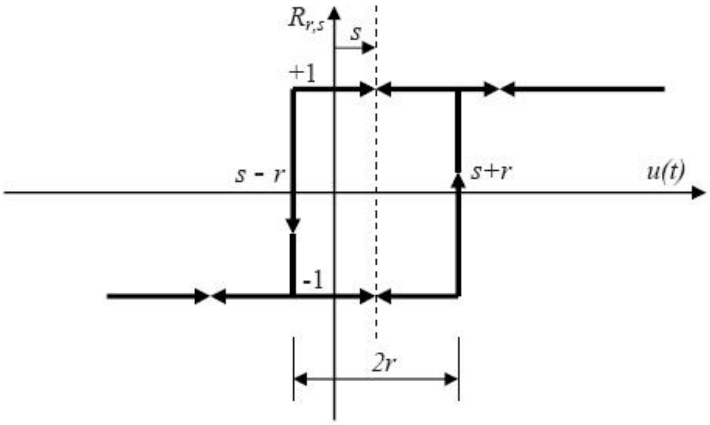

Figure 2.4: Preisach Relay, [41]

by the operator. With respect to $u(t)$, the operator produces successively larger clockwise loops as time progresses. The elastic-plastic operator is often considered the counterpart to the backlash operator. The two are related by: for all $u \in C(\mathbb{R}_+)$, $\mathcal{E}_{h,\xi}(u) + \mathcal{B}_{h,\xi}(u) = u$.

2.3 Preisach Model

One of the most powerful hysteresis models is the Preisach model. It was originally developed in the 1930s to describe the hysteresis observed by magnetic materials. There are several variations on the Preisach model based on physical phenomena, which will be reviewed later. There are many resources that discuss the Preisach model, among them, [11], [12], [25] and [40]. Though not presented here, an interesting description of the Preisach model using the play and stop operators can be found in [4].

2.3.1 Model Definition

The Preisach model is defined as a weighted sum of a continuum of relays. This will be reflected in a double integral, which will be made clear after a few definitions. Consider first the Preisach relay.

Preisach Relay

The Preisach relay is crucial to the definition of the Preisach model. The relay (see Figure 2.4) has a value of +1 or -1, which is analogous to a simple magnetic dipole

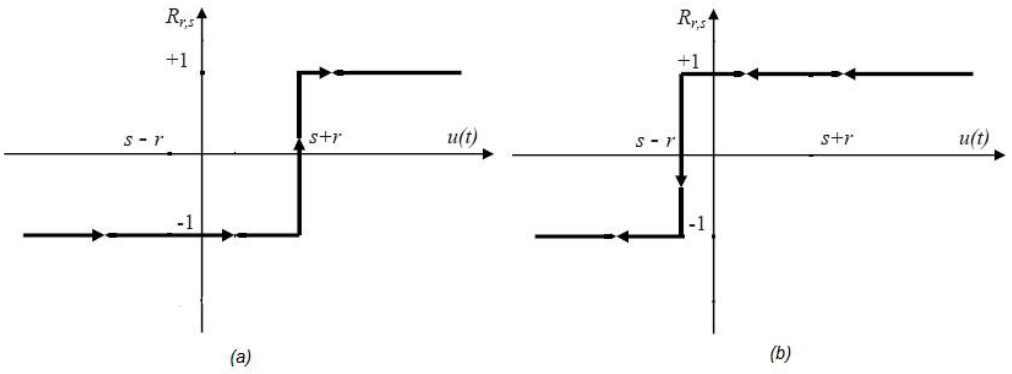

Figure 2.5: Preisach Relay while a) increasing the input $u(t)$, b) decreasing the input $u(t)$

that can only take on a value of ± 1. The relay has two parameters: r and s. The centre of the relay is denoted by s, while the half-width of the relay is denoted by r. Physically, r can be thought of as the resistance towards switching and s is the critical magnetization where switching can occur. Finally, to determine the output of the relay, a history of the relay is required. To illustrate this, suppose the input $u(t)$, lies between $s - r$ and $s + r$. According to Figure 2.4, there are two possible outputs for the relay.

Consider Figure 2.5. Following the left figure, suppose $u(t) < s - r$. Since there is only one input, the relay has a value of -1. In order for the relay to switch, $u(t)$ must be increased past $s + r$ for the relay to switch to +1. Analogously, on the right, suppose $u(t) > s + r$, then $u(t)$ must be decreased past $s - r$ for the relay to switch to -1. To resolve the previous dilemma, if $u(t)$ lies between $s - r$ and $s + r$, then the relay takes on the value of the most recent output. Finally, each pair of parameters (r, s) (note r must be nonnegative since it represents a half-width) has a one-to-one correspondence with a specific relay. With this definition in place, the actual model can now be introduced. The issue of initial states will be dealt with in the following section.

2.3.2 Preisach Operator

The Preisach operator is described as follows,

$$y(t) = \int_0^\infty \int_{-\infty}^\infty R_{r,s}(u(t))\mu(r,s)dsdr, \tag{2.2}$$

where $R_{r,s}$ is the relay with centre s and half width r, $u(t)$ is the input, $\mu(r, s)$ is the weight function and $y(t)$ is the output of the model. The weight function must

be integrable, that is, $y(t)$ in equation (2.2) must always be finite. This is reminiscent of an induced magnetic field (input) producing a magnetization (output) on a magnet. At first glance, there appears to be a difficulty in implementation due to the infinite double integral. Storage of all the history appears impossible. Furthermore, measuring a continuum of relays would raise issues with computation. However, several simplifications can be made, which lead to simpler computation.

2.3.3 Preisach Plane

The first of these simplifications is based upon physical systems having limitations. The system is assumed to exhibit saturation in the presence of a large enough input. As well, it is clear that in any physical computation, the integral cannot be evaluated exactly, so an approximation of a finite sum of selected relay outputs is considered instead.

The Preisach plane is a two-dimensional graphical construction with r on the x-axis, and s on the y-axis. Each point represents a potential relay (with r and s to be the parameters of the relay). Since r represents the half-width, which must be positive, the discussion is limited to points/relays on the right half of the Preisach plane. Next, only relays that have the capability of switching will be considered. Referring back to the Preisach Relay (see Figure 2.4), note that $s - r$ and $s + r$ are the switching points for a given relay with parameters r and s. Therefore only relays that satisfy $-u_{sat} \leq s - r \leq s + r \leq u_{sat}$ are of interest. Note that this has effectively changed the bounds from being infinite to finite.

The next statements deal with the initial state of the Preisach Plane. If the system is initialized (prior to any input), then relays with $s > 0$ and $s < 0$ will be assumed to have values of -1 and $+1$ respectively. If $s = 0$, then the relay will remain at 0 until the input causes the relay to switch (increased past $s-r$ or $s+r$). All of these assumptions result in the Preisach plane in Figure 2.6. As a side note, other sources of literature (for example [36] and [17]) define the Preisach plane so that the end result is a 135 degree counter-clockwise rotation of the description seen here. This is merely a change of coordinates and the two forms are otherwise identical.

To determine the output, all the relays in each of the regions marked $+1$ and -1 are summed. The Preisach boundary is made of line segments, having slopes of 1 and -1 as well as 0 (from the initial state see Figure 2.6). It is important to note that the $r = 0$ point of the boundary will always have the same value as the current input. To demonstrate the operation of the plane, an example will be considered. Suppose the input is increased monotonically from $u(t) = 0$ to $u(t) = 3$, see Figure 2.7 (left). Then the Preisach boundary will produce a line segment with slope -1.

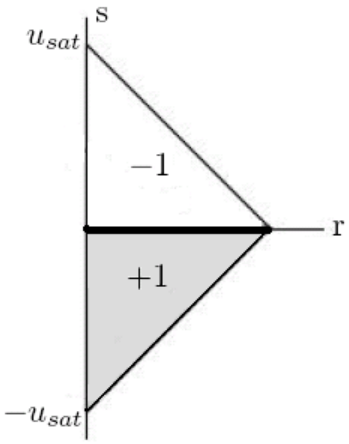

Figure 2.6: Preisach Plane (Initialized)

This is consistent with the previous definitions, since the line segment produced is in fact $s + r = 3$, indicating that all the relays $s + r \leq 3$ have switched to the $+1$ state. Suppose the input is now decreased monotonically to $u(t) = -1$, then the result is another line segment of slope $+1$, described by $s - r = 1$. In Figure 2.7 (right), the relays with both $s + r \leq 3$ and $s - r \geq 1$ have switched back to an output of -1. Note that the Preisach boundary has a corner, indicating that the input was once at $u(t) = 3$, (but now is at $u(t) = -1$). Further non-monotonic changes in the input would result in different corners in the Preisach boundary. It is clear that the Preisach boundary contains information regarding the history of the input. The next property regarding the Preisach plane will demonstrate this.

Continuing the previous example, suppose that the input is now increased monotonically from $u(t) = -1$ to $u(t) = 4$. As $u(t)$ increases, a new line segment with -1 slope will be introduced, hence introducing a corner indicating that the input was once at $u(t) = -1$ (See Figure 2.8 (left)). But as the input increases past $u(t) = 3$, both these corners will be wiped out, yielding only a single line segment of slope -1. At $u(t) = 4$, there will be only a single line segment: $s + r = 4$ (See Figure 2.8 (right)). That is, the Preisach boundary only retains information about the most recent extrema. If the input is increased or decreased past previous extrema, then that part of the memory is wiped out. Not surprisingly, this is known as the *wiping out property*. With regard to computation, an alternative definition can be made that uses the Presiach boundary $\psi(t, r)$ at time t. Consider

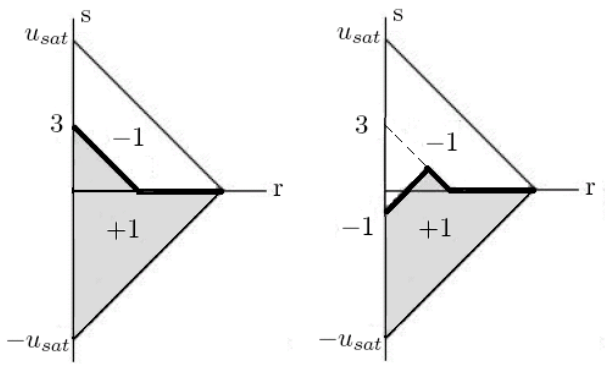

Figure 2.7: Left: Increasing the input to $u(t) = 3$, Right: Then Decreasing the input to $u(t) = -1$

$$y(t) = \int_0^\infty \int_{-\infty}^\infty R_{r,s}(u(t))\mu(r,s)dsdr \tag{2.3}$$

$$= 2\int_0^\infty \int_{-\infty}^{\psi(t,r)} \mu(r,s)dsdr - \int_0^\infty \int_{-\infty}^\infty \mu(r,s)dsdr \tag{2.4}$$

$$= 2\int_0^\infty \int_0^{\psi(t,r)} \mu(r,s)dsdr + \int_0^\infty \int_{-\infty}^0 \mu(r,s)dsdr - \int_0^\infty \int_0^\infty \mu(r,s)dsdr \tag{2.5}$$

$$= 2\int_0^\infty \int_0^{\psi(t,r)} \mu(r,s)dsdr + y_{ip}. \tag{2.6}$$

where y_{ip} is the output of the system evaluated with the Preisach plane shown in Figure 2.6. This definition is mathematically equivalent to (2.2), though from a computational perspective is simpler. The change from the initial state is modeled by the boundary, thus only the relays that switch value need to be considered.

Preisach Boundary and Backlash Operator

As an interesting sidenote, the Preisach boundary has a strong connection to the backlash operator. Consider first the boundary (ψ) as a function of r on the Preisach plane. This boundary will change over time according to an input $u(t)$. Let $\psi(t,r)$ denote the value of the boundary at position r and time t corresponding to the input history of $u(t)$. This mathematical relationship can be described with

$$\psi(t,r) = \mathcal{B}_{r,0}(\text{median}\,(-u_{sat}, u(t), u_{sat})),$$

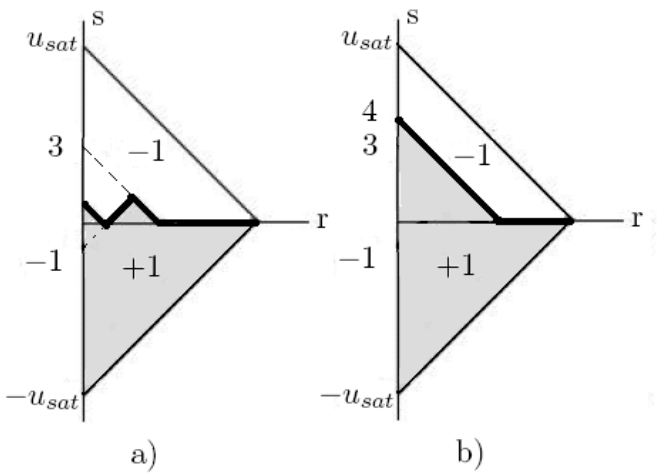

Figure 2.8: Wiping Out Property

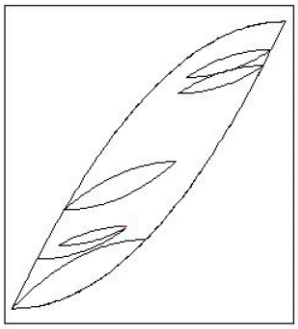

Figure 2.9: Minor Loops within a Major Loop in a Hysteretic System, from [41]

where r is the backlash factor and the second parameter (0) is the initial condition on the backlash operator. The median function is just the middle of the three values, ensuring that the saturation limits are in place. Should the input $u(t)$ be increased higher than u_{sat}, u_{sat} becomes the new input. While the Preisach plane can be defined without the backlash operator, this property will be used in theoretical developments in a future chapter. More details can be found in Section 2.1 of [4].

Major Loop

To obtain the major loop, (monotonically) increase $u(t)$ past u_{sat}, then (monotonically) decrease $u(t)$ below $-u_{sat}$, followed by (monotonically) increasing $u(t)$ past u_{sat}. The last two changes should trace out the major loop. A minor loop is any loop produced inside the major loop. See Figure 2.9 for a graphical example.

2.3.4 Weight Function

It remains to discuss how the weight function is identified. There are several approaches to this problem. A general form of the weight function can be assumed (for example, see Section 2.3.5), with varying parameters to be found through optimization of error in comparison to experimental data. Optimization may not yield a good result if an inappropriate shape is chosen. A popular choice for identifying the weight function is to discretize the Preisach plane into squares of equal size where the weight function is assumed to be constant over each square region. In literature, this process is referred to performing a discretization of level L, where L represents the number of squares along the centre. Thus the whole Preisach plane would have L^2 components. Assuming a proper identification technique is used for each square, the higher the level of discretization L, the better the accuracy.

The identification of each square can be performed by evaluating experimental data obtained in a very specific manner. The identification of a single square will be described. The corners of the square will be referred to in this description as labeled in Figure 2.10. The region of the desired square will be denoted Ω. The following algorithm will yield an expression for the weight function inside Ω.

1. Decrease u so that it is less than $-u_{sat}$ (note all relays will have output -1).
2. Increase u until the Preisach boundary coincides with the line segment formed by points 1 and 2 in Figure 2.10. This is described by u_{12} in Figure 2.11.
3. Decrease u until the Preisach boundary coincides with the line segment formed by points 1 and 3 in Figure 2.10. This is described by u_{13} in Figure 2.11.
4. Denote the output after this procedure y_1 (the process to obtain 1 as a corner in the Preisach boundary).

One may follow a similar algorithm to produce corners 2, 3, 4 in Figure 2.11 in the Preisach boundary, and label the outputs y_2, y_3, y_4 respectively. In the following, $\mathcal{P}_{y_i}$ is the Preisach plane obtained by following the procedure above to obtain y_i. The region Ω_1 is described by Figure 2.11 (b). Consider the quantity:

$$\begin{aligned}(y_1 - y_2) &= \left(\int\int_{\mathcal{P}_{y_1}} R_{r,s}(u(t))\mu(r,s)drds - \int\int_{\mathcal{P}_{y_2}} R_{r,s}(u(t))\mu(r,s)drds \right), \\ &= \left(\int\int_{\Omega_1} (+1)\mu(r,s)drds - \int\int_{\Omega_1} (-1)\mu(r,s)drds \right), \\ &= 2\int\int_{\Omega_1} \mu(r,s)drds.\end{aligned}$$

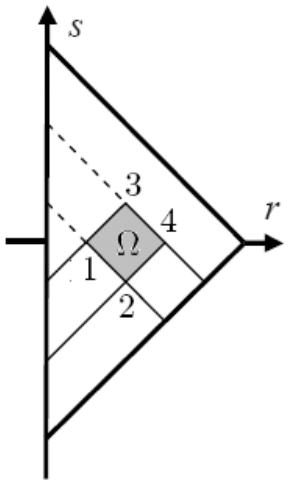

Figure 2.10: An arbitrary square in a piecewise-constant weight function

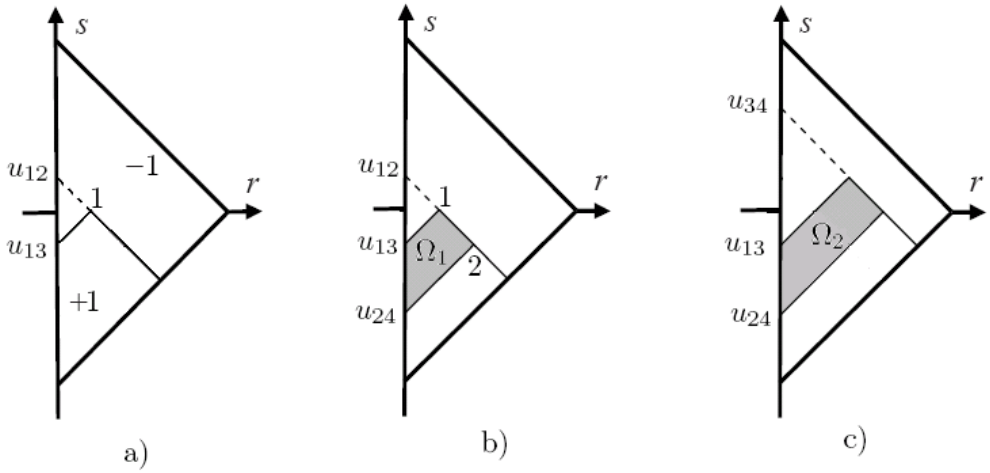

Figure 2.11: a) Preisach Plane in obtaining corner 1, b) The region Ω_1, c) The region Ω_2

It is easy to see that a similar region (but one that includes the square of interest) can be produced by considering the quantity $(y_3 - y_4)$. Denote this region Ω_2 (see Figure 2.11 c)). Then the following expression will result in a weight function for the square of interest. The side length of the square will be denoted c. The value μ_Ω is the constant value of the weight function in the region Ω.

$$\begin{aligned}
\frac{1}{2c^2}\left((y_3 - y_4) - (y_1 - y_2)\right) &= \frac{1}{2c^2}\left(2\int\int_{\Omega_2}\mu(r,s)drds - 2\int\int_{\Omega_1}\mu(r,s)drds\right), \\
&= \frac{1}{c^2}\int\int_{\Omega}\mu(r,s)drds, \\
&= \frac{1}{c^2}\mu_\Omega\int\int_{\Omega}drds, \\
&= \mu_\Omega.
\end{aligned}$$

The second last step is a result of the weight function assumed constant over this region. The experimental data used to identify the weight function is a set of first-order descending curves. For a discretization of level L ($L \in \mathbb{N}$), $L+1$ first-order descending curves are required. Suppose the range of the outputs in the major loop is divided into L equally spaced intervals (resulting in $L+1$ equally spaced points). Then the ith curve ($i \in 1, 2, ..., L+1$) is obtained by decreasing the input $u(t)$ below $-u_{sat}$ (so that all the relays are in the -1 state, then increasing the input monotonically to the ith point, followed by decreasing the input monotonically back to $-u_{sat}$. This is very similar to the procedure outlined above to obtain the square region Ω. The differences are that the procedure is performed $L+1$ times (once for each curve), and in the third step, $u(t)$ is decreased monotonically back down to $-u_{sat}$, while sampling at each potential square corner. This approach is attractive because it is simple both experimentally and computationally.

2.3.5 Physical Preisach Model

There have been efforts made (for example [33], [34]) to model magnetic effects from a physical perspective, yielding what is known as the physical Preisach model. The identification of the Preisach weight function in this context is done by assuming a general shape, and optimizing parameters to fit with experimental data. Other extensions include extending the relay so that it can take other values (other than just $+1$ and -1). The general shape and operation would still be the same, however, the top and bottom components will have a positive slope instead of fixed values (see Figure 2.12). This physical relay is modeled after the Gibbs Energy.

In the case of a magnetostrictive material, the variable M_I is the least amount of magnetization seen before switching from the positive to negative state. The

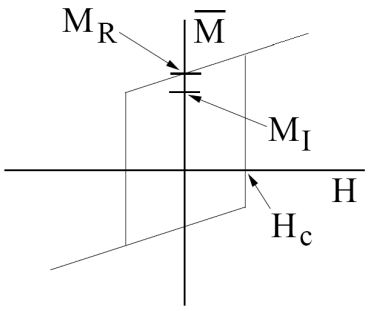

Figure 2.12: Physical Preisach Relay, see [33]

value M_R is the magnetization observed when the applied magnetic field is 0. The local magnetization is denoted by M, representing the amount of magnetization of that specific dipole. The coercive field H_C, or switching point, is the same as $r + s$ in the phenomenological model. The interaction field, H_I plays the same role as s. Instead of different centre locations, the same definition, but with an offset of H_I is used. Finally H is the applied magnetic field. For a visual representation of these values with the Gibbs energy, the reader is referred to Section 2 of [33].

With this different formulation, the model equation itself becomes

$$M(H) = \int_0^\infty \int_{-\infty}^\infty \nu_1(H_c)\nu_2(H_I)\overline{M}(H + H_I; H_c; \xi)dH_I dH_C. \tag{2.7}$$

where ξ represents the last known position (whether it is on the positive or negative part of the relay). The weight function components ν_1 and ν_2 in [33] are given by

$$\begin{aligned} \nu_1(H_c) &= \frac{c_1}{I_1} e^{-[\ln(H_c/\overline{H_C})/2c]^2}, \\ \nu_2(H_I) &= c_2 e^{-H_I^2/2b^2}, \\ I_1 &= \int_0^\infty \nu_1(H_c)dH_C. \end{aligned}$$

where c_1, c_2, and b are positive real parameters obtained through optimization in accordance to provided data. These are not the only choices for the weight function. There are however some general criteria that should be followed. Both functions should follow certain decay properties. The function ν_2 should be even. Extensions have been made in [42] and [33] to include the effects of compressive loads on the hysteresis of magnetostrictives.

The definition of three operators have been provided, but it should be mentioned that they are in fact hysteresis operators as described by Definition 2.0.4. Recall

that hysteresis operators must be both causal and rate-independent. The backlash, elastic-plastic and Preisach operators satisfy this definition. It is clear that they are causal. Rate-independence for each operator follows with a simple substitution verifying that the equality in equation (2.1) holds.

2.4 Other Models

There are many more hysteresis models that have not been discussed. The hysteresis models discussed thus far are described by operators acting on functions. The following hysteresis model is described by systems of differential equations. The Duhem model is a very general model that has a purely mathematical basis. Other models can be easily found in literature. The reader is referred to [32] for more general models regarding hysteresis. For specifics to magnetic and magnetostrictive materials, a wide variety of hysteresis models can be fonud in [39] and [40].

2.4.1 Duhem Model

The Duhem model was developed at the end of the last century by a French mathematician Pierre Duhem [4]. The model is used widely to model friction, and the Maxwell-slip model is a special case of the Duhem model [29]. Only the previous step of the input in terms of memory is required to determine whether is increasing, decreasing or stationary. The definition takes the form of a differential equation:

$$w'(t) = f_+(t, v, w)(v'(t))_+ - f_-(t, v, w)(v'(t))_-, w(0) = w_0.$$

where $(v'(t))_+ = 1$ if $v(t)$ is increasing at t and 0 otherwise, its counterpart $(v'(t))_- = -1$ when $v(t)$ is decreasing and 0 otherwise. The functions f_+ and f_- can be chosen to satisfy an application. The solution to this system can be written as a series of ODEs on finite time intervals where the input is monotonely nonincreasing or nondecreasing. Each ODE would depend on the solution and endpoint of the previous one for its initial value. It is not too difficult to see that the input-output graph (see Figure 2.13) could produce a loop-like behaviour. In this very simple example, $v(t)$ is a sawtooth function with an amplitude of 1 and a period of 2:

$$f_+(t, v, w) = 2\pi \sin(2\pi t),$$
$$f_-(t, v, w) = 2\pi \cos(2\pi t),$$

The Duhem model in contrast to the other models presented holds very general assumptions and the hysteresis depends entirely on the chosen functions. The reader is referred to [28], and [29] for more information on its derivation and properties. The Duhem model may define a hysteresis operator, depending on the chosen functions in its definition.

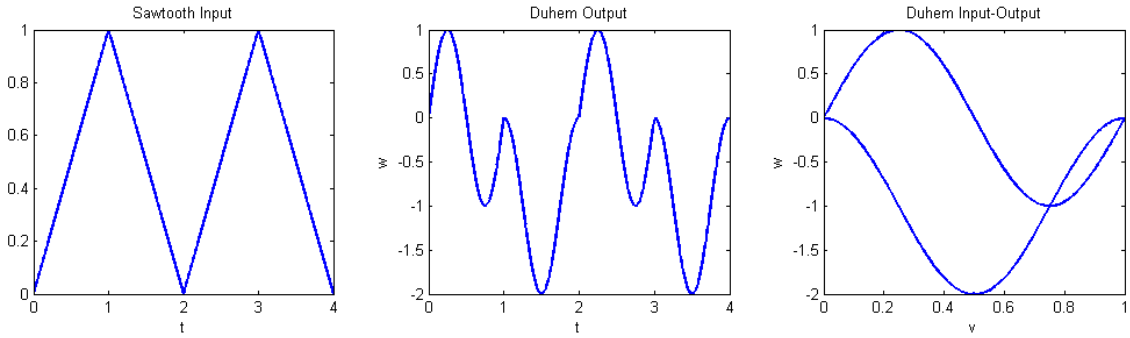

Figure 2.13: Left: Input, Center: Output, Right: Input-Output

Chapter 3

PID Control of Hysteretic Systems

3.1 Introduction

PID control is a well understood branch of control theory. In this chapter, two groups of hysteretic systems will be controlled by PID controllers in order to track a constant reference signal. A brief introduction to PID controllers and literature review is presented in the following section. In [41], a system experiencing hysteresis is controlled with a PI controller. These mathematical results are presented in Section 3.3. An extension is made in Section 3.4 to include a linear first-order system and some similar properties and results are shown.

In [18], a second-order system experiencing hysteresis in the actuator is controlled to track a constant reference signal. These results are discussed in Section 3.5. A verification is presented in Section 3.6 that the same results hold for a general first order system. The assumptions of [18] and [41] are compared in Section 3.5.3. Finally, a literature survey discussing other popular methods of control in the context of hysteresis systems is presented.

3.1.1 PID Controllers

PID controllers are commonly used in feedback control. The goal of the controller is to steer the system to follow a given reference signal. The error is defined as the difference between the output and a reference signal. Proportional, integral and derivative components of the error can be found in the PID Controller. For the following controller, $K_P, K_I, K_D > 0$ are the proportional, integral and derivative control parameters respectively. The general form of the PID controller is:

$$u(t) = K_P e(t) + K_I \int_0^t e(\tau) d\tau + K_D e'(t). \tag{3.1}$$

The Laplace transform of a function $f \in C(\mathbb{R}_+)$ is

$$(\mathcal{L}\{f(t)\})(s) = \hat{f}(s) = \int_0^\infty f(t)e^{-st}dt.$$

It is convenient to write the PID controller and other linear transformations in terms of a transfer function. A transfer function is a representation of a linear operator in the Laplace domain, defined by the Laplace transform of the output divided by the Laplace transform of the input. For the PID controller described above, if $e(0) = 0$,

$$\frac{\hat{u}(s)}{\hat{e}(s)} = K_P + \frac{K_I}{s} + K_D s.$$

Proportional control changes the controller by an amount that is proportional to the error. The system can become unstable if the value of K_P is too high. Conversely, if K_P is too low, then the controller may not be responsive to large errors. Integral control considers previous values of error, and adjusts the input accordingly. A larger value of K_I will eliminate steady-state error faster but may cause overshoot (the state moves past the reference signal and then returns to stabilize). Derivative control affects the controller by considering the derivative of the error. Applying derivative control reduces the rate of change of the controller, and hence the overshoot is decreased. The derivative control is sensitive to noise. The derivative of the noise is usually unbonuded. More information regarding PID controllers can be found in [26].

3.1.2 Lebesgue and Hardy Spaces

The notion of Lebesgue and Hardy spaces will be used throughout the chapter. More information can be found in [8] and [9]. The space of $L^p(\mathbb{R}_+)$ functions will now be introduced.

Lebesgue Spaces: $L^p(\mathbb{R}_+)$

For $1 \leq p < \infty$ and a function f

$$\|f\|_p = \left(\int_0^\infty |f(t)|^p dt\right)^{\frac{1}{p}}.$$

In the case of $p = \infty$,

$$\|f\|_\infty = \sup_{t\in\mathbb{R}_+} |f(t)|.$$

A function f belongs to an $L^p(\mathbb{R}_+)$ space if its $L^p(\mathbb{R}_+)$-norm is finite. Next, the set of functions that are locally $L^p(\mathbb{R}_+)$ where $p \in \mathbb{N}\bigcup\{\infty\}$) will be introduced. Recall the truncation property defined earlier in the beginning of Chapter 2. A function $f \in L^p_{loc}$ if for every $T > 0$,

$$\|f_T\|_P < \infty.$$

Hardy Spaces: $H^2(\mathbb{C}_+)$ and $H^\infty(\mathbb{C}_+)$

The results in this chapter require the definition of two Hardy spaces. A more specific version of the definition found in [8, Definition A.6.14] is presented here.

Definition 3.1.1. *A complex-valued function $f \in H^2(\mathbb{C}_+)$ if it is holomorphic on the right-half complex plane and*

$$\|f\|^2_{H^2} := \sup_{x>0} \left(\frac{1}{2\pi} \int_{-\infty}^{\infty} \|f(x+iy)\|^2 \, dy \right) < \infty. \tag{3.2}$$

Definition 3.1.2. *A complex-valued function $f \in H^\infty(\mathbb{C}_+)$ if it is holomorphic on the right-half complex plane and*

$$\|f\|_{H^\infty} := \sup_{Re(s)>0} |f(s)| = \sup_{\omega\in\mathbb{R}} |f(iw)| < \infty. \tag{3.3}$$

3.2 PID Control of Hysteretic Systems in Literature

Before the main work is presented, a brief overview of other PID-related work available in the literature regarding stability of controlled hysteretic systems will be mentioned. Each of the hysteresis models are described in their respective papers. In [16], a second-order system with hysteretic effects in the spring term, modeled by the Bouc-Wen model, is controlled using a PID controller. The Bouc-Wen model is a specific case of a rate-independent Duhem model. The closed loop signals are shown to satisfy boundedness, and the Routh-Hurwitz criterion is used to demonstrate asymptotic stability of the error. A similar study can be found in [18] (expanded further in [22]), where the effects and control of a hysteretic spring is considered. The hysteresis operator is formulated in the same manner as in Section 3.5.2. Experimental data is presented in both works. A PID controller combined with inverse compensation (discussed in Section 3.7.3) approach where

the constants are determined experimentally is used in [14]. Shape memory alloy actuators represented by a Preisach model are controlled in [1] with use of fuzzy logic components and a PID controller. Lyapunov methods are used to demonstrate stability. Finally, in [5], a PID controller is used alongside a feedback linearization loop and repetitive controller on a system exhibiting Maxwell slip model hysteresis. Stability is obtained with a small gain theorem.

3.3 Stability and Robust Position Control of Hysteretic Systems

The position control of a hysteretic system using a PI controller is discussed in [41]. For arbitrary reference signals, the closed-loop system is shown to be BIBO-stable with a gain of one. In the case of a constant reference signal, zero-state error and monotonically decreasing error are guaranteed. A bound on the time to reach an arbitrarily small error is found. All the material in this section can be found in [4] and [41].

3.3.1 Background and Assumptions

Several sets that deal with extensions of existing functions are defined. These sets will be useful in the context of proving existence and uniqueness of solutions in future sections. For every $\delta > 0$, $0 \leq t_1 \leq t_2$, $w \in C([0, t_1])$, let

$$B_1(w, t_1, t_2) := \{u \in C([0, t_2]) \mid u_{t_1} = w_{t_1}\}.$$

The set B_1 is the set of all continuous extensions of w from t_1 to t_2.

Some assumptions on the hysteresis operator (Definition 2.0.4) are required and will be applied throughout the next few theorems. In the following assumptions, $y(t) = \Phi(u(t))$, where Φ is a hysteresis operator.

(A1) If $u(t)$ is continuous, then $y(t)$ is continuous.

(A2) There exists $\lambda > 0$, such that for all $0 \leq t_1 \leq t_2$, $w \in C([0, t_1])$, $u_1, u_2 \in B_1(w, t_1, t_2)$,

$$\sup_{t_1 \leq \tau \leq t_2} |\Phi(u_1)(\tau) - \Phi(u_2)(\tau)| \leq \lambda \sup_{t_1 \leq \tau \leq t_2} |u_1(\tau) - u_2(\tau)|$$

(A3): Let $t_f > t_i \geq 0$. If for every $t \in [t_i, t_f]$, $u(t_i) \geq u(t)$, then $y(t_i) \geq y(t_f)$. Similarly, if for every $t \in [t_i, t_f]$, $u(t_i) \leq u(t)$, then $y(t_i) \leq y(t_f)$. (In the context of hysteresis loops, only counter-clockwise loops may be observed. In Figure 3.1a, the first statement of **(A3)** is violated, whereas it is satisfied in Figure 3.1b.)

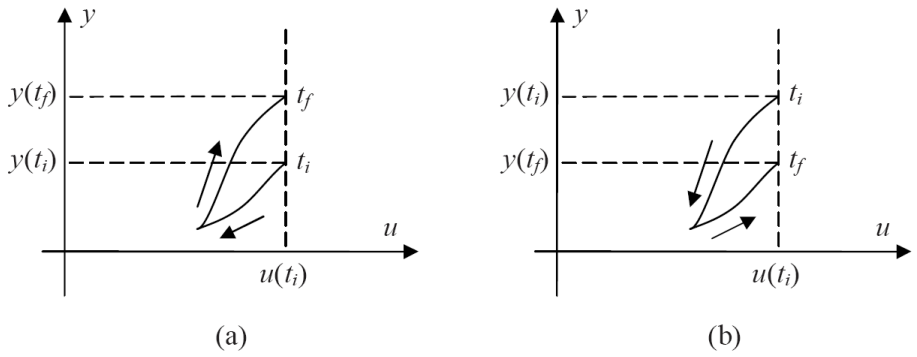

Figure 3.1: (a) Clockwise Hysteresis Loop, (b) Counter-Clockwise Hysteresis Loop, from [41]

(A4): There exists $u_{sat} > 0$, y_+ and y_- such that if $u(t) \geq u_{sat}$, then $(\Phi u)(t) = y_+$ and $(\Phi(-u))(t) = y_-$. This property is known as *saturation.*

The norm used throughout [41] is the infinity norm, defined by

$$\|f\|_\infty = \sup_{t \in \mathbb{R}_+} |f(t)|.$$

It will be shown that the Preisach model satisfies the given assumptions. The reader is referred to Section 2.3 for a complete definition of the Preisach model. Several conditions are required for the Preisach model to satisfy **(A1)-(A4)**.

Theorem 3.3.1. *[41, Theorem 5] If $\mu(r, s)$ is bounded with compact support, then assumptions **(A1)** and **(A2)** are satisfied with*

$$\lambda := 2 \int_0^\infty \sup_{s \in \mathbb{R}} |\mu(r, s)| \, dr < \infty.$$

Outline of Proof: Assumption **(A1)** can be proven using the results of Propositions 2.4.9 and 2.4.11 in [4]. With regard to **(A2)** being satisfied, the Preisach operator can be written as:

$$y(t) = \int_0^\infty \int_0^{\psi(t,r)} 2\mu(r, s) ds dr + y_{ip},$$

where $\psi(t, r)$ represents the Preisach boundary at time t. The value $y_{ip} \in \mathbb{R}$ is first introduced in equation (2.6). If $\psi_1(t, r)$ and $\psi_2(t, r)$ are the boundaries produced

by input histories $u_1(t)$ and $u_2(t)$, respectively at time t, then

$$\begin{aligned}
|y_1(t) - y_2(t)| &= \left| \int_0^\infty \int_0^{\psi_1(t,r)} 2\mu(r,s)dsdr - \int_0^\infty \int_0^{\psi_2(t,r)} 2\mu(r,s)dsdr \right|, \\
&= \left| \int_0^\infty \int_{\psi_2(t,r)}^{\psi_1(t,r)} 2\mu(r,s)dsdr \right|, \\
&\leq 2 \int_0^\infty \sup_{s\in\mathbb{R}} \mu(r,s)dr \, \|\psi_1(t) - \psi_2(t)\|_\infty , \\
&\leq 2 \int_0^\infty \sup_{s\in\mathbb{R}} \mu(r,s)dr \, \|u_1 - u_2\|_\infty .
\end{aligned}$$

A detailed proof of the last two lines is provided in Lemmas 2.3.2 and 2.4.8 in [4]. □

Theorem 3.3.2. *[41, Theorem 6] If $\mu(r,s) \geq 0$ for every r, s,* **(A3)** *holds.*

Proof. Let $t_f > t_i \geq 0$. Suppose u is such that for every $t \in [t_i, t_f]$, $u(t) \leq u(t_i)$. Comparing the state of the system at t_f and t_i, let Ω_+ denote the set of relays that switched from -1 to $+1$ and let Ω_- be the set of relays that switched from -1 to $+1$.

$$\begin{aligned}
y(t_f) - y(t_i) &= \iint_{\Omega_+} (+1)\mu(r,s)\mathrm{drds} + \iint_{\Omega_-} (-1)\mu(r,s)\mathrm{drds} \\
&\quad - \left[\iint_{\Omega_+} (-1)\mu(r,s)\mathrm{drds} + \iint_{\Omega_-} (+1)\mu(r,s)\mathrm{drds} \right] \\
&= 2 \iint_{\Omega_+} \mu(r,s)\mathrm{drds} - 2 \iint_{\Omega_-} \mu(r,s)\mathrm{drds}
\end{aligned}$$

Since $u(t) \leq u(t_i)$ for every $t \in [t_i, t_f]$, no relays could have switched from -1 to $+1$. Hence the set Ω_+ is empty. This, together with the property that $\mu(r,s) \geq 0$ for all r, s, implies that

$$y(t_f) - y(t_i) = -2 \iint_{\Omega_-} \mu(r,s)\mathrm{drds} \leq 0.$$

Therefore $y(t_f) \leq y(t_i)$, as required. For the second statement, with the assumption that $u(t) \geq u(t_i)$, the set Ω_- can be shown to be empty by an analogous argument, so $y(t_f) \geq y(t_i)$ as required. □

Finally, the Preisach model will be shown to satisfy **(A4)**.

Theorem 3.3.3. *[41, Theorem 7] Assume there is $u_{sat} > 0$ such that $\mu(r,s) = 0$ for $|r+s|$ or $|r-s|$ larger than $u_{sat} > 0$, and define*

$$\begin{aligned}
y_+ &= \int_{-\infty}^\infty \int_0^\infty \mu(r,s)\, drds \\
y_- &= \int_{-\infty}^\infty \int_0^\infty -\mu(r,s)\, drds.
\end{aligned}$$

*If $u(t) \geq u_{sat}$ or $u(t) \leq -u_{sat}$, then $y(t)$ is equal to y_+ or y_- respectively, satisfying **(A4)**.*

Proof. Let $u(t) \geq u_{sat}$. If the switching point, $r + s$ (refer to Figure 2.4) of a relay is past u_{sat}, its weight must be 0. All the relays that correspond to when $\mu \neq 0$ are in the $+1$ state. By applying the definition of y, if $u(t) \geq u_{sat}$, then $y(t) = y_+$. The analagous argument is true, if $u(t) \leq -u_{sat}$, then $y(t) = y_-$. □

The Preisach model has been shown to satisfy assumptions **(A1)** - **(A4)** provided that reasonable assumptions on μ are satisfied. In particular, **(A1)** - **(A4)** hold if the weight function μ, is both nonnegative and has compact support. In the context of physical systems, the weight function at a point represents the contribution of the relays with a specific configuration. This value must intuitively be nonnegative. The notion of a weight function having compact support assumes that relays that require extensive actuation do not have a considerable impact on the output. If the contribution coming from relays that require large actuation is significant, then u_{sat} can be increased accordingly. An infinite amount of actuation is not realistic for a physical system, so a suitable u_{sat} can be chosen.

3.3.2 Stability of the Closed-Loop System

It will be shown that the controlled hysteretic system described below is BIBO (Bounded Input Bounded Output)-stable.

Definition 3.3.4. *Let an operator $R : C(I) \to C(I)$. R is **BIBO-stable** if for every $u \in C(I)$, $Ru \in C(I)$, and there exists ρ such that:*

$$||(Ru)||_\infty \leq \rho||u||_\infty.$$

The smallest such ρ is known as the gain.

The output is defined as $y = \Phi u$. The controller will have both proportional and integral components of the error, e. A diagram is provided in Figure 3.2. For the remainder of the section, *closed-loop system* will refer to the following four equations,

$$e(t) = r(t) - y(t) \tag{3.4}$$

$$f(t) = \int_0^t e(\tau)\mathrm{d}\tau \tag{3.5}$$

$$u(t) = K_P e(t) + K_I f(t) \tag{3.6}$$

$$y(t) = \Phi[u(t)] \tag{3.7}$$

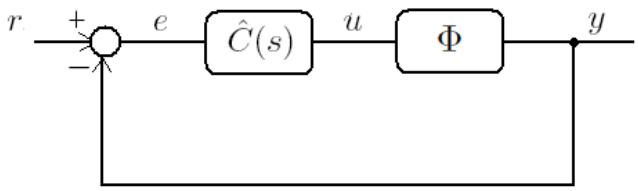

Figure 3.2: Closed-Loop System, from [41]

The transfer function of the controller, C is $\hat{C}(s) = \dfrac{\hat{u}(s)}{\hat{e}(s)} = K_P + \dfrac{K_I}{s}$, where K_I and K_P are chosen control parameters. With regard to the system parameters, the following two assumptions are required.

(B1) $0 \leq K_P\lambda < 1$, and $K_I > 0$, where $\lambda > 0$ is the Lipschitz constant described in **(A2)**.

(B2) The reference signal, $r(t)$ is continuous (that is, $r(t) \in C(\mathbb{R}_+)$).

Theorem 3.3.5. *[41, Theorem 4] If Φ is a hysteresis operator, and satisfies **(A3)** and **(A4)**, then $y_- \leq y(t) \leq y_+$ for every t.*

Proof. If $|u(t)| > u_{sat}$, assumption **(A4)** implies that $y \in \{y_+, y_-\}$. Otherwise, let $u(t_i)$ and $y(t_i)$ be the input and output of the system at an arbitrary time t_i. If $u(t_i) \leq u_{sat}$, monotonically increase u to $u(t_f) > u_{sat}$ (where $t_f > t_i$). From **(A3)**, $y(t_i) \leq y(t_f)$, and from the saturation property in **(A4)**, $y(t_f) = y_+$, and hence $y(t_i) \leq y_+$. An opposite argument with a monotone decrease will result in $y(t_i) \geq y_-$. Since t_i was chosen arbitrarily, this holds for all possible t. □

The next lemma will demonstrate the existence and uniqueness of the solution to the closed-loop system on a small interval.

Lemma 3.3.6. *[41, Lemma 9] Assume **(A1)**, **(A2)**, **(B1)**, **(B2)** are satisfied. For every $t_0 \geq 0$ such that the closed-loop system has a unique solution, u on $[0, t_0]$, the closed-loop system will have a unique solution u on $C([t_0, t_0 + \bar{t}))$, where*

$$\bar{t} = \frac{1 - K_P\lambda}{2\lambda K_I}.$$

Proof. Let $x \in C([0, t_0])$. Define the operator

$$(Gx)(t) = K_I \int_0^t (r(\tau) - (\Phi x)(\tau))\mathrm{d}\tau + K_P(r(t) - (\Phi x)(t)).$$

If G is a contraction map, then by the Contraction Mapping Theorem [27, Thm 3.15.2] there will exist a unique fixed point. Note that in this case,

$$\begin{aligned}(Gu)(t) &= K_I \int_0^t (r(\tau) - (\Phi u)(\tau))\mathrm{d}\tau + K_P(r(t) - (\Phi u)(t)) \\ &= K_I \int_0^t e(\tau)\mathrm{d}\tau + K_p e(t), \text{ since } y = \Phi u \\ &= K_I f(t) + K_P e(t) \\ &= u(t),\end{aligned}$$

and so u is a fixed point of G.

In order for the contraction mapping theorem to apply, two conditions must be satisfied. The operator must map functions in the space of interest back into the same space, namely $C([0, t_0+\bar{t}))$. Since r is continuous, all the subsequent functions (u, y, e, and f) are continuous. The second condition is that the operator must be Lipschitz, with a Lipschitz constant that is strictly less than 1. Let $w \in C([0, t_0])$ and $u_1, u_2 \in B_1(w, t_0, t_0 + \bar{t})$. Recall that this means $u_1 = u_2 = w$ in the interval $[0, t_0]$. It will be shown that the contraction condition is satisfied on $[t_0, t_0 + \bar{t})$.

$$\begin{aligned}&\max_{t_0 \le t \le t_0+\bar{t}} |(Gu_1)(t) - (Gu_2)(t)| \\ &= \max_{t_0 \le t \le t_0+\bar{t}} \left| K_I \int_0^t [(\Phi u_1)(t) - (\Phi u_2)(t)]\mathrm{d}\tau + K_P[(\Phi u_1)(t) - (\Phi u_2)(t)] \right| \\ &\le K_I \max_{t_0 \le t \le t_0+\bar{t}} \left| \int_0^t [(\Phi u_1)(t) - (\Phi u_2)(t)]\mathrm{d}\tau \right| + K_p\lambda \max_{t_0 \le t \le t_0+\bar{t}} |u_1(t) - u_2(t)| \\ &\le K_I \max_{t_0 \le t \le t_0+\bar{t}} \int_{t_0}^{t_0+\bar{t}} |(\Phi u_1)(t) - (\Phi u_2)(t)|\, \mathrm{d}\tau + K_p\lambda \max_{t_0 \le t \le t_0+\bar{t}} |u_1(t) - u_2(t)| \\ &\le K_I \max_{t_0 \le t \le t_0+\bar{t}} |(\Phi u_1)(t) - (\Phi u_2)(t)| \int_{t_0}^{t_0+\bar{t}} \mathrm{d}\tau + K_p\lambda \max_{t_0 \le t \le t_0+\bar{t}} |u_1(t) - u_2(t)| \\ &\le (K_I\bar{t} + K_p)\lambda \max_{t_0 \le t \le t_0+\bar{t}} |u_1(t) - u_2(t)|\end{aligned}$$

Recall from assumption **(B1)**, $0 \le K_P\lambda < 1$ and $K_I > 0$. For $\bar{t}$ small enough, the condition will be satisfied. In fact, if $\bar{t} = \frac{1-K_P\lambda}{2\lambda K_I}$,

$$\begin{aligned}&(K_I\bar{t} + K_P)\lambda \\ &= \left(\frac{1 - K_P\lambda}{2\lambda} + K_P\right)\lambda \\ &= \frac{1 + K_P\lambda}{2} \\ &< 1, \text{ as required. } \square\end{aligned}$$

Extended uniqueness and maximal solution arguments are discussed in the following theorem.

Theorem 3.3.7. *[41, Theorem 10] Given that **(A1)**, **(A2)**, **(B1)** and **(B2)** hold, then the closed-loop system (3.4) - (3.7) has a unique solution for all $t \geq 0$.*

Proof. Let T be the set of all $\tau > 0$ such that there exists a solution on $[0, \tau]$. This set is nonempty from the previous lemma. Define $t^* = \sup T$ and $u^* : [0, t^*] \to \mathbb{R}$ by

$$u^*(t) = u_\tau(t), t \in [0, \tau), \tau < t^*.$$

If the maximal interval is not open, then t^* is finite. By Lemma 3.3.6, $t^* \geq \bar{t}$. If t^* is finite, then $t^* \geq \bar{t}$ implies $t^* > \frac{\bar{t}}{2}$. There is a unique solution u^* on $[0, t^* - \frac{\bar{t}}{2}]$, and hence by Lemma 3.3.6, the solution u^* can be extended to $[0, t^* + \frac{\bar{t}}{2})$. Thus t^* is not the supremum of T. By this argument, the existence of u^* can be extended to $C([0, \infty))$. Along with **(A1)**, this implies that $y \in C([0, \infty))$. With regard to uniqueness, suppose there are two solutions $u_1(t)$, and $u_2(t) \in C([0, \infty))$. Let a_0 be the largest time such that $u_1 = u_2$ on $[0, a_0)$. By Lemma 3.3.6, $a_0 \geq \bar{t} > 0$. By continuity, the limits of $u_1(t)$ and $u_2(t)$ must agree at a_0. Thus the solutions u_1 and u_2 agree on $[0, a_0]$. By Lemma 3.3.6, there is actually a unique solution on $[0, a_0 + \bar{t})$. These arguments imply the existence and uniqueness of $u(t) \in C([0, \infty))$. By **(A1)**, since $u \in C([0, \infty)), y \in C([0, \infty))$. $\square$

The closed-loop system will be shown to be BIBO-stable.

Theorem 3.3.8. *[41, Theorem 11] Assume that the closed-loop system has a unique solution for $u, y \in C([0, \infty))$ and assumptions **(A3)**, **(B1)** and **(B2)** hold. Assume $u(0) = 0$. If $|y(0)| \leq \|r\|_\infty$, then $\|y\|_\infty \leq \|r\|_\infty$. The closed-loop system is BIBO-stable with a gain of 1.*

Proof. Let $\mathrm{L} = \|r\|_\infty$. Assume there exists $t_f \geq 0$ such that $y(t_f) > L$. Let t_{maxu} be the first time such that u reaches its maximum on the interval $[0, t_f]$. Similarly, let t_{maxf} be defined in the same manner for f. From the assumptions, y and r are continuous, so e is continuous. As well,

$$\begin{aligned} e(t_f) &= r(t_f) - y(t_f) \\ &\leq L - y(t_f) \\ &< 0. \end{aligned}$$

There exists a neighbourhood around t_f such that $e(t) < 0$. Since $f'(t) = e(t) < 0$, f must be strictly decreasing in this neighbourhood. As a result, $f(t)$ is not maximized at t_f. That is, $t_{maxf} \neq t_f$.

If $t_{maxf} \neq 0$, f is maximized at t_{maxf}, implying $f'(t_{maxf}) = e(t_{maxf}) = 0$. Taking the contrapositive statement, if $e(t_{maxf}) \neq 0$, then $t_{maxf} = 0$. Next two cases are considered:

Case 1: $K_P > 0$
By definition, $u(t_{maxu}) \geq u(t)$ for all $t \in [0, t_f]$. Assumption **(A3)** implies that $y(t_{maxu}) \geq y(t_f)$. By the definition of t_{maxu}, $u(t_{maxu}) \geq u(t_{maxf})$ and so $f(t_{maxf}) \geq f(t_{maxu})$. From the definition of u:

$$K_I f(t_{maxu}) + K_P e(t_{maxu}) \geq K_I f(t_{maxf}) + K_P e(t_{maxf}) \tag{3.8}$$

Since $K_I, K_P > 0$, and $f(t_{maxf}) \geq f(t_{maxu})$, inequality (3.8) implies

$$e(t_{maxf}) \leq e(t_{maxu}).$$

Note that $e(t_{maxu}) = r(t_{maxu}) - y(t_{maxu}) \leq L - y(t_f) < 0$. Therefore, $e(t_{maxf}) < 0$. As shown above, this implies $t_{maxf} = 0$. Finally,

$$u(0) = K_P e(0) = K_P e(t_{maxf}) < 0.$$

The contrapositive of the theorem has been proven: If $u(0) = 0, K_P > 0$, then $\|y\|_\infty \leq \|r\|_\infty$.

Case 2: $K_P = 0$
The input u is reduced to $u(t) = K_I f(t)$. It is clear that $f(t_{maxf}) \geq f(t)$. Multiplying both sides by K_I yields $u(t_{maxf}) \geq u(t)$, for every $t \in [0, t_f]$ and **(A3)** imply that $y(t_{maxf}) \geq y(t_f)$.

Thus, $e(t_{maxf}) = r(t_{maxf}) - y(t_{maxf}) \leq L - y(t_f) < 0$. (Recall that at the beginning of the proof that $y(t_f) > L$ is assumed). Therefore $e(t_{maxf}) \neq 0$ implies $t_{maxf} = 0$. Finally,

$$\begin{aligned} y(0) &= y(t_{maxf}) \\ &\geq y(t_f) \\ &> L \\ &= \|r\|_\infty . \end{aligned}$$

As a result, $y(0) > \|r\|_\infty$. This result is the contrapositive of the theorem statement. Hence if $u(0) = 0$, and $|y(0)| \leq \|r\|_\infty$, then $\|y\|_\infty \leq \|r\|_\infty$. □

3.3.3 Tracking

The performance of tracking a signal is discussed in Section 4 of [41], and the results are shown here. Some interesting results are proved pertaining to the special case

where the reference signal is a constant, including a bound on the time to reach any arbitrarily small error.

Theorem 3.3.9. *[41, Theorem 12] Let r be constant on an interval $[t_0, T]$, where $t_0 > 0$. Assume that the closed-loop system has a unique solution for $u, y \in C([t_0, T])$, and **(A3)** and **(B1)** hold. For $\rho \geq 0$, if*

$$|r - y(t_0)| \leq \rho,$$

then

$$|r - y(t_1)| \leq \rho, \text{ for every } t_1 \in [t_0, T].$$

Proof. Assume for some $t_1 > t_0$, $r - y(t_1) = e(t_1) < -\rho$. As in previous proofs, let t_{maxf} and t_{maxu} be the first times at which f and u respectively are maximized on the interval $[t_0, t_1]$ respectively. The error e is continuous because r and y are continuous, and hence f is continuously differentiable. Note that since $e(t_1) = f'(t_1) < 0$, $t_{maxf} \neq t_1$. This implies that if $e(t_{maxf}) \neq 0$, then $t_{maxf} = t_0$. This will be useful later in the proof. If $K_P > 0$, then $u(t_{maxf}) \leq u(t_{maxu})$. This implies that

$$K_P e(t_{maxf}) + K_I f(t_{maxf}) \leq K_P e(t_{maxu}) + K_I f(t_{maxu}) \leq K_P e(t_{maxu}) + K_I f(t_{maxf}).$$

Therefore,

$$K_P e(t_{maxf}) \leq K_P e(t_{maxu}).$$

By assumption **(A3)**,

$$\begin{aligned} &u(t_{maxu}) \geq u(t) \text{ for every } t \in [t_0, t_1] \text{ implies that} \\ &y(t_{maxu}) \geq y(t_1). \end{aligned}$$

By this property and the definition of $e(t)$,

$$\begin{aligned} &r - y(t_{maxu}) \leq r - y(t_1), \text{ implies that} \\ &e(t_{maxu}) \leq e(t_1). \end{aligned}$$

Thus

$$\begin{aligned} e(t_{maxf}) &\leq e(t_{maxu}) \\ &\leq e(t_1) \\ &= r - y(t_1) \\ &< -\rho. \end{aligned}$$

Therefore $e(t_{maxf}) \neq 0$ implies $t_{maxf} = t_0$ and inequality $e(t_0) = r - y(t_0) < -\rho$ is shown.

If $K_P = 0$, then $u(t) = K_I f(t)$. Since $K_I > 0$, u and f will be maximized at the same time. The inequality becomes

$$\begin{aligned} e(t_{maxf}) &= e(t_{maxu}) \\ &\leq e(t_1) \\ &= r - y(t_1) \\ &< -\rho. \end{aligned}$$

Again $e(t_0) < -\rho$, as required. An analogous proof arguing that

$$r - y(t_1) > \rho$$

implies

$$e(t_0) > \rho$$

completes the proof. □

Since the error must always decrease monotonically, an overshoot cannot occur. Finally, a bound on the time to reach any arbitrarily small error is found. This implies zero steady-state error.

Theorem 3.3.10. *[41, Theorem 13] Let $t_0 \geq 0$, and r be a constant reference signal on $[t_0, \infty)$. Assume that $u, y \in C([t_0, \infty))$ are unique solutions to the closed-loop system and that **(A3)**, **(A4)**, and **(B1)** hold. If $y_- \leq r \leq y_+$, then for every $\epsilon > 0$,*

$$|r - y(t)| \leq \epsilon, \text{ for every } t \geq \bar{t} + t_0,$$

where $\bar{t} = \dfrac{\frac{u_{sat}}{K_I} + |f(t_0)|}{\epsilon}$. Thus asymptotic tracking is achieved, that is:

$$\lim_{t \to \infty} y(t) = r.$$

.

Proof. Assume that there exists some $t \geq \bar{t} + t_0$ and $\epsilon > 0$, such that $r - y(t) > \epsilon$. Since a monotonic decrease in the absolute value of the error is guaranteed in the previous theorem,

$$|r - y(t')| = |e(t')| > \epsilon, \text{ for every } t' \in [t_0, t]. \tag{3.9}$$

Integrating (3.9) from t_0 to $t_0 + \bar{t}$ yields:

$$\begin{aligned}
&\int_{t_0}^{t_0+\bar{t}} e(t')\mathrm{dt}' > \epsilon\bar{t} \\
&f(t_0+\bar{t}) > f(t_0) + \epsilon\bar{t}, \text{ using the definition of } \bar{t}, \\
&f(t_0+\bar{t}) > \frac{u_{sat}}{K_I}.
\end{aligned}$$

Since $t \geq t_0 + \bar{t}$, $e(t_0 + \bar{t}) \geq e(t) > \epsilon$. Therefore,

$$\begin{aligned}
u(t_0+\bar{t}) &= K_P e(t_0+\bar{t}) + K_I f(t_0+\bar{t}) \\
&\geq K_P\epsilon + u_{sat} \\
&\geq u_{sat}.
\end{aligned}$$

By the saturation assumption **(A4)**, $y(t_0 + \bar{t}) = y_+$. Altogether:

$$e(t_0+\bar{t}) = r - y(t_0+\bar{t}) = r - y_+ > \epsilon > 0.$$

This implies $r > y_+$. Analogously, if $y(t) - r < \epsilon$, then $r < y_-$. The contrapositive of the theorem has been proven. Thus, for every $\epsilon > 0$, there is a $\bar{t}$ such that:

$$|r - y(t)| < \epsilon$$

for all $t \geq \bar{t} + t_0$. Hence also, $\lim_{t\to\infty} y(t) = r$. □

Therefore, a bound on time is guaranteed to reach a diminishing error. Thus a constant reference signal can be asymptotically tracked.

3.4 Extensions to include a Linear System

Suppose a linear system with transfer function $\hat{G}(s)$ is introduced into the original set of equations presented in Section 3.3.2 after the hysteresis operator. This modification introduces a component into the system that could represent the modelling of dynamics in a hysteretic actuator. See Figure 3.4 for the new system. While similar results hold for a linear system of arbitrary order, the results will be demonstrated for a linear first-order system. The extension to higher-order systems will be discussed later. In the next few equations, the notation exp is used to denote the exponential as to avoid confusion with the error function $e(t)$. The resulting

set of equations are

$$e(t) = r(t) - y(t), \tag{3.10}$$

$$\hat{C}(s) = K_P + \frac{K_I}{s+\epsilon} \tag{3.11}$$

$$u(t) = K_P e(t) + K_I \exp(\text{-}\epsilon t) \int_0^t \exp(\epsilon\tau) e(\tau) d\tau, \tag{3.12}$$

$$v(t) = \Phi(u(t)), \tag{3.13}$$

$$\hat{G}(s) = \frac{M}{s+\sigma} \tag{3.14}$$

$$y'(t) = Mv(t) - \sigma y(t), \tag{3.15}$$

where Φ is a hysteretic operator satisfying assumptions **(A1)** - **(A4)**. The controller has been changed to a practical PI controller, where $\epsilon > 0$ is small. The pole of the integral component has been shifted off of the imaginary axis and into the left-half of the complex plane. This is generally the case in practical application.

3.4.1 Existence and Uniqueness

The aim is to provide existence and uniqueness proofs analogous to those in Section 3.3.2.

Lemma 3.4.1. *Assume a hysteresis operator Φ satisfies **(A1)**, **(A2)** and **(B2)**, with Lipschitz constant λ. Let $M, \sigma, K_P, K_I > 0$. For every $t_0 \geq 0$ such that the closed-loop system described by equations (3.10) to (3.15) has a unique solution, u on $[0, t_0]$, the closed-loop system will have a unique solution u on $C([t_0, t_0 + \bar{t}))$, where $\bar{t}$ is chosen such that*

$$0 < \bar{t} < \frac{\sigma}{\lambda M K_I}(1 - K_P \lambda \frac{\sigma}{M})$$

Let $x \in C([0, t_0))$. Define the operator F as follows,

$$\begin{aligned} &F[x(t)] \\ =&K_I e^{\text{-}\epsilon t} \int_0^t e^{\epsilon\tau} \left(r(\tau) - M e^{\text{-}\sigma\tau} \int_0^\tau e^{\sigma s} \Phi(x(s)) ds \right) d\tau \\ &+ K_P \left(r(t) - M e^{\text{-}\sigma t} \int_0^t e^{\sigma\tau} \Phi(x(\tau)) d\tau \right). \end{aligned}$$

It can be verified that the operator has a fixed point $u(t)$. Proceeding with familiar arguments, it is clear that if a function $x(t)$ is continuous, and by **(B2)** $r(t)$

is continuous, hence $F[x(t)]$ is a continuous function. An estimate of the difference of the operator F acting on functions $u_1, u_2 \in B(w, t_0, t_0 + \bar{t})$ yields

$$
\begin{aligned}
&\|F(u_1) - F(u_2)\|_\infty \\
=& \max_{t_0 \le t \le t_0+\bar{t}} |F[u_1(\cdot)](t) - F[u_2(\cdot)](t)| \\
\le& \|\Phi(u_1) - \Phi(u_2)\|_\infty |M| \max_{t_0 \le t \le t_0+\bar{t}} \left| K_I e^{-\epsilon t} \int_{t_0}^{t} e^{\epsilon\tau} \epsilon^{-\sigma\tau} \int_{t_0}^{\tau} e^{\sigma s} ds d\tau + K_P e^{-\sigma t} \int_{t_0}^{t} e^{\sigma\tau} d\tau \right| \\
\le& \frac{|M|}{\sigma} \lambda \|u_1 - u_2\|_\infty \max_{t_0 \le t \le t_0+\bar{t}} \left| K_I e^{-\epsilon t} \int_{t_0}^{t} e^{\epsilon\tau} d\tau + K_P \right| \\
\le& \frac{|M|}{\sigma} \lambda (K_P + K_I \bar{t}) \|u_1 - u_2\|_\infty .
\end{aligned}
$$

If $\bar{t}$ is chosen within the bounds mentioned in the theorem statement, then the contraction mapping theorem assumptions are satisfied, and hence a unique solution exists on $C([t_0, t_0 + \bar{t}))$. □

Corollary 3.4.2. *Assume a hysteresis operator Φ satisfies **(A1)**, **(A2)** and **(B2)** with Lipschitz constant λ. Let $M, \sigma, K_P, K_I > 0$. Then equations (3.10) to (3.15) have a unique solution for $u \in C([0, \infty))$ and $y \in C([0, \infty))$.*

The proof of Corollary 3.4.2 is analogous to the proof of Theorem 3.3.7.

3.4.2 Stability

The system will be shown to be BIBO-stable for a range of parameters (see Definition 3.3.4 for a definition of BIBO-stability). The incremental gains of each of the components of the system will be found, and then combined using an incremental gain theorem found in [9]. First, a useful lemma is presented that requires the definition of a convolution of two functions. A multiplication of functions in the Laplace domain is equivalent to a convolution in the time-domain. A convolution of two functions $f,\ g \in C(\mathbb{R}_+)$ is denoted by $f \star g$ and is defined by

$$(f \star g)(t) = \int_0^t f(\tau) g(t - \tau) d\tau.$$

In the context of linear systems, the L^∞ gain of an operator is the L^1 norm of the inverse Laplace transform of the transfer function.

Lemma 3.4.3. *[26, Thm 3.11] Suppose for a general input, output and plant denoted by u, y and $\hat{G}$ respectively so that*

$$\hat{y}(s) = \hat{G}(s)\hat{u}(s).$$

Then

$$\|y\|_\infty \leq \|g\|_1 \|u\|_\infty ,$$

where g is the inverse Laplace transform of $\hat{G}$.

Proof

$$\begin{aligned}
y(t) &= (g \star u)(t) \\
&= \int_0^t g(t-\tau)u(\tau)d\tau \\
\|y\|_\infty &= \max_{t\in\mathbb{R}_+} \left| \int_0^t g(t-\tau)u(\tau)d\tau \right| \\
&\leq \max_{t\in\mathbb{R}_+} \int_0^t |g(t-\tau)||u(\tau)|d\tau \\
&\leq \left(\max_{t\in\mathbb{R}_+} \int_0^t |g(t-\tau)|d\tau \right) \|u\|_\infty \\
&= \left(\max_{t\in\mathbb{R}_+} \int_0^t |g(\tau)|d\tau \right) \|u\|_\infty \\
&= \|g\|_1 \|u\|_\infty \, \square
\end{aligned}$$

Estimates on upper bounds for the gains of the linear components of the system can be easily found if $\hat{G}$ is a first-order system. If $g(t)$ and $c(t)$ are the inverse Laplace transforms of $\hat{G}(s)$ and $\hat{C}(s)$ respectively,

$$\begin{aligned}
g(t) &= M \exp(\text{-}\sigma t), \\
\|g\|_1 &= \frac{|M|}{\sigma}, \\
c(t) &= K_P \delta(t) + K_I \exp(\text{-}\epsilon t), \\
\|c\|_1 &= K_P + \frac{K_I}{\epsilon}.
\end{aligned}$$

Definition 3.4.4. *The **incremental gain** $\tilde{\gamma}$ of an operator $H : L^\infty(\mathbb{R}_+) \to L^\infty(\mathbb{R}_+)$ is defined as*

$$\tilde{\gamma} = \inf\{\gamma \in \mathbb{R}_+ | \, \|H(x_1) - H(x_2)\|_\infty \leq \gamma \|x_1 - x_2\|_\infty , \text{ for every } x_1, x_2 \in L^\infty(\mathbb{R}_+)\}.$$

Assumption **(A2)** implies that the Lipschitz constant λ is an upper bound to the incremental gain of the hysteresis operator Φ. A small gain theorem is used. For a range of chosen parameters, closed-loop BIBO stability is guaranteed. A specific case of a theorem from [9] is presented regarding a fairly general closed-loop system described by

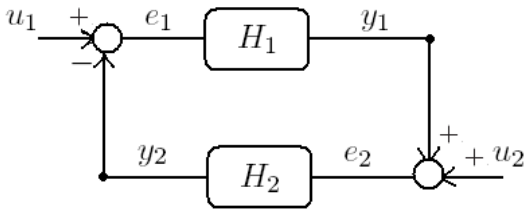

Figure 3.3: Closed-Loop System defined by (3.16) - (3.19)

$$e_1(t) = u_1(t) - y_2(t), \tag{3.16}$$
$$e_2(t) = u_2(t) + y_1(t), \tag{3.17}$$
$$y_1(t) = H_1(e_1(t)), \text{ and} \tag{3.18}$$
$$y_2(t) = H_2(e_2(t)). \tag{3.19}$$

The assumptions on the equations will be made specific in the following theorem.

Theorem 3.4.5. *[9, Thm 3.3.1] Consider the feedback system shown in Figure 3.3, and defined by (3.16) - (3.19). Suppose $H_1, H_2 : L^\infty_{loc} \to L^\infty_{loc}$, and there are constants $\tilde{\gamma}_1$ and $\tilde{\gamma}_2$ such that for every $T \in \mathbb{R}_+$ and $u_1, u_2 \in L^\infty_{loc}$,*

$$\|(H_1u_1)_T - (H_1u_2)_T\|_\infty \leq \tilde{\gamma}_1 \|u_{1T} - u_{2T}\|_\infty ,$$
$$\|(H_2u_1)_T - (H_2u_2)_T\|_\infty \leq \tilde{\gamma}_2 \|u_{1T} - u_{2T}\|_\infty .$$

If in addition, the solution corresponding to $u_1 = u_2 = 0 \in L^\infty$, then $u_1, u_2 \in L^\infty$ implies that $e_1, e_2 \in L^\infty$, that is, the system is BIBO-stable.

Theorem 3.4.6. *If the parameters described in equations (3.10) to (3.15) satisfy*

$$\frac{M}{\sigma}\lambda\left(K_P + \frac{K_I}{\epsilon}\right) < 1,$$

then $r(t) \in L^\infty(\mathbb{R}_+)$ implies $e(t), u(t), v(t), y(t) \in L^\infty(\mathbb{R}_+)$.

Proof. Choose $H_1 = G \circ \Phi \circ C$, where G and C are the operators that correspond to the transfer functions $\hat{G}(s)$ and $\hat{C}(s)$. Define $H_2 = I$ (the identity operator), with gain $\tilde{\gamma}_2 = 1$. To apply Theorem 3.4.5 to the system at hand, the following are chosen: $u_2 = 0, e_1 = e, u_1 = r, y_2 = e_2 = y_1 = y$.

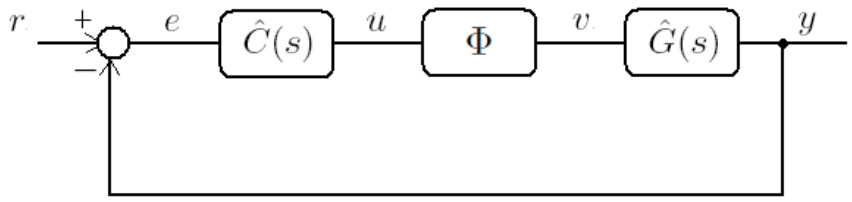

Figure 3.4: Closed-Loop System defined by equations (3.10) - (3.15)

$$\begin{aligned}\|(G\circ\Phi\circ C)(u_1)-(G\circ\Phi\circ C)(u_2)\|_\infty &= \|G\left((\Phi\circ C)(u_1)-(\Phi\circ C)(u_2)\right)\|_\infty \\ &\leq \frac{|M|}{\sigma}\left\|\Phi\left(C(u_1)\right)-\Phi\left(C(u_2)\right)\right\|_\infty \\ &\leq \frac{|M|}{\sigma}\lambda\left\|C(u_1-u_2)\right\|_\infty \\ &\leq \frac{|M|}{\sigma}\lambda\left(K_P+\frac{K_I}{\epsilon}\right)\left\|u_1-u_2\right\|_\infty .\end{aligned}$$

From this calculation, it is deduced that the small gain condition is

$$\tilde{\gamma_1}\tilde{\gamma_2} = \tfrac{|M|}{\sigma}\lambda(K_P+\tfrac{K_I}{\epsilon}) < 1.\square$$

Performing simulations and choosing different parameters has shown that this bound yields not a necessary, but only sufficient condition. The range in the parameters that govern the gain are very limited because of the small gain condition. These results hold for a linear system of arbitrary order, provided that $\|g\|_1$ is finite.

3.5 PID Control of Second-Order Systems with Hysteresis

Using a PID controller, the tracking of a constant piecewise reference signal on a second-order system experiencing hysteresis in the actuator is performed. Constant disturbances were added to both the system, and the input as a measure of robustness of the controller. Even with these disturbances, the tracking was found to be asymptotic. The results from [18] and [23] are described in this section.

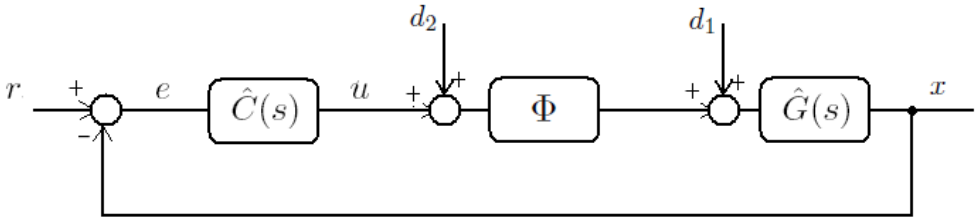

Figure 3.5: Closed-Loop System defined by equations (3.21) and (3.22)

3.5.1 Model

The spring-mass-damper system is a classical example of a physical system modeled by differential equations. The standard model without the presence of disturbances or controlling forces is described by

$$mx''(t) + cx'(t) + kx(t) = 0, x(0) = x_0, v(0) = v_0 \tag{3.20}$$

where

m is the mass of the object,
c is the damping constant,
k is the linear spring constant, and
$x(t)$ is the displacement at time t.

The parameters m, c, and k must all be positive. The control to be used is a PID controller. Letting $e(t) = x(t) - r$,

$$u(t) = -K_P e(t) - K_I \int_0^t e(\tau)d\tau - K_D \frac{d}{dt}(e(t)) + u_0,\ u(0) = u_0. \tag{3.21}$$

As discussed previously, the input to the system will exhibit hysteresis. Two constant disturbances d_1, d_2 are introduced as a measure of robustness to the controller. See Figure 3.5, $\hat{G}(s)$ is the second-order system described in equation 3.20. The modified system will have the form:

$$mx''(t) + cx'(t) + kx(t) = \Phi(u(t) + d_2) + d_1, x(0) = x_0, \tag{3.22}$$

$$x'(0) = v_0, \text{ and } u(0) = u_0$$

3.5.2 Assumptions on Hysteresis Operators

Some further assumptions are required in order to achieve the results found in the theorems in the next sections. There are six in total, but some necessary notation

must first be introduced.

Definition 3.5.1. *Let $W^{1,1}_{loc}(\mathbb{R}_+)$ denote the space of locally absolutely continuous functions. A function $f \in W^{1,1}_{loc}(\mathbb{R}_+)$ if there exists $g \in L^1_{loc}(\mathbb{R}_+)$ such that*

$$f(t) = f(0) + \int_0^t g(s)ds \text{ for all } t \in \mathbb{R}_+.$$

This is a smaller space than the set of continuous functions. According to the definition above, functions in this set must be locally L^1-differentiable. That is, on any interval, the derivative must be defined and bounded almost everywhere. Throughout this section, θ will denote the step function, that is $\theta(t) = 1$, for all $t \geq 0$.

For $w \in C([0,\alpha]), \alpha \geq 0, \gamma, \delta > 0$,

$$B(w;\delta,\gamma) := \{v \in C([0,\alpha+\gamma]) : v|_{[0,\alpha]} = w, \max_{t\in[\alpha,\alpha+\gamma]} |v(t) - w(\alpha)| \leq \delta\}. \quad (3.23)$$

With these notational definitions in place, the following assumptions can be stated.

For a hysteresis operator $\Phi : C(\mathbb{R}_+) \to C(\mathbb{R}_+)$,

(N1) If $u \in W^{1,1}_{loc}(\mathbb{R}_+)$, then $\Phi(u) \in W^{1,1}_{loc}(\mathbb{R}_+)$

The hysteresis operator must map continuous functions that have bounded derivatives almost everywhere to the same space of functions.

(N2) For $u \in W^{1,1}_{loc}(\mathbb{R}_+)$, Φ satisfies:

$$(\Phi(u))'(t)u'(t) \geq 0, \text{ a.e. } t \in I,$$

where a.e. means almost everywhere, and I is the domain of definition of u. Since $\Phi(u)$ depends on u, the following is implied:

$$u'(t) > 0 \text{ implies } (\Phi(u))'(t) \geq 0, \text{ and}$$
$$u'(t) < 0 \text{ implies } (\Phi(u))'(t) \leq 0$$

wherever $u'(t)$ is defined.

(N3) Φ is locally Lipschitz in the following manner: there exists $\lambda > 0$ such that for all $\alpha \geq 0$ and $w \in C([0,\alpha])$, there exists constants $\gamma, \delta > 0$ such that

$$\max_{t\in[\alpha,\alpha+\gamma]} |(\Phi(u))(t)-(\Phi(v))(t)| \leq \lambda \max_{t\in[\alpha,\alpha+\gamma]} |u(t)-v(t)|, \text{ for all } u,v \in B(w;\delta,\gamma).$$

Many hysteresis operators will satisfy a stronger condition, that is, a global Lipschitz condition

$$\sup_{t\in\mathbb{R}_+} |(\Phi(u))(t) - (\Phi(v))(t)| \leq \lambda \sup_{t\in\mathbb{R}_+} |u(t) - v(t)|, \text{ for all } u,v : C(\mathbb{R}_+) \longrightarrow \mathbb{R}_+.$$

holds. If this is true, then **(N3)** is obviously true.

(N4) For all $\alpha \in \mathbb{R}_+$ and all $u \in C([0,\alpha])$, there exists $c > 0$ such that

$$\max_{\tau\in[0,t]} |(\Phi(u))(\tau)| \leq c(1 + \max_{\tau\in[0,t]} |u(\tau)|), \text{ for all } t \in [0,\alpha).$$

The last two assumptions require some simple definitions.

Definition 3.5.2. *The numerical value set, denoted NVS* (Φ) *represents all the possible values that* Φ *can output.*

Definition 3.5.3. *A function* f *is* ***ultimately non-decreasing*** *(non-increasing) if there exists* $\tau \in \mathbb{R}_+$ *such that* f *is non-decreasing (non-increasing) on* $[\tau,\infty)$.

Definition 3.5.4. *A function* f *is* ***approximately ultimately non-decreasing*** *(non-increasing)* if for all $\epsilon > 0$, there exists $\tau > 0$ and an ultimately non-decreasing (non-increasing function g such that for all $t > \tau$,

$$|f(t) - g(t)| < \epsilon$$

The term *approximately ultimately non-decreasing (non-increasing)* is a broader definition than *ultimately non-decreasing (non-increasing)* since functions that have decaying oscillations (even if they continue to oscillate as $t \to \infty$) are included.

(N5) If $u \in \mathbb{R}_+$ is approximately ultimately non-decreasing and $\lim_{t\to\infty} u(t) = \infty$, then $(\Phi(u))(t)$ and $(\Phi(-u))(t)$ converge to sup NVS Φ and inf NVS Φ, respectively as $t \to \infty$.

(N6) If, for $u \in C(\mathbb{R}_+)$, $\lim_{t\to\infty}(\Phi(u))(t)$ is in the interior of NVS Φ, then u is bounded.

The assumption **(N4)** is a limiting growth condition on Φ, relative to u. Assumptions **(N5)** and **(N6)** are similar in the sense that the behaviour of Φ must in some sense follow the behaviour of u.

These assumptions will be referred to frequently throughout the remainder of the section and will be required in proofs involving specific systems. Commonly used hysteresis operators that satisfy **(N1)** - **(N6)** include the backlash operator, elastic-plastic operator, and with some slight modifications (discussed later), the Preisach operator (see Section 3.5.3).

3.5.3 Comparison of Assumptions from Valadkhan/Morris Paper and Logemann Papers

A comparison of the assumptions on the hysteresis operator found in [41] and [18] will be made. As in their respective sections, the assumptions found in [41] will be denoted **(A1)-(A4)**, while those found in [23] and [18] will be denoted **(N1)-(N6)**. For consistency, $u(t)$ will be the input to the hysteresis operator, and $y(t) = \Phi(u(t))$ will be the output. The first comparison deals with **(A1)** and **(N1)**. They are as follows:

(A1) If $u(t)$ is continuous, then $y(t)$ is continuous.

(N1) If $u(t) \in W^{1,1}_{loc}(\mathbb{R}_+)$, then $y(t) \in W^{1,1}_{loc}(\mathbb{R}_+)$,

where $W^{1,1}_{loc}(\mathbb{R}_+)$ is the space of functions that are continuous and have a derivative in $L^1(\mathbb{R}_+)$. At first glance, the two assumptions look very similar, however **(N1)** deals with a smaller space than **(A1)**. It is important to note that neither assumption implies the other.

Next, a comparison is made between **(A2)** and **(N3)**, which both deal with the Lipschitz property of Φ acting on functions in $B_1(w, t_1, t_2)$ and $B(w, \delta, \gamma)$ respectively. The sets B_1 and B are similar, with different names for the parameters. **(A2)** provides a global Lipschitz condition for Φ, while **(N3)** is only a local Lipschitz condition (on Φ). Technically, **(A2)** is stronger. Following the introduction of **(N1)-(N6)**, [18] also describes a global Lipschitz condition, that is identical to **(A2)**.

(A3) will now be compared to **(N2)**:

(A3) Consider an arbitrary interval $[t_i, t_f]$. If for every $t \in [t_i, t_f]$, $u(t_i) \geq u(t)$, then $y(t_i) \geq y(t_f)$. Alternative, if for every $t \in [t_i, t_f]$, $u(t_i) \leq u(t)$, then $y(t_i) \leq y(t_f)$.

(N2) For $u \in W^{1,1}_{loc}(\mathbb{R}_+)$, Φ satisfies:

$$(\Phi(u))'(t)u'(t) \geq 0,$$

wherever $u'(t)$ is defined. Recall that this is equivalent to whenever $u(t)$ is increasing, $\Phi(u(t))$ is nondecreasing, and whenever $u(t)$ is decreasing, $\Phi(u(t))$ is nonincreasing. Since the interval in **(A3)** can be chosen arbitrarily, setting $t = t_f$ in the assumption yields that monotonicity in the sense of **(N2)** is preserved. Therefore, **(A3)** implies **(N2)**. The converse is not satisfied, since **(A3)** allows only for counter-clockwise loops while clockwise loops are not permitted. Assumption **(N2)** does not imply **(A3)**. Also note that in **(A3)**, there are no assumptions regarding the derivative of $u(t)$ and $\Phi(u(t))$ whereas these are required for **(N2)**.

The remainder of this section will show that **(A4)** either implies, or is a specific case of each of **(N4)-(N6)**. Recall that **(A4)** deals with the saturation of the system:

(A4) There exists some $u_{sat} > 0$, y_+, and y_- such that if $u(t) \geq u_{sat}$, then $\Phi(u(t)) = y_+$, and $\Phi(-u(t)) = y_-$.

First, a comparison to **(N4)** will be made:

(N4) For all $\alpha \in \mathbb{R}_+$, and all $u \in C([0, \alpha])$, there exists $c > 0$ such that

$$\max_{\tau \in [0,t]} |(\Phi(u))(\tau)| \leq c(1 + \max_{\tau \in [0,t]} |u(\tau)|), \text{ for every } t \in [0, \alpha).$$

Assumption **(N4)** places a bound on growth of $\Phi(u(t))$ that depends on $u(t)$. It is immediately obvious that **(N4)** does not imply **(A4)**, since an input $u(t)$ can be chosen that increases to infinity, resulting in $y(t)$ not having a finite bound on $y(t)$ as required by **(A4)**. Recall that from Theorem 3.3.5, assumptions **(A3)** and **(A4)** together imply that there exist y_+ and y_- such that $y_- \leq y(t) \leq y_+$ for every $t \geq 0$. To show that this implies **(N4)**,

Let $c = \max\{|y_+|, |y_-|\}$.

$$\begin{aligned}\max_{\tau\in[0,t]}|(\Phi(u))(\tau)| &= \max_{\tau\in[0,t]}|y(\tau)|\\ &\leq c,\\ &\leq c + c\max_{\tau\in[0,t]}|u(\tau)|,\\ &= c(1+\max_{\tau\in[0,t]}|u(\tau)|).\end{aligned}$$

Therefore assumptions **(A3)** and **(A4)** imply assumption **(N4)**.

In comparison to **(N5)**, **(A4)** is a specific case of **(N5)**.

(N5) If $u \in \mathbb{R}_+$ is approximately ultimately non-decreasing, and $\lim_{t\to\infty} u(t) = \infty$, then $\Phi(u(t))$ and $\Phi(-u(t))$ will converge to sup NVS Φ, and inf NVS Φ respectively, as $t \to \infty$.

Assuming **(A4)** yields: if $\lim_{t\to\infty} u(t) = \infty$, then $\lim_{t\to\infty} \Phi(u(t)) = \text{sup NVS}\Phi = y_+$, and $\lim_{t\to\infty} \Phi(-u(t)) = \text{inf NVS}\Phi = y_-$, hence satisfying **(N5)**. **(A4)** guarantees that sup NVS Φ and inf NVS Φ are reached by a finite $u(t)$, whereas in **(N5)** sup NVSΦ and inf NVSΦ need not be finite, and there need not exist a u_{sat} as described in **(A4)**. Thus Assumption **(A4)** implies Assumption **(N5)**. The converse is obviously not true.

Finally, it will be shown that assumptions **(A3)** and **(A4)** together imply **(N6)**:

(N6) If for $u \in C(\mathbb{R}_+)$, $\lim_{t\to\infty} \Phi(u(t)) \in$ int NVS Φ, then u is bounded.

Assumptions **(A3)** and **(A4)** (see Theorem 3.3.5) imply that NVS $\Phi = [y_-, y_+]$. This property along with the contrapositive of **(A4)** yields that if $y \in (y_-, y_+)$, then $|u(t)| < u_{sat}$. Hence, u is bounded. Therefore assumptions **(A3)** and **(A4)** imply assumption **(N6)**. The converse is not true. It is clear that assumption **(N6)** does not imply **(A3)**. To compare assumption **(N6)** with assumption **(A4)**, if NVS Φ is not a finite interval, then u_{sat} as described in assumption **(A4)** does not exist. If NVS Φ is a finite interval, then the contrapositive of **(N6)** only guarantees that for an unbounded $u \in C(\mathbb{R}_+)$, sup NVS Φ or inf NVS Φ is reached as u approaches infinity. This does not assert the existence of a u_{sat}. This is weaker than **(A4)** which guarantees that y_+ or y_- are reached as soon as $|u(t)| \geq u_{sat}$.

Also note that assumptions **(N1)** - **(N6)** can have NVS $\Phi = (-\infty, \infty)$, whereas assumptions **(A1)** - **(A4)** cannot.

To summarize the comparisons:

(A1) acts on a larger space than **(N1)** but the assumptions do not imply each other.
(A2) implies **(N3)**, (if the signals u and y are differentiable),
(A3) implies **(N2)**,
(A3) and **(A4)** imply **(N4)** – **(N6)**.

3.5.4 Integral Control In The Presence Of Hysteresis In The Input

A simplified version of a result found in [23, Thm 4.1] is presented. (In reference to the original paper, h, ϑ, ψ, g and u in [23] are replaced with 0, 0, the identity map, η, and x respectively.) The introduction of a space of functions similar to the L^p-space is required. Let $L^p_\alpha(\mathbb{R}_+)$ denote the space of α-exponentially weighted functions. That is, $f \in L^p_\alpha(\mathbb{R}_+)$ if

$$\int_0^\infty (f(t)e^{-\alpha t})^p dt < \infty.$$

Also,

$$\|f\|_{L^p_\alpha(\mathbb{R}_+)} = \left\|f(\cdot)e^{-\alpha \cdot}\right\|_p.$$

This is the space of functions that decrease faster than an exponential function with constant $\alpha < 0$.

Let $\mathcal{G} : L^2(\mathbb{R}_+) \to L^2(\mathbb{R}_+)$ be a linear, bounded, shift-invariant operator defined by $\mathcal{G}u = g \star u$, where $g \in L^1_\alpha(\mathbb{R}_+) + \mathbb{R}\delta_0$ for some $\alpha < 0$. The transfer function of $\mathcal{G}$ is the Laplace transform of g, (denoted $\hat{g}$). Note that $\hat{g} \in H^\infty(\mathbb{C}_+)$. The following assumptions are made on $\hat{g}$.

Assumption 3.5.5. *[23, Assumption **(L)**] Let $\hat{g}$ satisfy*

$$\hat{g}(0) := \lim_{s \to 0, Re\ s>0} \hat{g}(s) \text{ exists }, \hat{g}(0) > 0, \text{ and,}$$

$$\limsup_{s \to 0, Re\ s>0} \left| \frac{\hat{g}(s) - \hat{g}(0)}{s} \right| < \infty.$$

The material presented in this section is entirely done by Logemann and his associates. His work can be broken down into successive theorems, which are each steps to the final product.

Proposition 3.5.6. *[23, Prop 2.1] Assume there are $\mathcal{G}$, N, and r such that*

(a) $\mathcal{G} : L^2(\mathbb{R}_+) \to L^2(\mathbb{R}_+)$ satisfies assumption 3.5.5;
(b) $N : \mathbb{R}_+ \times \mathbb{R} \to \mathbb{R}$ satisfying

$$0 \leq N(t,\xi)\xi \leq a\xi^2, \text{ for every } (t,\xi) \in [t_0,\infty) \times \mathbb{R}$$

(c) $r \in L^2(\mathbb{R}_+) + \mathbb{R}\theta$.

If v is a global solution to

$$v(t) = r(t) - \int_0^t (\mathcal{G}(N(\cdot, v)))(\tau)d\tau$$

then

(i) $v - r \in L^\infty(\mathbb{R}_+)$;
(ii) $N(\cdot, v) \in L^2(\mathbb{R}_+)$;
(iii) $\int_0^t N(\tau, v(\tau))d\tau$ converges to a finite limit as $t \to \infty$.

Before proving results regarding the system presented in the next theorem, it is necessary to establish the existence and uniqueness of a solution for the system. Since the proof is rather long, it will be presented in Appendices A.1 and A.2. The actual existence and uniqueness proof is for a more general system (Appendix A.1). It is shown in Appendix A.2 that the system (3.25) is a special case of the system in Appendix A.1. The proof uses a standard ODEs argument that asserts the existence and uniqueness of a solution on a small interval by using the contraction mapping theorem. Further arguments are made to extend uniqueness to all of $\mathbb{R}_+$.

The following lemmas will be referred to in the proof of the next theorem. For the first lemma, it can intuitively thought that f_2 ultimately dominates f_3.

Lemma 3.5.7. *[23, Lemma 2.2] Let $g \in W^{1,1}_{loc}(\mathbb{R}_+)$ satisfy*

$$g' = f_1(f_2 - f_3), \tag{3.24}$$

where $f_1 \notin L^1(\mathbb{R}_+)$ is non-negative and bounded, $\lim_{t\to\infty} f_2(t) = l \neq 0$ and $f_3 \in L^p(\mathbb{R}_+)$, where $1 \leq p < \infty$. Then the following statements hold.

1. *If $l < 0$, then g is approximately ultimately non-increasing and $\lim_{t\to\infty} g(t) = -\infty$.*
2. *If $l > 0$, then g is approximately ultimately non-decreasing and $\lim_{t\to\infty} g(t) = \infty$.*

Lemma 3.5.8. *[21, Lemma 3.2c)] Let $\Phi : C(\mathbb{R}_+) \to C(\mathbb{R}_+)$ be a hysteresis operator satisfying **(N1)** - **(N6)**, with Lipschitz constant λ. For any $u \in W^{1,1}_{loc}(\mathbb{R}_+)$, there exists a measurable function $d_u : \mathbb{R}_+ \to [0, \lambda]$ such that*

$$(\Phi(u))'(t) = d_u(t)u'(t), \ \text{a.e. } t \in \mathbb{R}_+.$$

Theorem 3.5.9. *[23, Thm 4.1] Consider the system*

$$x' = \kappa(\rho - \eta - (\mathcal{G} \circ \Phi)(x)), \ x(0) = x_0 \tag{3.25}$$

with the following assumptions:

1. *$\mathcal{G} : L^2(\mathbb{R}_+) \to L^2(\mathbb{R}_+)$ is a linear, bounded, and shift-invariant operator, as described above, satisfying Assumption 3.5.5;*
2. *$\eta \in L^2(\mathbb{R}_+)$;*
3. *Φ is a hysteresis operator, satisfying (N1) - (N6) with associated Lipschitz constant λ_1;*
4. *There exists $\mu \in \overline{\text{NVS}}\ \Phi$ such that $\rho = \hat{g}(0)\mu$;*
5. *$\kappa : \mathbb{R}_+ \to \mathbb{R}$ is measurable, non-negative and bounded with:*

$$\limsup_{t\to\infty} \kappa(t) < \frac{1}{\lambda_1 |f(\hat{g})|},$$

where $f(\hat{g}) = \inf_{\omega\in\mathbb{R}^*} \ Re \left(\frac{\hat{g}(i\omega)}{i\omega}\right)$.

Then there exists a unique solution $x \in W^{1,1}_{loc}(\mathbb{R}_+)$ to (3.25) and the following statements hold:

1. *$(\Phi(x))' \in L^2(\mathbb{R}_+)$ and the limit $\Phi^\infty := \lim_{t\to\infty}(\Phi(x))(t)$ exists and is finite.*
2. *The signal $w = \eta + (\mathcal{G} \circ \Phi)(x)$ can be decomposed into $w = w_1 + w_2$ where w_1 is continuous and has a finite limit:*

$$w_1^\infty = \lim_{t\to\infty} w_1(t) = \hat{g}(0)\Phi^\infty,$$

and $w_2 \in L^2(\mathbb{R}_+)$. Under the additional assumption that:

$$\lim_{t\to\infty}(\eta(t) + \Phi(x(0))(\mathcal{G}\theta(t) - \hat{g}(0))) = 0, \tag{3.26}$$

$$\lim_{t\to\infty} w_2(t) = 0.$$

3. *If $\kappa \notin L^1(\mathbb{R}_+)$, then $w_1^\infty = \rho$ and the error signal $e = \rho - w$ can be decomposed as $e = e_1 + e_2$ where e_1 is continuous and $e_2 \in L^2(\mathbb{R}_+)$. If additionally, (3.26) holds, then $\lim_{t\to\infty} e(t) = 0$.*

4. *If μ described in the assumptions is in the interior of NVS Φ, then x is bounded.*

Proof.[Proof of Theorem 3.5.9] Each result in the theorem will be shown separately.

(1) The aim here is to apply Proposition 3.5.6 to the signal

$$\tilde{w} := w - \rho = \eta + (\mathcal{G} \circ \Phi)(x) - \rho.$$

By the assumptions in the theorem, there exists μ such that $\rho = \hat{g}(0)\mu$. By Lemma 3.5.8,

$$\begin{aligned}(\Phi(x))'(t) &= d_x(t)x'(t)\\ &= d_x(t)\kappa(t)(\rho - \eta - (\mathcal{G}\circ\Phi)(x))\\ &= -d_x(t)\kappa(t)\tilde{w}(t).\end{aligned}$$

Define $N(t,\xi) = \kappa(t)d_x(t)\xi$. Integrating yields

$$(\Phi(x))(t) = (\Phi(x))(0) - \int_0^t N(\tau, \tilde{w}(\tau))d\tau.$$

Applying the operator $\mathcal{G}$ on both sides yields

$$(\mathcal{G}\circ\Phi(x))(t) = \mathcal{G}(\Phi(x(0))\theta)(t) - \mathcal{G}\left(\int_0^t N(\tau,\tilde{w}(\tau))(\tau)d\tau\right).$$

By linearity and shift-invariance of $\mathcal{G}$,

$$(\mathcal{G}\circ\Phi(x))(t) = (\Phi(x(0)))(\mathcal{G}\theta)(t) - \int_0^t (\mathcal{G}(N(\tau,\tilde{w}(\tau))))(\tau)d\tau$$

Adding $\eta - \hat{g}(0)\mu$ to both sides,

$$(\mathcal{G}\circ\Phi(x))(t) + \eta(t) - \hat{g}(0)\mu = \eta - \hat{g}(0)\mu + \Phi(x(0))(\mathcal{G}\theta)(t) - \int_0^t \mathcal{G}(N(\cdot,\tilde{w}))(\tau)d\tau. \tag{3.27}$$

Defining

$$r := \eta - \hat{g}(0)\mu\theta + (\Phi(x))(0)\mathcal{G}\theta,$$

equation (3.27) can be written

$$\tilde{w}(t) = r(t) - \int_0^t \mathcal{G}(N(\tau, \tilde{w}(\tau)))(\tau)d\tau. \tag{3.28}$$

Equation (3.28) has the same form as that found in Proposition 3.5.6. It remains to verify that the hypotheses on the components of (3.27) hold. Consider an operator $\mathcal{H}$: $L^2_{loc}(\mathbb{R}_+) \to L^2_{loc}(\mathbb{R}_+)$ defined by:

$$(\mathcal{H}v)(t) := \int_0^t (\mathcal{G}v(\tau) - \hat{g}(0)v(\tau))d\tau. \tag{3.29}$$

where $\mathcal{G}$ is the previously described convolution operator. The transfer function of $\mathcal{H}$ is the Laplace transform of the corresponding function h. This is given by $\hat{h}(s) = \dfrac{\hat{g}(s) - \hat{g}(0)}{s}$. Note also that the inverse Laplace transform of $\hat{h}$ is the function $\mathcal{G}\theta - \hat{g}(0)\theta$. It is clear from Assumption 3.5.5 that $\hat{h} \in H^\infty(\mathbb{C}_+)$. It can also be shown that $\hat{h} \in H^2(\mathbb{C}_+)$. Let $r > 0$. For $\mathrm{Re}(s) > 0$ and $|s| > r$,

$$\begin{aligned}
|\hat{h}(s)| &= \left|\frac{\hat{g}(s) - \hat{g}(0)}{s}\right| \\
&\leq \frac{\sup\limits_{\mathrm{Re}(s)>0} |\hat{g}(s)| + \sup\limits_{\mathrm{Re}(s)>0} |\hat{g}(s)|}{|s|} \\
&= \frac{2||\hat{g}||_{H^\infty}}{|s|} \\
&= \left(\frac{1+|s|}{|s|}\right)\frac{2||\hat{g}||_{H^\infty}}{1+|s|} \\
&= \left(\frac{1}{|s|} + 1\right)\frac{2||\hat{g}||_{H^\infty}}{1+|s|} \\
&\leq \left(\frac{1}{r} + 1\right)\frac{2||\hat{g}||_{H^\infty}}{1+|s|} \\
&= \frac{M_1}{1+|s|}
\end{aligned}$$

where $M_1 = 2(\frac{1}{r} + 1)||\hat{g}||_{H^\infty}$. For $|s| < r$ and $\mathrm{Re}(s) > 0$,

$$\begin{aligned}
|\hat{h}(s)| &\leq ||\hat{h}||_{H^\infty} \\
&= \frac{(1+|s|)||\hat{h}||_{H^\infty}}{1+|s|} \\
&\leq \frac{(1+r)||\hat{h}||_{H^\infty}}{1+|s|} \\
&= \frac{M_2}{1+|s|}.
\end{aligned}$$

where $M_2 = (1+r)||\hat{h}||_{H^\infty}$. Choose $\gamma = \max\{M_1, M_2\}$. By Assumption 3.5.5 and $\hat{g}, \hat{h} \in H^\infty(\mathbb{C}_+)$, $\gamma < \infty$. The transfer function $\hat{h}$ is bounded by $\frac{\gamma}{1+|s|}$ for all of $\mathrm{Re}(s) > 0$. It is clear that this transfer function belongs in $H^2(\mathbb{C}_+)$, so $\hat{h} \in H^2(\mathbb{C}_+)$.

By the Paley-Wiener Theorem [8, Appendix 6.21], $\mathcal{G}\theta - \hat{g}(0)\theta \in L^2(\mathbb{R}_+)$, which consequently implies that $\mathcal{G}\theta \in L^2(\mathbb{R}_+) + \mathbb{R}\theta$ since $\hat{g}(0) \in \mathbb{R}$. Thus the first and third conditions in Proposition 3.5.6 are satisfied. To show the second condition, note that

$$0 \leq N(t,\xi)\xi \leq \lambda_1 \kappa(t)\xi^2.$$

By the assumption on κ (assumption 5 in the theorem statement), there exists $0 < a < 1/|f(\mathcal{G})|$ and $t_0 \geq 0$ such that

$$0 \leq N(t,\xi)\xi \leq a\xi^2, \text{ for every } (t,\xi) \in [t_0,\infty) \times \mathbb{R}.$$

Thus Proposition 3.5.6 can be applied, yielding that $N(\cdot, \tilde{w}) \in L^2(\mathbb{R}_+)$ and the limit of $\int_0^t N(\tau, \tilde{w}(\tau))d\tau$ as $t \to \infty$ exists and is finite. Hence $(\Phi(x))' = -N(\cdot, \tilde{w}) \in L^2(\mathbb{R}_+)$, and

$$\lim_{t\to\infty}(\Phi(x))(t) = (\Phi(x))(0) - \lim_{t\to\infty}\int_0^t N(\tau, \tilde{w}(\tau))d\tau$$

exists and is finite, which proves the first result of Theorem 3.5.9.

(2) Let $w_1 := \hat{g}(0)\Phi(x)$ and let $w_2 := \eta + (\Phi(x))(0)(\mathcal{G}\theta - \hat{g}(0) + \mathcal{H}((\Phi(x))')$. Note that

$$\begin{aligned}
&(\mathcal{H}(\Phi(x))')(t) \\
&= \int_0^t \left(\mathcal{G} \circ (\Phi(x))'(\tau) - \hat{g}(0)(\Phi(x))'(\tau)\right) d\tau \\
&= (\mathcal{G}\circ\Phi)(x(t)) - (\mathcal{G}\circ\Phi)(x(0)) - \hat{g}(0)\left[(\Phi(x))(t) - (\Phi(x))(0)\right].
\end{aligned}$$

It is easily verified that w_1 and w_2 form a valid decomposition of w. By result (1), $w_1^\infty := \hat{g}(0)\Phi^\infty$ exists and is finite. Considering the components of w_2, $\eta \in L^2(\mathbb{R}_+)$, and from the proof of result (1), it was argued by the Paley-Wiener Theorem (see [8, Appendix 6.26]) that $\mathcal{G}\theta - \hat{g}(0)\theta \in L^2(\mathbb{R}_+)$. Also, by Assumption 3.5.5, $\hat{h} \in H^\infty(\mathbb{C}_+)$, which implies that $\mathcal{H}$ maps $L^2(\mathbb{R}_+)$ to itself. From result (1), $(\Phi(x))' \in L^2(\mathbb{R}_+)$, so $\mathcal{H}(\Phi(x))') \in L^2(\mathbb{R}_+)$. Therefore $w_2 \in L^2(\mathbb{R}_+)$.

With the additional assumption described in the result of (2), the first two terms of $w_2 \to 0$ as $t \to \infty$. It remains to show that $\lim_{t\to\infty}(H(\Phi(x)'))(t) = 0$. Since $\mathcal{H}$ is bounded, linear, and shift-invariant, there exists a function h where

$\mathcal{H}((\Phi(x))') = h \star (\Phi(x))'$. Again by the Paley-Wiener Theorem (see [8, Appendix 6.26]), h (whose Laplace transform is in $H^2(\mathbb{C}_+)$) belongs in $L^2(\mathbb{R}_+)$. From Appendix C of [9], the term $(H(\Phi(x)'))(t)$ is a convolution of two functions in $L^2(\mathbb{R}_+)$ and hence has a zero limit.

(3) Rewrite the system (3.25) as

$$x' = \kappa(\rho - w_1 - w_2). \tag{3.30}$$

The aim is to prove $\lim_{t\to\infty} w_1 = w_1^\infty = \rho$. Suppose $w_1^\infty > \rho$. Lemma 3.5.7 can be used with $g = x$, $f_1 = \kappa$, $f_2 = \rho - w_1$ and $f_3 = w_2$. Then x is approximately ultimately non-increasing and $\lim_{t\to\infty} x(t) = -\infty$. Hence by **(N5)**,

$$\lim_{t\to\infty} \Phi(x(t)) = \Phi^\infty = \inf \text{ NVS } \Phi.$$

Since it was assumed in the theorem statement that $\mu \in \overline{\text{NVS}}\ \Phi$,

$$\rho = \hat{g}(0)\mu \geq \hat{g}(0)\Phi^\infty = w_1^\infty.$$

A contradiction is reached. If the same argument is made for $w_1^\infty < \rho$, the conclusion that $w_1^\infty = \rho$ is reached. Finally, in letting $e_1 = \rho - w_1$ and $e_2 = -w_2$, the required decomposition for the additional property that $\lim_{t\to\infty} e(t) = 0$ is achieved.

(4) Two cases will be considered independently based on whether or not κ belongs to $L^1(\mathbb{R}_+)$. Suppose it does, considering the system in the form above in (3.30), w_1 is bounded, and $w_2 \in L^2(\mathbb{R}_+)$. By the fact that $\kappa \in L^1(\mathbb{R}_+)$ and that it is bounded, the L^2-norm of κ must also be bounded. Note that

$$\begin{aligned}
\|\kappa\|_2 &= \left(\int_0^\infty (\kappa(t))^2 d\tau\right)^{\frac{1}{2}} \\
&\leq \left(\max_{t\in[0,\infty)} |\kappa(t)|\right)^{1/2} \left(\int_0^\infty |\kappa(t)| d\tau\right)^{1/2} \\
&= \|\kappa\|_\infty^{\frac{1}{2}} \|\kappa\|_1^{\frac{1}{2}} \\
&< \infty
\end{aligned}$$

Finally, $\kappa(\rho - w_1 - w_2)$ will be shown to belong to $L^1(\mathbb{R}_+)$. For the first two terms, ρ and w_1 are both bounded so $\kappa\rho$ and κw_1 both belong to $L^1(\mathbb{R}_+)$. For the last term, an appeal is made to Hölder's inequality. Since both κ and w_2 are in $L^2(\mathbb{R}_+)$,

$$\|\kappa w_2\|_1 \leq \|\kappa\|_2 \|w_2\|_2 < \infty.$$

Hence $x' \in L^1(\mathbb{R}_+)$, and is integrable and hence x is bounded. If $\kappa \notin L^1(\mathbb{R}_+)$, then by result (3), $w_1(t) \to \rho$ as $t \to \infty$. Therefore $w_1 = \hat{g}(0)\Phi(x)$ implies that $\Phi^\infty \in \text{int}(\text{NVS}(\Phi))$. By **(N6)**, x is bounded. $\square$

Next, the main result of the section is presented.

Theorem 3.5.10. *[18, Thm 3.2] Let $g \in L^1_\alpha(\mathbb{R}_+) + \mathbb{R}\delta_0$ for some $\alpha < 0$, where δ_0 is the Dirac distribution with support at 0. Let $r_1, r_2 \in \mathbb{R}, \kappa > 0$ and $q \in L^2(\mathbb{R}_+)$ with $\lim_{t\to\infty} q(t) = 0$.*

*Let $\Phi : C(\mathbb{R}_+) \to C(\mathbb{R}_+)$ be a hysteresis operator that satisfies assumptions **(N1)** - **(N6)** with associated Lipschitz constant $\lambda > 0$.*

Let $\hat{g}$ denote the Laplace Transform of g, and $\hat{g}(0) > 0$, $r_1 + \dfrac{r_2}{\hat{g}(0)} \in \overline{NVS}\,\Phi$, and define $f(\hat{g}) = \inf_{\omega\in\mathbb{R}^*} Re\left(\dfrac{\hat{g}(i\omega)}{i\omega}\right)$. For every κ such that

$$0 < \kappa < \begin{cases} \frac{1}{\lambda|f(\hat{g})|}, & f(\hat{g}) \neq 0 \\ \infty, & f(\hat{g}) = 0 \end{cases}, \tag{3.31}$$

and $y_0 \in \mathbb{R}$, there exists a unique solution $y \in W^{1,1}_{loc}(\mathbb{R}_+)$ to

$$y' = \kappa(r_1(g \star \theta) + q + r_2\theta - (g \star \Phi(y))), y(0) = y_0 \in \mathbb{R}, \tag{3.32}$$

such that $\lim_{t\to\infty} y'(t) = 0$, and $\lim_{t\to\infty}(\Phi(y))(t) = r_1 + \dfrac{r_2}{\hat{g}(0)}$ and $(\Phi(y))' \in L^2(\mathbb{R}_+)$.

Moreover, if $r_1 + \dfrac{r_2}{\hat{g}(0)} \in \text{int}\ \overline{\text{NVS}}\ \Phi$, then y is bounded.

This result is pertinent because it describes asymptotic properties and will be useful in showing asymptotic tracking in the next theorem. Theorem 3.5.10 states the limit of the hysteresis operator and guarantees that the solution of the differential equation (3.32) tends to zero as t tends to infinity.

Proof: It will be shown that this current setup satisfies the previous theorem with (3.32) taking the role of (3.25). First, since $g \in L^1_\alpha(\mathbb{R}_+) + \mathbb{R}\delta_0$ with $\alpha < 0$, hence $\hat{g}$ is holomorphic and bounded on the open right-half plane. Furthermore, $-tg(t) \in L^1_\alpha(\mathbb{R}_+) + \mathbb{R}\delta_0$ since the exponential decay will eventually dominate the polynomial factor. Its Laplace transform $\hat{g}'(s)$ must also exist, and

$$|\hat{g}'(0)| < \infty, \text{ and}$$

$$\limsup_{s\to 0, \text{Re } s>0} \left|\frac{\hat{g}(s) - \hat{g}(0)}{s}\right| = |\hat{g}'(0)|$$

From the assumptions of this theorem $\hat{g}(0) > 0$ thus Assumption 3.5.5 is satisfied. Next, by the Final Value Theorem, $g \star \theta - \hat{g}(0) \to 0$ as $t \to \infty$ where θ is the unit step function. Also $g \star \theta - \hat{g}(0) \in L^2(\mathbb{R}_+)$ by the Paley-Wiener Theorem, since its Laplace transform is in $H^2(\mathbb{C}_+)$. Comparing (3.32) with the system found in Theorem 3.5.9, let $\rho = \hat{g}(0)r_1 + r_2$ and $\eta = r_1(\hat{g}(0) - g \star \theta) - q$, which is in $L^2(\mathbb{R}_+)$ since each term is in $L^2(\mathbb{R}_+)$.

Therefore Theorem 3.5.9 can be applied to (3.32). The properties $\lim_{t\to\infty} y'(t) = 0$, $(\Phi(y))' \in L^2(\mathbb{R}_+)$, and $\lim_{t\to\infty}(\Phi(y))(t)$ exists are true. Moreover, y is bounded, provided that $r_1 + \frac{r_2}{\hat{g}(0)}$ is an interior point of NVS Φ. Finally, it is claimed that $\Phi^\infty = r_1 + r_2/\hat{g}(0)$. This can be verified from equation (3.32) by applying the properties shown already. As $t \to \infty$, $y'(t) \to 0$, $q \to 0$, $(g \star \theta)(t) \to \hat{g}(0)$ and $(g \star \Phi(y))(t) \to \hat{g}(0)\Phi^\infty$ by use of the Final Value Theorem. As $t \to \infty$, equation (3.32) becomes

$$0 = \kappa(r_1\hat{g}(0) + r_2 - \hat{g}(0)\Phi^\infty)$$

Dividing both sides by κ and rearranging the terms yields

$$\Phi^\infty = r_1 + \frac{r_2}{\hat{g}(0)}. \square$$

3.5.5 PID Control of Systems with Hysteresis

In this section, asymptotic tracking of the system (3.22) is presented. See Figure 3.5. The transfer function $\hat{G}(s)$ is the second-order system described in equation (3.22). It is shown that through the manipulation of the control parameters, the desired closed-loop properties can be achieved even without the presence of derivative control.

Theorem 3.5.11. *[18, Thm 4.3] Let $\Phi : C(\mathbb{R}_+) \to C(\mathbb{R}_+)$ be a hysteresis operator satisfying (N1) - (N6), with associated Lipschitz constant $\lambda > 0$. Let $r, d_1, d_2 \in \mathbb{R}$ and assume that $rk - d_1 \in \overline{\text{NVS}}\ \Phi$.* Consider two cases,

Case (a): *$K_D = 0$ and $K_P, K_I > 0$ such that*

(A) $0 < K_I < \frac{K_P k}{c} < \frac{ck}{\lambda m}$.

Case (b): *$K_P, K_I, K_D > 0$ such that*

(B1) $0 < K_I < \infty$,

(B2) $K_P > \dfrac{cK_I}{k}$,

(B3) $K_D > \dfrac{mK_P}{c}$,

Then there exists a unique solution $x \in C^2(\mathbb{R}_+)$ of the closed-loop system given by (3.22) such that

$$\lim_{t\to\infty} x(t) = r \ , \ \lim_{t\to\infty} x'(t) = 0, \ \lim_{t\to\infty} x''(t) = 0, \ \lim_{t\to\infty} (\Phi(u + d_2\theta))(t) = rk - d_1$$

Moreover, if $rk - d_1$ is an interior point of NVS Φ, then the control signal u given by (3.1) is bounded.

It is useful to know the steady-state result of the control under the hysteretic effects. Note that asymptotic tracking of a constant reference signal is the result of this theorem.

Proof. The aim of this proof is to demonstrate that the system satisfies the assumptions of Theorem 3.5.10. Several functions must first be defined and it will be shown that those functions live in the desired spaces.

Let $p(s) := ms^2 + cs + k$, let h be the solution of the initial value problem

$$p\left(\frac{d}{dt}\right) h = 0, \ h(0) = 0, \ h'(0) = \frac{1}{m},$$

and let ρ be the solution of the initial-value problem

$$p\left(\frac{d}{dt}\right) \rho = 0, \ \rho(0) = x_0, \ \rho'(0) = v_0.$$

By direct substitution, the function x

$$x = h \star \left[\Phi\left(-K_P(x - r\theta) - K_D x' - K_I \textstyle\int_0^{\cdot}(x(\tau) - r)d\tau + (u_0 + d_2)\theta\right) + d_1\theta\right] + \rho,$$

satisfies the system (3.22). Define $w(t) = u(t) + d_2$. The following calculation can easily be verified by direct substitution. The Dirac distribution δ_0 is the identity element of convolution, and differentiation of a convolution yields: $(g \star h)'(t) = g(t)h(0) + g \star h' = g(t) \star h(0)\delta_0 + (g \star h')(t)$ (see Appendix A.3). Thus, for all $t \geq 0$,

$$\begin{aligned} w(t) &= u(t) + d_2 \\ &= -K_P(x - r) - K_D x' - K_I \int_0^{\cdot} (x(\tau) - r)d\tau + u_0 + d_2. \end{aligned}$$

Differentiating and defining

$$g := \frac{K_D}{K_I}\left[h'' + \frac{1}{m}\delta_0\right] + \frac{K_P}{K_I}h' + h,$$

and

$$q := -\frac{K_D}{K_I}\rho'' - \frac{K_P}{K_I}\rho' - \rho.$$

yields

$$\begin{aligned} w' &= -K_P x' - K_D x'' - K_I(x - r\theta) && (3.33)\\ &= K_I(r\theta + q - d_1 g \star \theta - g \star \Phi(w)), && (3.34) \end{aligned}$$

where

$$w(0) = -K_P(x_0 - r) - K_D v_0 + u_0 + d_2.$$

Note that w' has the form of y' in Theorem 3.5.10 with $\kappa = K_I, r_1 = -d_1$, and $r_2 = r$. With this setup in mind, the rest of the assumptions will be shown to hold. The denominator of both of the transfer functions of h and ρ is $p(s)$, whose roots are: $\frac{-c \pm \sqrt{c^2 - 4km}}{2}$, which clearly have negative real part. The poles of the transfer functions of h and ρ all lie in the left-half complex plane, which implies that the functions and their derivatives decay exponentially and are hence in $L^2(\mathbb{R}_+)$. See Appendix A.4 for a detailed explanation.

Because linear combinations of h, ρ and their derivatives are exponentially decaying, $q \in L^2(\mathbb{R}_+)$ and $\lim_{t\to\infty} q(t) = 0$, and $g \in L^1_\alpha(\mathbb{R}_+) + \mathbb{R}\delta_0$ for some $\alpha < 0$. The Laplace transform of g is

$$\hat{g}(s) = \frac{1}{K_I}\frac{K_D s^2 + K_P s + K_I}{ms^2 + cs + k}.$$

Therefore $\hat{g}(0) = 1/k > 0$. Also, by assumption $rk - d_1 = r_2/\hat{g}(0) + r_1 \in \overline{\text{NVS}}\ \Phi$. It remains to show that K_I satisfies the role of κ as described in Theorem 3.5.10, by verifying (3.31). Consider

$$
\begin{aligned}
f(\hat{g}) &= \inf_{\omega\in\mathbb{R}^*} \operatorname{Re}\left(\frac{\hat{g}(i\omega)}{i\omega}\right) \\
&= \inf_{\omega\in\mathbb{R}^*} \operatorname{Re}\left(\frac{K_D(i\omega)^2 + K_P i\omega + K_I}{K_I(m(i\omega)^3 + c(i\omega)^2 + ki\omega)}\right) \\
&= \inf_{\omega\in\mathbb{R}^*} \operatorname{Re}\left(\frac{-K_D\omega^2 + K_I + K_P i\omega}{K_I(-c\omega^2 + i(k\omega - m\omega^3))} \cdot \frac{-c\omega^2 - i(k\omega - m\omega^3)}{-c\omega^2 - i(k\omega - m\omega^3)}\right) \\
&= \inf_{\omega\in\mathbb{R}^*} \frac{1}{K_I}\left(\frac{K_D c\omega^4 - K_I c\omega^2 + K_P k\omega^2 - K_P m\omega^4}{c^2\omega^4 + (k\omega - m\omega^3)^2}\right), \text{let } \xi = \omega^2 \text{ vary from } (0,\infty) \\
&= \inf_{\xi\in\mathbb{R}_+} \frac{1}{K_I}\left(\frac{(K_P k - K_I c) + \xi(K_D c - mK_P)}{m^2\xi^2 + (c^2 - 2mk)\xi + k^2}\right) \\
&= \inf_{\xi\in\mathbb{R}_+} \left(\frac{(K_P k - K_I c) + \xi(K_D c - mK_P)}{K_I((m\xi - k)^2 + c^2\xi)}\right).
\end{aligned}
$$

where $\xi = \omega^2$ and let $\zeta : \mathbb{R}_+ \to \mathbb{R}$ be defined by

$$
\zeta(\xi) = \frac{(kK_P - cK_I) + \xi(cK_D - mK_P)}{K_I((m\xi - k)^2 + c^2\xi)}.
$$

At this point, each of the two cases are considered separately and are each shown to satisfy (3.31).

Case (a): Let $K_D = 0$, and assume **(A)** holds. From **(A)**, $kK_P - cK_I > 0$. The denominator of ζ is positive for all $\xi \geq 0$. Since $K_D = 0$, if $\xi > \frac{kK_P - cK_I}{mK_P}$, then $\zeta(\xi) < 0$. Thus $f(\hat{g})$ defined above is negative. Also,

$$
f(\hat{g}) \geq \inf_{\xi\in\mathbb{R}_+} \mu(\xi),
$$

where $\mu(\xi) := \dfrac{-mK_P\xi}{K_I((m\xi - k)^2 + c^2\xi)}$. The function μ attains a global minimum over $\mathbb{R}_+$ at $\xi = k/m$, and hence

$$
0 > f(\hat{g}) \geq \mu(k/m) = -\frac{mK_P}{c^2 K_I}.
$$

By **(A)**, $1 < c^2/(\lambda m K_P)$, hence

$$0 < K_I < \frac{K_I c^2}{\lambda m K_P} \leq \frac{1}{\lambda |f(\hat{g})|}.$$

Thus, if $K_D = 0$, (3.31) is satisfied by choosing $\kappa = K_I$.

It remains to show that the hypothesis holds for **Case b)**. Let $K_P, K_I, K_D > 0$ and **(B1)**, **(B2)**, **(B3)** hold, then both terms in the numerator of ζ are positive, as is the denominator, so $\zeta(\xi) \geq 0$ for all $\xi \in \mathbb{R}_+$. Along with $f(\hat{g}) = \lim_{\xi \to \infty} \zeta(\xi) = 0$, $K_I = \kappa$ can take on any real value, hence the assumption in equation (3.31) is satisfied.

Therefore, all the hypotheses of Theorem 3.5.10 are satisfied. Hence, there exists a unique solution $w \in C^1(\mathbb{R}_+)$ to (3.34), such that $w'(t) \to 0$ and $(\Phi(w))(t) \to rk - d_1$ as $t \to \infty$. Finally, consider (3.34),

$$K_D e'' + K_P e' + K_I e = -w',$$

with $-w'$ as the input to the system. Since $K_P, K_I > 0$, and $K_D \geq 0$ and $w'(t) \to 0$ as $t \to \infty$ (shown above), $e(t) \to 0$ (that is, $x(t) \to r$). By an application of the Final Value Theorem, $e'(t) = x'(t) \to 0$ as $t \to \infty$. From equation (3.33), as t approaches ∞, $x''(t)$ approaches 0 since all the other components decay to 0. Finally, if $r_1 + r_2/\hat{g}(0) = -d_1 + rk \in \text{int NVS } \Phi$, then boundedness of w, and hence by its definition, boundedness of u follows. □

3.6 Verification of Results for First-Order System

The work presented in [18] is in the context of second-order systems. A verification that the results hold true for a first-order system is given here. Logemann's approach (building on successive theorems) will be especially useful in this context. As in the previous setup, $u(t)$ is the PID controller (3.21). Consider

$$Mx'(t) + \sigma x(t) = \Phi(u(t) + d_2) + d_1, x(0) = x_0. \tag{3.35}$$

The results of applying Theorem 3.5.10 to the first-order system (3.35) are summarized in the following corollary.

Corollary 3.6.1. *Let $\Phi : C(\mathbb{R}_+) \to C(\mathbb{R}_+)$ be a hysteresis operator satisfying **(N1)** - **(N6)**, with associated Lipschitz constant $\lambda > 0$. Let $r, d_1, d_2 \in \mathbb{R}$ and assume that $r\sigma - d_1 \in \overline{\text{NVS}}\ \Phi$.* Let $M, \sigma > 0$. Consider two cases,

Case (a): *$K_D = 0$ and let $K_P, K_I > 0$ such that:*

(A) $0 < K_I < \frac{K_P \sigma}{M}$

Case (b): *Let $K_P, K_I, K_D > 0$ such that:*

(B1) $0 < K_I < \infty$,

(B2) $K_P > \dfrac{K_I M}{\sigma}$,

(B3) $K_D < \dfrac{M(K_P\sigma - MK_I)}{\sigma^2}$,

Then there exists a unique solution $x(t)$ of the closed-loop system given by equation (3.35) such that

$$\lim_{t\to\infty} x(t) = r \ , \ \lim_{t\to\infty} x'(t) = 0, \ \lim_{t\to\infty} (\Phi(u + d_2\theta))(t) = r\sigma - d_1.$$

Moreover, if $r\sigma - d_1$ is an interior point of NVS Φ, then the control signal u given by equation (3.1) is bounded.

Proof. The structure of this proof is very similar to that of Theorem 3.5.11.

Let $p(s) := Ms + \sigma$, and h be the solution of the initial value problem

$$p\left(\frac{d}{dt}\right) h = 0, \ h(0) = \frac{1}{M}.$$

Similarly, let ρ be the solution to the initial value problem:

$$p\left(\frac{d}{dt}\right) \rho = 0, \ \rho(0) = x_0.$$

As before, define $x(t)$ which satisfies equation (3.35), and define $w(t)$, $q(t)$ and $g(t)$ in the same manner as for the proof of Theorem 3.5.11:

$$\begin{aligned}
x &= h \star [\Phi(u + d_2)\theta + d_1\theta] + \rho, \\
w &= u + d_2\theta, \\
w' &= K_I(r\theta + q - d_1 g \star \theta - g \star \Phi(w)), \\
q &= -\frac{K_D}{K_I}\rho'' - \frac{K_P}{K_I}\rho' - \rho, \\
g &= \frac{K_D}{K_I}[h'' + h'(0)\delta_0] + \frac{K_P}{K_I}[h' + \frac{1}{M}\delta_0] + h.
\end{aligned}$$

Since ρ and h are exponentially decaying functions, $q \in L^2(\mathbb{R}_+)$ and $g \in L^1_\alpha(\mathbb{R}_+) + \mathbb{R}\delta_0$, for some $\alpha < 0$. The Laplace transform of g yields

$$\hat{g}(s) = \frac{1}{K_I} \frac{MK_P s + MK_I - K_D s\sigma}{M(Ms + \sigma)}, \text{ where } \hat{g}(0) = \frac{1}{\sigma} > 0.$$

It remains to show that κ, or in the present context K_I, satisfies the required assumption in each of the cases, but first, a calculation of $f(\hat{g})$ must be performed. Again, let

$$\begin{aligned} f(\hat{g}) &= \inf_{\omega \in \mathbb{R}^*} \operatorname{Re}\left(\frac{\hat{g}(i\omega)}{i\omega}\right), \\ &= \inf_{\xi \in \mathbb{R}_+} \left(\zeta(\xi)\right). \end{aligned}$$

Note that $\xi = \omega^2 > 0$. After some algebraic computations, the following becomes the equation to be minimized:

$$\zeta(\xi) = \frac{1}{K_I} \frac{-M^2 K_I + MK_P\sigma - K_D\sigma^2}{M^3\xi + M\sigma^2}.$$

Case (a): Let $K_D = 0$, and **(A)** hold. The third term in the numerator disappears. By condition **(A)**, K_P and K_I must be chosen such that $-MK_I + K_P\sigma > 0$. Hence, the function ζ is always positive, and approaches 0 as ξ becomes arbitrarily large. The assumption (3.31) is satisfied with $f(\hat{g}) = 0$.

Case (b): Let $K_D > 0$, such that **(B1)**, **(B2)** and **(B3)** hold. Under a similar argument as case (a), ζ is positive and $\zeta \to 0$ as $\xi \to \infty$.

Hence all the required assumptions are satisfied, and Theorem 3.5.10 can be applied. By the same arguments used at the end of Theorem 3.5.11, the conclusions of this corollary follow.

□

3.7 Other Forms of Control of Hysteretic Systems

While the work presented in this thesis is focused on the PID control of hysteretic systems, there has been some control work done outside of this area. A brief overview of other methods of control applied to hysteretic systems will be presented here. The modeling of the hysteretic system may vary from paper to paper, and may include models not mentioned in the modelling section. Several papers are concerned with specific applications such as the control of magnetostrictives. The focus here is on the control method rather than the hysteresis model, and on the results achieved (for example, stability and tracking).

3.7.1 Optimal Control

The optimal control problem is well known in the literature. Suppose there are a set of differential equations that govern the dynamics of a system. The system is subject to some inputs, and there are certain optimization criteria that need to be met. The optimal control law is the solution that satisfies the optimization criteria while at the same time minimizing a cost functional that is chosen based on design parameters. For a physical example, consider the well-known inverted pendulum and cart system. There is a pendulum that is free to swing about an axis of rotation, attached to a cart that can exhibit motion on a one dimensional track. The control can accelerate the cart back and forth. Given an initial angle of the pendulum and starting reference point on the track, the optimization criteria requires the system to balance the pendulum upright, while bringing the cart to a desired origin point. The state-space formulation considers four states: position and velocity of each of the pendulum (angular quantities in this case) and the cart. The cost function is chosen to be some combination of those four quantities.

In [3], a general system is introduced that can contain hysteretic components modeled by the Preisach model. They find viscosity solutions to the derived Hamilton-Jacobi-Bellman equation, which are solutions that can have points where the solution is not differentiable, but still satisfies the system in an appropriate sense. The value function is shown to be bounded. The same concept is evaluated by the same author while considering the play operator and the Prandtl-Ishlinskii operator in [2]. An example of a special case of optimal control, linear quadratic regulator, can be found in [31], applied to a hysteretic system.

3.7.2 Sliding Mode Control

Contrary to many other control theory formulations, the control law produced by sliding mode control is not continuous. The control switches between different

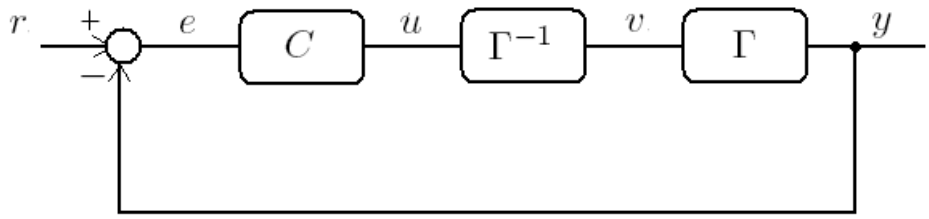

Figure 3.6: A controlled hysteretic system with inverse compensation

smooth control laws. Intuitively, the method used to drive the system towards the stable equilibrium is dependent on its position relative to the equilibrium. The movement towards this surface is known as a sliding mode. Continuing with the cart-pendulum example mentioned previously, the stable surface is the pendulum in the upright position and the cart returning to its origin on the track. A sliding mode controller for this system can take on two values, a positive or negative value with the same magnitude. The input is driven towards the equilibrium, should it in some sense exceed it, a switch to the other value will occur and vice-versa.

In [20], a sliding-mode enhanced adaptive (see below regarding adaptive control) control method is applied towards a piezoelectric actuation system. By employing Lyapunov stability methods, the system is shown to exhibit system stability and tracking convergence. Position control using a sliding-mode based robust controller of a shape memory alloy actuator is proposed in [35] and experimental results are discussed. The modeling and control of Terfenol-D, a magnetostrictive is discussed in [30]. Using the Jiles-Atherton model as a basis to describe the inherent hysteresis, a sliding mode controller was shown experimentally to have better tracking than a PID controller in the presence of uncertainties and unmodeled components. The results were shown experimentally, while the focus of this thesis has been on theoretical results.

3.7.3 Inverse Compensation

Efforts have been made to include components in the controller that consider inverse compensation to a hysteresis operator. In theory, this is a clever idea to have the effects of the hysteresis negated. Inverse compensation can be used with any type of control. This inverse operator simply has to be placed directly in front of the hysteresis operator. According to Figure 3.6, the control problem is reduced to controlling a non-hysteretic system. The operator C is a general controller to the system.

The drawback is in the difficulty of deriving this inverse. In application, approximations to an inverse are formulated. In [31], the control of a magnetostrictive material from a physical perspective, by using the Jiles-Atherton model is considered. Since then, the Jiles-Atherton model has not been as commonly used as a model to describe magnetic hysteresis due to its improper closure of minor loops, however the techniques used to obtain this inverse model are still of interest. As a practical application, a magnetostrictive material is modeled to be a cantilever beam, and controlled using linear quadratic regulator, a form of optimal control. In [13], an inverse compensation model is proposed for the physical Presiach model based on Gibbs energy. In [36], inverses for both the Preisach model and a physical model are constructed. The inversion error is shown to be bounded in magnitude. In fact, in both [17] and [36], algorithms (in the Preisach model context) are given to approximate the input to the hysteresis to yield the desired output. For [36], $\bar{H}$, an approximate input is recovered from M, in no more than a sum of the corners in the Preisach boundary and the discretization level. In [14], an inverse to the Preisach model is used to construct the controller. Experimental data is presented. The focus in these papers was to provide working inverse models to hysteresis rather than to formulate results regarding stability and tracking.

3.7.4 Adaptive Control

In adaptive control, the control law changes according to system variables. To clarify, consider the example of the control of stabilizing the flight of an aeroplane. As fuel is being consumed, the mass of the aeroplane decreases. This change in mass can be compensated in the control law. One such method is in [37], where the authors perform adaptive identification of the inverse to the Preisach model (see above section on inverse compensation). This update is performed on the piecewise-continuous weight function, which in turn requires an update to the inverse. Two identification schemes are presented, one based on the hysteretic output and the other based on time-difference of the output. The former is found to be more effective, as it achieves asymptotic tracking. Experimental data is shown with a magnetostrictive material, Terfenol-D.

In a more general sense, adaptive control can be an update to the parameters of the control law. In [43] and [45], adaptive control laws are used to control a general class of nonlinear ODEs, to which the input exhibits stop and play hysteresis. In both sources, stability is shown by finding a Lyapunov function. In [15], a control law for a second-order spring-mass-damper system using the Bouc-Wen model for hysteresis in the spring component is proposed. Expressions that bound the errors of transient displacement, asymptotic displacement, transient velocity, and asymptotic velocity are provided.

Chapter 4

Simulations

Computations were performed using MATLAB® to visualize and simulate some of the theory presented. Three hysteresis operators were considered: backlash, elastic-plastic and Preisach operators. As an application, one can consider the tracking of a certain signal (for example, constants, ramps, sinusoids etc.) by an actuator that exhibits hysteresis. Originally, Simulink® was considered in performing these simulations however the programming of the Preisach model in Simulink proved to be a challenge. Instead, all of the simulations were performed in MATLAB® using a Runge-Kutta fourth order fixed-step ODE solver. The code is available in Appendix B.

4.1 System Description

Recall that the equations that govern the closed-loop system (3.10) - (3.15) are:

$$\begin{aligned} e(t) &= r(t) - y(t), \\ u(t) &= K_P e(t) + K_I \exp(\text{-}\epsilon t) \int_0^t \exp(\epsilon\tau) e(\tau) d\tau, \\ v(t) &= \Phi(u(t)), \\ y'(t) &= Mv(t) - \sigma y(t), \end{aligned}$$

where Φ represents the hysteresis operator. Refer to Figure 3.4, where $\hat{G}(s) = \frac{M}{s+\sigma}$. Since this is in fact a closed loop, the entire system can be rewritten as a single equation, dependent on $r(t)$ and $y(t)$. This equation becomes

$$y'(t) = -\sigma y(t) + M\Phi\left[K_P\left(r(t) - y(t)\right) + K_I \exp(\text{-}\epsilon t) \int_0^t \exp(\epsilon\tau)\left(r(\tau) - y(\tau)\right) d\tau\right]. \tag{4.1}$$

As mentioned above, the fourth-order Runge-Kutta numerical scheme is used. Note that equation (4.1) is written in the form $y'(t) = f(t, y)$. Given y_n, time t_n and timestep h, the method to obtain y_{n+1} is the following,

$$\begin{aligned} k_1 &= f(t_n, y_n), \\ k_2 &= f(t_n + \frac{1}{2}h, y_n + \frac{1}{2}hk_1), \\ k_3 &= f(t_n + \frac{1}{2}h, y_n + \frac{1}{2}hk_2), \\ k_4 &= f(t_n + h, y_n + hk_3), \\ k &= \frac{1}{6}(k_1 + 2k_2 + 2k_3 + k_4) \\ y_{n+1} &= y_n + hk \\ t_{n+1} &= t_n + h. \end{aligned}$$

A weighted average of the slopes k, considered at four different points varying from t_n to t_{n+1} is used to compute the next input value. Since the chosen method was an explicit scheme, a relatively small timestep was used. In all simulations the timestep never exceeded $h = 0.01$s. The integral in Equation (4.1) is computed by a simple trapezoidal rule. This was chosen for the sake of computational simplicity. Finally, the history of the input $u(t)$ in calculating k_1 to k_4 was chosen to not have an affect on another. To clarify, the input history used to calculate k_1 to k_4 is the same. Only the last value of the input $u(t)$ differed according to the definitions of the coefficients.

The numerical scheme was entirely self-written. Despite the superiority of the built-in techniques available in MATLAB®, an issue arose with the need to access the solution in previous timesteps as the solution was being computed. The output function, y, was provided only at the end of the computation. Accessing previous timesteps that the hysteresis operator required as the solution was being solved proved to be a challenge. Regardless of whether or not this was possible through modifying the code, it was much quicker to implement a self-written solver.

4.2 Implementation of Hysteresis Operators

The implementation of the hysteresis operators is discussed in the following section. Both the backlash and the elastic operators are programmed to work very quickly, while the Preisach model being a much more complex and difficult model to implement, took longer to run, but less than thirty seconds to produce a ten-second long simulation on a dual 1.66 GHz Processor.

4.2.1 Backlash Operator and Elastic-Plastic Operator

Using the notation provided in its definition, recall that the backlash operator takes the parameters ξ and h (denoted by *bfac* in the code) in addition to the input history to determine its current value. The initial value is given by the parameter ξ. The lagging factor h represents a dead zone, that the input must first overcome in order to see a change in the output. Upon close inspection, only the current value of the input, as well as the two previous timesteps (rather than the entire input history) are required. The need for the previous timesteps, is to determine if the input changes direction (from increasing to decreasing or vice versa). Should the input change direction, the current interval would no longer be monotone. A new interval must begin, that is, $i = i + 1$, $t_i = t$, and $\mathcal{B}_{h,\xi}(u(t_i))$ is updated to $\mathcal{B}_{h,\xi}(u(t))$. The function b_h is programmed exactly as it is defined.

The elastic-plastic operator is programmed in the same fashion. The code uses the variable *efac* rather than h, since h is used for the timestep length. The only difference compared to the backlash operations was the need for the value of $u(t_i)$ in addition to $\mathcal{E}_{h,\xi}(u(t_i))$. Similar to the latter value, $u(t_i)$ is fed through the system as an input and an output that changes only to $u(t)$ should it change direction. The function e_h was straightforward to program.

4.2.2 Preisach Operator

First, a gridsize and a saturation value u_{sat} of the input is chosen (recall assumption **(A4)**). Together, the two parameters determine the size of the array (2 round($\frac{u_{sat}}{gridsize}$), round($\frac{u_{sat}}{gridsize}$) required to represent the Preisach plane. The top right and bottom right portions are always 0, as they are not part of the Preisach plane. The grid is rotated compared to the original definition given in Section 2.3. This change facilitated the input of the Preisach plane into a matrix (see Figure 4.1).

At each time step, $u(t)$ is provided. The cells affected by the boundary are modified, and the corresponding cells that switch their relays are updated. For example, Figure 4.1 represents the an initialized Preisach plane with $u_{sat} = 10$ and $gridsize = 1$, where the input has been increased from $u = 0$ to $u = 5$. The plane and the boundary are both drawn onto the matrix. The model allows for cells to take values other than $+1$ and -1. Should the boundary traverse a cell, a fractional value dependent on the amount of area in each of the $+1$ or the -1 regions is considered. See Figure 4.2, the input has been monotonically increased from $u = 0$, to $u = 7$, then monotonically decreased to $u = 2.5$.

The weight function used is based on experimental data of Terfenol-D, a magnetostrictive material. This data was obtained by Sina Valadkhan [39]. The method described previously where the Preisach plane is subdivided into square-shaped cells where a constant value is assumed over each cell is used. A detailed explanation of

	1	2	3	4	5	6	7	8	9	10
1	-0.5000	0	0	0	0	0	0	0	0	0
2	-1	-0.5000	0	0	0	0	0	0	0	0
3	-1	-1	-0.5000	0	0	0	0	0	0	0
4	-1	-1	-1	-0.5000	0	0	0	0	0	0
5	-1	-1	-1	-1	-0.5000	0	0	0	0	0
6	0	-1	-1	-1	-1	-0.5000	0	0	0	0
7	1	0	-1	-1	-1	-1	-0.5000	0	0	0
8	1	1	0	-1	-1	-1	-1	-0.5000	0	0
9	1	1	1	0	-1	-1	-1	-1	-0.5000	0
10	1	1	1	1	0	-1	-1	-1	-1	-0.5000
11	1	1	1	1	1	1	1	1	1	0.5000
12	1	1	1	1	1	1	1	1	0.5000	0
13	1	1	1	1	1	1	1	0.5000	0	0
14	1	1	1	1	1	1	0.5000	0	0	0
15	1	1	1	1	1	0.5000	0	0	0	0
16	1	1	1	1	0.5000	0	0	0	0	0
17	1	1	1	0.5000	0	0	0	0	0	0
18	1	1	0.5000	0	0	0	0	0	0	0
19	1	0.5000	0	0	0	0	0	0	0	0
20	0.5000	0	0	0	0	0	0	0	0	0

Figure 4.1: MATLAB® Preisach Plane at $u = 5$ (from $u = 0$)

	1	2	3	4	5	6	7	8	9	10
1	-0.5000	0	0	0	0	0	0	0	0	0
2	-1	-0.5000	0	0	0	0	0	0	0	0
3	-1	-1	-0.5000	0	0	0	0	0	0	0
4	-1	-1	-1	-0.5000	0	0	0	0	0	0
5	-1	-1	-1	-1	-0.5000	0	0	0	0	0
6	-1	-0.7500	-0.1250	-1	-1	-0.5000	0	0	0	0
7	-0.7500	0.7500	1	0	-1	-1	-0.5000	0	0	0
8	0.7500	1	1	1	0	-1	-1	-0.5000	0	0
9	1	1	1	1	1	0	-1	-1	-0.5000	0
10	1	1	1	1	1	1	0	-1	-1	-0.5000
11	1	1	1	1	1	1	1	1	1	0.5000
12	1	1	1	1	1	1	1	1	0.5000	0
13	1	1	1	1	1	1	1	0.5000	0	0
14	1	1	1	1	1	1	0.5000	0	0	0
15	1	1	1	1	1	0.5000	0	0	0	0
16	1	1	1	1	0.5000	0	0	0	0	0
17	1	1	1	0.5000	0	0	0	0	0	0
18	1	1	0.5000	0	0	0	0	0	0	0
19	1	0.5000	0	0	0	0	0	0	0	0
20	0.5000	0	0	0	0	0	0	0	0	0

Figure 4.2: MATLAB® Preisach Plane: $u = [0, 7, 2.5]$

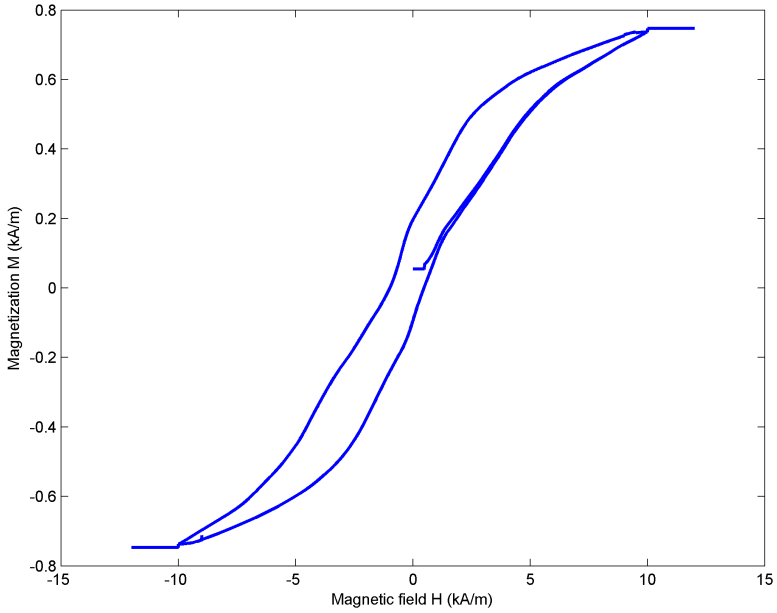

Figure 4.3: Preisach Major Loop with Terfenol-D Data

this weight function can be found in [39]. The weight function is a matrix of the same size as the grid for the Preisach plane, which is then multiplied cell by cell with the Preisach plane for a given input history. The sum of the entries of the resultant matrix is multiplied by the area of each grid. This value is the output of the Preisach model at that timestep. A major loop of the hysteresis can be found in Figure 4.3. The reader is referred to Section 1.4 of [25] for an alternate numerical implementation of the Preisach model.

4.3 Results

While the theory presented in this thesis does not cover the stability and tracking of ramps and sinusoids, their simulation is presented here to demonstrate the effectiveness of a PI controller for these applications. The stability results found in Section 3.4 provide a range of parameters for which stability is guaranteed. Since the aim was to use a practical PI controller, the parameter ϵ was chosen to be small to mimic a pure integral controller. It is shown however in Section 3.6 that for a first order system, the conditions that had to be satisfied for asymptotic tracking were

$$0 < K_I < \frac{K_P \sigma}{M} \text{ and } K_P > 0.$$

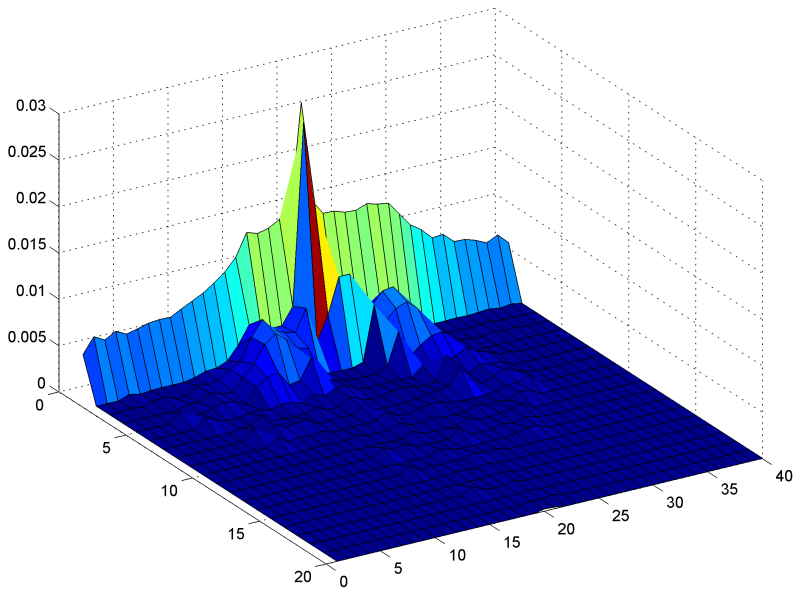

Figure 4.4: Weight Function from Terfenol-D Data

The parameters $\sigma = M = 1$ were used in performing the simulations. The required conditions became $0 < K_I < K_P$, $K_P > 0$. The performance became better for larger values of K_I and K_P provided that the necessary conditions were satisfied. With practical application however, these parameters are limited by the maximum output of an actuator. It will be seen that these conditions are not necessary, but only sufficient for stability.

4.3.1 Tracking a Constant Reference Signal

Backlash and Elastic-Plastic Operators

A reference signal of $r(t) = 1$ was tracked with the backlash and elastic-plastic operators acting on the controller. In Figure 4.5, both the backlash factor and the elastic-plastic factor were set to 3 with 0 initial condition. The controller parameters were chosen to be $K_P = 10$, and $K_I = 5$. In comparison to the controller acting with no hysteresis, an overshoot is produced with the backlash operator. The nature of the backlash operator is that the output is a delayed version of the input. When a larger control effort is required, the system must wait until the backlash is overcome. This delay in control effort causes the system to drift past the desired value. The elastic-plastic operator has a limit in terms of control effort that can be exerted, resulting in the slower response seen in Figure 4.5.

Should the conditions be violated, the system may still be stable. The effect

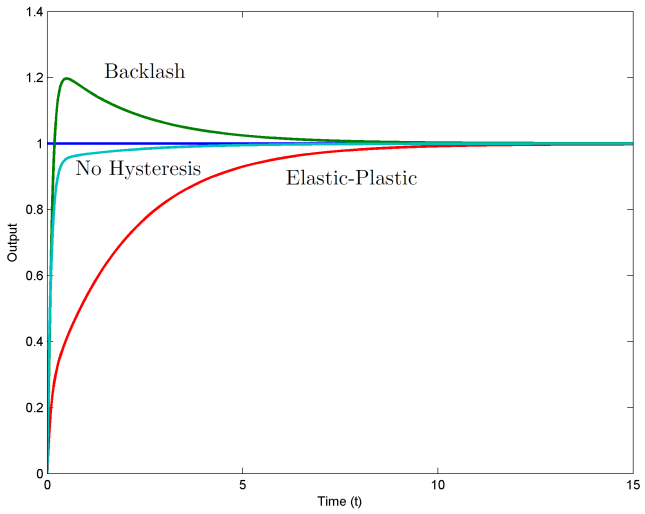

Figure 4.5: Tracking of a Constant Reference Signal: Backlash and Elastic-Plastic, $K_P = 10$, $K_I = 5$, $bfac = 3$, $efac = 3$

of using $K_I > K_P$ is shown for the backlash operator with $K_P = 5$ and $K_I = 10$ in Figure 4.6. It can be seen in Figure 4.6 that the system is stable, but tracking occured very slowly as many overshoots (and undershoots) were observed. The reasoning behind the overshoots was the same as previously described. The system exhibited change only after enough error was accumulated in the integral. As the output of the system approached the reference signal, the error $e(t)$ decreased, requiring an even longer time for the integral to grow.

Preisach Operator

Since assumptions **(A1)** - **(A4)** were shown to imply **(N1)** - **(N6)**, the results shown in Section 3.6 are applicable to the Preisach operator. The piecewise constant function can be approximated arbitrarily closely by a continuous function. The major loop produced by the Terfenol-D data has an upper limit of 0.7468, so only values between -0.7468 and 0.7468 can be tracked. This is shown in Figure 4.3.

4.3.2 Tracking Of Other Reference Signals

Although the theory presented in this thesis only covers the tracking of constant reference signals, the application of tracking other signals can be performed with suitable parameters. Figures 4.8 and 4.9 demonstrate the tracking of a piecewise ramp function with the three programmed hysteresis operators. The ramp function in Figure 4.9 is scaled due to the saturation of the Preisach model for the given weight function. The tracking of sinusoidal functions with varying amplitude can

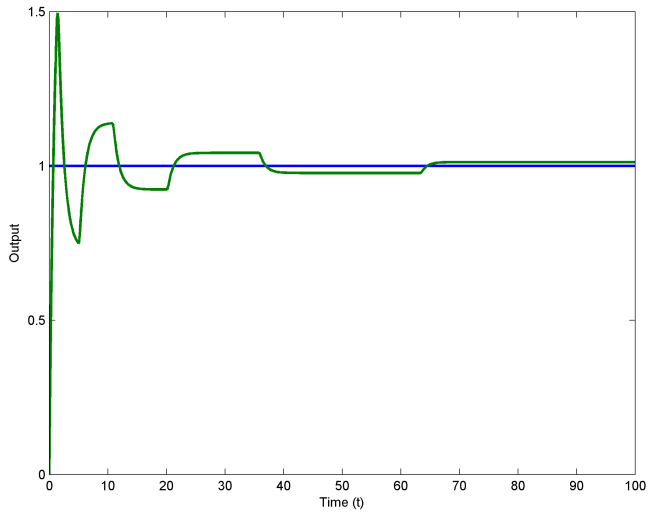

Figure 4.6: Tracking of a Constant Reference Signal: Backlash, $K_P = 5$, $K_I = 10$, $bfac = 3$

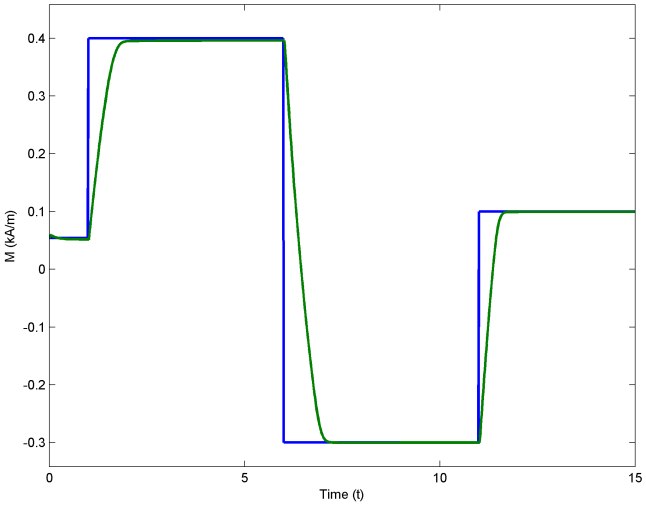

Figure 4.7: Tracking of a Piecewise Constant: Preisach Operator, $K_P = 100$, $K_I = 10$

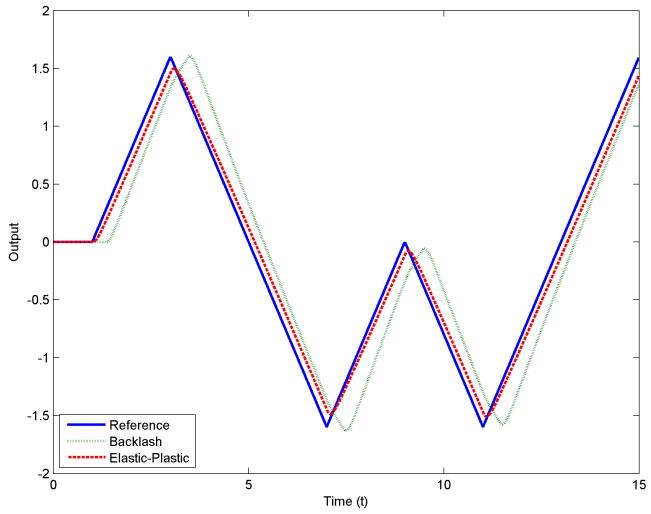

Figure 4.8: Tracking of a Piecewise Ramp Function: Backlash and Elastic Plastic Operators, $K_P = 10$, $K_I = 5$

be seen in Figures 4.10 and 4.11.

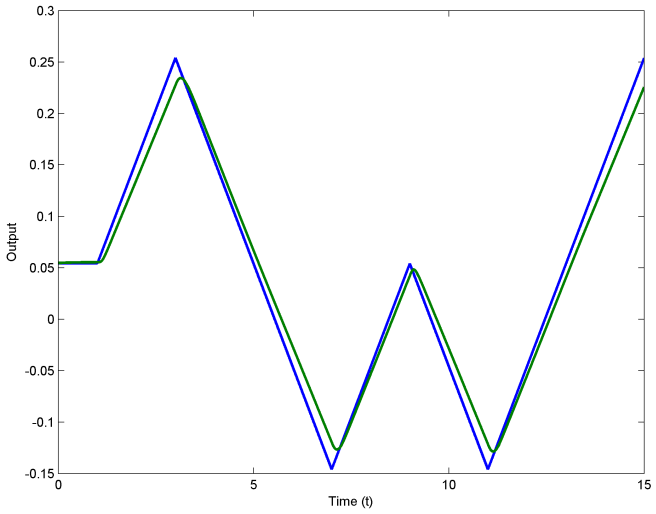

Figure 4.9: Tracking of a Piecewise Ramp Function: Preisach Operator, $K_P = 100$, $K_I = 10$

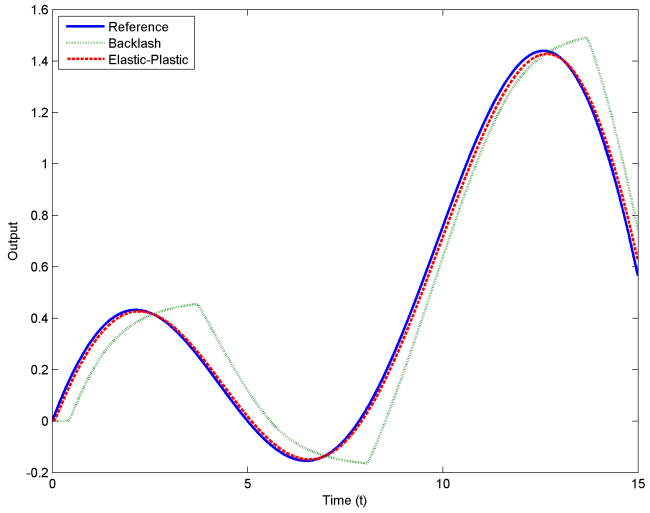

Figure 4.10: Tracking of a Sinusoidal Function with Varying Amplitude: Backlash and Elastic Plastic Operators, $K_P = 20$, $K_I = 10$, $r(t) = 0.2(5 - t)\sin(0.4t)$

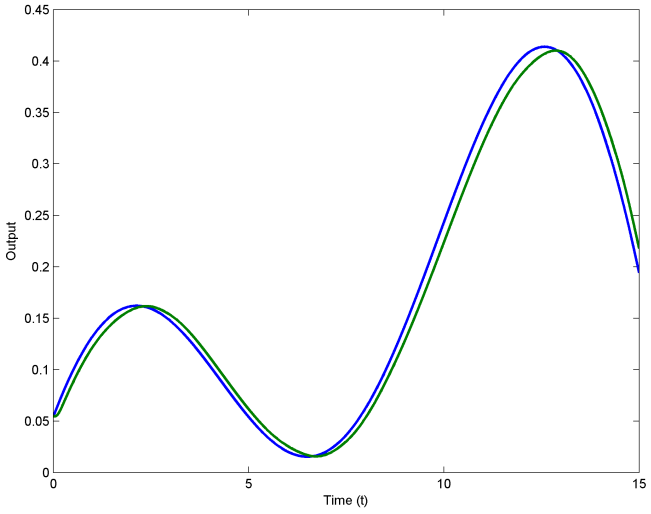

Figure 4.11: Tracking of Sinusoidal Function with Varying Amplitude: Preisach Operator, $K_P = 100$, $K_I = 40$, $r(t) = 0.05(5 - t)\sin(0.4t) + 0.0540$

Chapter 5

Conclusions and Future Work

In this thesis the control of systems with hysteresis was mathematically investigated. A review of hysteresis models was presented including a detailed formulation of the Preisach, backlash and elastic-plastic models. An overview of some of the other control methods employed to solve this control problem were discussed.

The control of two similar hysteretic systems has been the focus of this thesis. The first system whose output exhibited hysteretic effects, used a PI controller to track a reference signal. A BIBO-stability property is shown for continuous signals, and the tracking of a constant signal was shown to be asymptotic. In particular, a bound on the time to reach an arbitrarily small error was found. The original plant is extended to include a first-order system, and stability is shown for a range of parameters. Some simulations were performed on this first-order system.

The second system described the PID control of a second-order system. The input to the second-order system was modeled to include hysteresis. The tracking for a constant reference signal was shown to be asymptotic. The results were then verified for a first order system. Both systems included hysteresis described by two different sets of assumptions. The assumptions for each of these systems were compared, and the assumptions used for the first system was found to be essentially a subset of the those used in the second system.

Possible avenues of future work include extending the results for both systems to linear systems of arbitrary order. Such an extension would allow for better modelling of the actuator. Experimental results suggest that this bound is only a sufficient condition for stability. Alternative theory could be investigated that would guarantee stability and tracking for a larger range of parameters.

APPENDICES

Appendix A

Proofs and Details

Detailed calculations/details and proofs that were omitted in other sections are presented here.

A.1 Existence and Uniqueness Proof

The reasoning behind defining the following conditions may not be intuitive, but will become more apparent in subsequent theorems as to why they were defined in that manner. Logemann breaks his findings into successive theorems, which are each small steps to the final product. As a result, an existence uniqueness proof will be provided for a more general system, than that of Theorem 3.5.9. The pertinent system is:

$$x'(t) = (F(u))(t), \qquad t > \alpha, \tag{A.1}$$
$$x(t) = w(t), \qquad t \in [0, \alpha], \tag{A.2}$$

where $\alpha \geq 0$ and $w \in C([0, \alpha])$, (if $\alpha = 0$, then $C([0, \alpha]) = \mathbb{R}$). Assume that $F : C(\mathbb{R}_+) \to L^1_{\text{loc}}(\mathbb{R}_+)$ is causal and satisfies **(H1) and (H2)** where:

(H1) For all $a \geq 0$ and $v \in C([0, a])$, there exist $\delta > 0$, $\gamma > 0$, and a function $f : [0, \gamma] \to \mathbb{R}_+$, with $f(0) = 0$, continuous, such that for all $\epsilon \in (0, \gamma]$.

$$\int_a^{a+\epsilon} |(F(v_1))(\tau) - (F(v_2))(\tau)| \mathrm{d}\tau \leq f(\epsilon) \max_{\tau \in [a, a+\epsilon]} |v_1(\tau) - v_2(\tau)|,$$
$$\text{for all } v_1, v_2 \in C(w; \delta, \epsilon)$$

where $B(v; \delta, \epsilon) := \{p \in C([0, \alpha + \epsilon]) : p|_{[0,\alpha]} = v, \max_{t \in [\alpha, \alpha+\gamma]} |p(t) - v(\alpha)| \leq \delta\}$. This was defined earlier in Equation (3.23) to be the ϵ - long extensions of $v(t)$ from α,

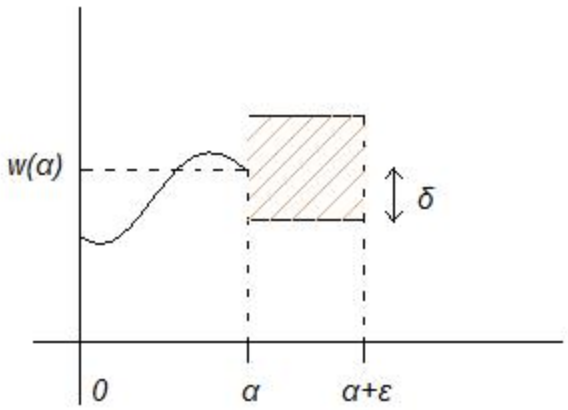

Figure A.1: Depicting the set $B(w; \delta, \epsilon)$

that are within δ of $v(\alpha)$. This set is depicted in Figure A.1. An element of the set $B(v; \delta, \epsilon)$ must be identical to the function v from $[0, \alpha]$ and continuous, within (and including) the boundary of shaded box from $(\alpha, \alpha + \epsilon]$.

The second hypothesis is:

(H2) For all $a > 0$ and $v \in C([0, a))$, there exists $c > 0$ such that

$$\int_0^t |(F(v))(\tau)| \mathrm{d}\tau \leq c(1 + \max_{\tau \in [0,t]} |v(\tau)|), \text{ for all } t \in [0, a).$$

The existence and uniqueness claim is as follows:

Lemma A.1.1. *For every $\alpha \geq 0$ and every $w \in C([0, \alpha])$, there exists a unique solution x of (A.1), defined on a maximal interval $[0, t_{max})$ with $t_{max} > \alpha$. Moreover, if $t_{max} < \infty$, then*

$$\limsup_{t \to t_{max}} |x(t)| = \infty.$$

Proof. First, existence and uniqueness will be established on a small interval, then uniqueness will be established on the maximal solution, then finally it will be shown that if $t_{max} < \infty$ then the solution becomes unbounded.

Step 1. Existence and uniqueness on a small interval.

The aim here is to define an operator that has a fixed point, which is a solution to Equation (A.1). If the operator is a contraction mapping, then the fixed point must be unique, and hence existence and uniqueness can be established on a small interval. First, the desired operator, acting on $y \in C([0, \alpha + \epsilon])$ is:

$$(\Gamma^\epsilon(y))(t) = \begin{cases} w(t), & t \in [0, \alpha] \\ w(\alpha) + \int_\alpha^t (F(y))(\tau) \mathrm{d}\tau, & t \in (\alpha, \alpha + \epsilon], \end{cases}$$

with the metric $d(v_1, v_2) = \max_{\tau \in [\alpha, \alpha+\epsilon]} |v_1(\tau) - v_2(\tau)|$. Since the range of the functions in $C(w; \delta, \epsilon)$ on $[\alpha, \alpha + \epsilon]$ is a closed set, then $(B(w; \delta, \epsilon), d)$ is a complete metric space. It remains to show that for small enough $\epsilon \in (0, \gamma]$, Γ^ϵ acting on $B(w; \delta, \epsilon)$ is a contraction map. As a result, the following two properties must be shown.

1) $\Gamma^\epsilon(B(w; \delta, \epsilon)) \subset B(w; \delta, \epsilon)$.

2) There exists $0 < \lambda \leq 1$ that for every $v_1, v_2 \in B(w; \delta, \epsilon)$,

$$d(\Gamma^\epsilon(v_1)), (\Gamma^\epsilon(v_2))) \leq \lambda d(v_1, v_2).$$

For the first condition, consider the definition of Γ^ϵ. Given $v \in B(w; \delta, \epsilon)$, it is clear that $\Gamma^\epsilon(v) = w$ on $[0, \alpha]$ and that it is continuous on $[0, \alpha + \epsilon]$. It remains to show that for small enough ϵ, $\Gamma^\epsilon(v)$ does not escape the δ-bound. Defining the following function facilitates the next calculation.

$$\tilde{w}(t) = \begin{cases} w(t), & t \in [0, \alpha] \\ w(\alpha), & t \in (\alpha, \alpha + \epsilon]. \end{cases}$$

It is clear that $\tilde{w}$ belongs to $B(w; \delta, \epsilon)$. Considering $t \in [\alpha, \alpha + \epsilon]$, an estimation yields:

$$
\begin{aligned}
|((\Gamma^\epsilon)(v))(t) - w(\alpha)| &= \left| \int_\alpha^t (F(v))(\tau) \mathrm{d}\tau \right| \\
&\leq \int_\alpha^t |(F(v))(\tau)| \mathrm{d}\tau \\
&\leq \int_\alpha^{\alpha+\epsilon} |(F(v))(\tau)| \mathrm{d}\tau \\
&\leq \int_\alpha^{\alpha+\epsilon} |(F(v))(\tau) - (F(\tilde{w}))(\tau)| \mathrm{d}\tau + \int_\alpha^{\alpha+\epsilon} |(F(\tilde{w}))(\tau)| \mathrm{d}\tau, \text{ by (H1)}, \\
&\leq f(\epsilon) \max_{\tau \in [\alpha, \alpha+\epsilon]} |v(\tau) - w(\alpha)| + \int_\alpha^{\alpha+\epsilon} |(F(\tilde{w}))(\tau)| \mathrm{d}\tau \\
&\leq f(\epsilon)\delta + \tilde{f}(\epsilon),
\end{aligned}
$$

where $\tilde{f}(\epsilon) = \int_\alpha^{\alpha+\epsilon} |(F(\tilde{w}))(\tau)| \mathrm{d}\tau$. The first term approaches 0 because $f(\epsilon) \to 0^+$ as $\epsilon \to 0^+$. Since $F(\tilde{w}) \in L^1_{loc}(\mathbb{R}_+)$, taking $\epsilon \to 0^+$ results in $\tilde{f}(\epsilon) \to 0^+$. Given δ, ϵ can be shrunk small enough that $|((\Gamma^\epsilon)(v))(t) - w(\alpha)| = |\int_\alpha^t (F(v))(\tau)\mathrm{d}\tau| \leq \delta$. Let ϵ_1 be the largest of such ϵ. Note that such an ϵ_1 can be found, since it the inequality includes the endpoint. Thus for $\epsilon \in (0, \epsilon_1]$, $\Gamma^\epsilon(B(w; \delta, \epsilon)) \subset B(w; \delta, \epsilon)$. Next, since $\Gamma^\epsilon(v_1) = \Gamma^\epsilon(v_2)$ on $t \in [0, \alpha]$ only $t \in [\alpha, \alpha + \epsilon]$ need to be considered.

$$
\begin{aligned}
|\Gamma^\epsilon(v_1) - \Gamma^\epsilon(v_2)| &\leq \int_\alpha^{\alpha+\epsilon} |(F(v_1))(\tau) - (F(v_2))(\tau)| \mathrm{d}\tau \\
&\leq f(\epsilon) d(v_1, v_2).
\end{aligned}
$$

Since this is valid for all $t \in [0, \alpha + \epsilon]$, the max case is included. Again by shrinking ϵ, $f(\epsilon) < 1$ can be achieved. Let ϵ_2 be such an ϵ (the same largest argument made for ϵ_1 cannot be made here since it is a strict inequality). Take $\epsilon^* = \min(\epsilon_1, \epsilon_2)$. For all $\epsilon \in (0, \epsilon^*]$, Γ^ϵ is a contraction map on $B(w; \delta, \epsilon)$. There exists a unique solution x to the system (A.1) on $B(w; \delta, \epsilon)$. However, this does not exclude the case that other solutions could exist outside of this space. That is, other solutions could protrude out of the shaded box when the boundary is reached. For this reason, let $\epsilon^{**} \leq \epsilon^*$ be the first time the boundary is reached (if the boundary is not reached then let $\epsilon^{**} = \epsilon^*$). If $t \in [\alpha, \alpha + \epsilon^{**})$, $|x(t) - w(\alpha)| < \delta$, no other solutions can exist on this interval. Thus, there exists a unique solution $x \in C([0, \alpha + \epsilon^{**}])$ to (A.1).

Step 2 Extended Uniqueness.

The idea is to apply Step 1 repeatedly using the subsequent $\alpha + \epsilon^{**}$ as the new α. Uniqueness will be demonstrated to hold in this process. Let $x_1 \in C([0, \alpha_1))$ and $x_2 \in C([0, \alpha_2))$ be solutions to (A.1) on their respective domains of definition.

Let $\beta := \min\{\alpha_1, \alpha_2\}$. Claim that $x_1 = x_2$ on $[0, \beta)$. Seeking a contradiction, define:

$$\alpha^* := \inf\{t \in [0, \beta) : x_1(t) \neq x_2(t)\} < \beta,$$

That is, α^* is the last point on which the functions x_1, x_2 are equal. Let $x(t) = x_1(t) = x_2(t)$ on $[0, \alpha^*]$. Apply Step 1 again on α^*, so that there exists ϵ such that $0 < \epsilon < \beta - \alpha^*$, where there exists a unique solution x on $C([0, \alpha^* + \epsilon])$, contradicting the definition of α^*.

Step 3 Existence of a maximal solution.

If Steps 1 and 2 are applied successively, then a unique maximal solution is obtained. Formally, let T be the set of all $\tau > \alpha$ s.t. there exists a solution x^τ to (A.1) on the interval $[0, \tau)$. From Step 1, T $\neq 0$. Let $t_{max} := \sup$ T and define $x : [0, t_{max}) \to \mathbb{R}$ by setting $x(t) = x^\tau(t)$ for $t \in [0, \tau)$ where $\tau \in$ T. Since this applies to all $\tau \in$ T, then this is the maximal solution of (A.1). Uniqueness follows from Step 2.

Step 4 If $t_{max} < \infty$, x is unbounded.

This is the last claim of Lemma A.1.1. It will be shown via a contrapositive proof. Consider x bounded on $[0, t_1)$ where $t_1 < \infty$. Integrating A.1 yields:

$$x(t) = x(\alpha) + \textstyle\int_\alpha^t (F(x))(\tau) \mathrm{d}\tau, \text{ for all } t \in [\alpha, t_1)$$

By(H2), there exists $c > 0$ such that,

$$\int_\alpha^t |(F(x))(\tau)| \mathrm{d}\tau \leq c(1 + \sup_{\tau \in [0, t_1]} |x(\tau)|) < \infty,$$

so $F(x) \in L^1([0, t_1])$, and $\lim_{t \to t_1} x(t)$ exists and is finite. Step 1 can be applied. However, since t_1 was arbitarily chosen, this argument works for all $t_1 \in (0, \infty)$. Therefore $t_{max} = \infty$. □

A.2 Showing (3.25) satisfies Lemma A.1

The system in (3.25) will be shown to satisfy **(H1)** and **(H2)**, and that there is no finite escape time (that is from Lemma A.1, x must be bounded locally). Let $F : C(\mathbb{R}_+) \to L^1_{loc}(\mathbb{R}_+)$ be defined by

$$F(v) := \kappa(\rho - \eta - (\mathcal{G} \circ \Phi)(v))$$

To show that F satisfies **(H1)**. Let $a \geq 0$, and $v \in C([0, a])$.

$$\begin{aligned}
\int_a^{a+\epsilon} |(F(v_1))(\tau) - (F(v_2))(\tau)| \mathrm{d}\tau &= \int_a^{a+\epsilon} |\kappa(t)(\mathcal{G}(\Phi(v_1) - \Phi(v_2)))(\tau)| \mathrm{d}\tau \\
&\leq \|\kappa\|_{L^\infty(\mathbb{R}_+)} \int_a^{a+\epsilon} |\kappa(t)(\mathcal{G}(\Phi(v_1) - \Phi(v_2)))(\tau)| \mathrm{d}\tau \\
&\text{by Holder's inequality, using the function itself 1} \\
&\leq \sqrt{\epsilon} \|\kappa\|_{L^\infty(\mathbb{R}_+)} \|\mathcal{G}\| \|(\Phi(v_1) - \Phi(v_2))\|_{L^2([a,a+\epsilon])} \\
&\leq \epsilon \|\kappa\|_{L^\infty(\mathbb{R}_+)} \|\mathcal{G}\| \|(\Phi(v_1) - \Phi(v_2))\|_{C([a,a+\epsilon])}, \text{ by (N3)} \\
&\leq \epsilon\lambda_1 \|\kappa\|_{L^\infty(\mathbb{R}_+)} \|\mathcal{G}\| \|(v_1 - v_2)\|_{C([a,a+\epsilon])}
\end{aligned}$$

Assumption **(H1)** holds with

$$f(\epsilon) := \epsilon\lambda_1 \|\kappa\|_{L^\infty(\mathbb{R}_+)} \|\mathcal{G}\|.$$

To establish **(H2)**, let $a > 0$, $v \in C([0, a))$. For $t \in [0, a)$,

$$\begin{aligned}
\int_0^t |(F(v))(\tau)| \mathrm{d}\tau &\leq \|\kappa\|_{L^\infty(\mathbb{R}_+)} \int_0^t |\rho - \eta(\tau) - ((\mathcal{G} \circ \Phi)(v))(\tau)| \mathrm{d}\tau, \\
&\leq \|\kappa\|_{L^\infty(\mathbb{R}_+)} [\rho t + \int_0^t |\eta(\tau)| \mathrm{d}\tau + \int_0^t |(\mathcal{G}(\Phi(v)))(\tau)| \mathrm{d}\tau], \\
&\leq \|\kappa\|_{L^\infty(\mathbb{R}_+)} [\rho a + \int_0^a |\eta(\tau)| \mathrm{d}\tau + \int_0^t |(\mathcal{G}(\Phi(v)))(\tau)| \mathrm{d}\tau].
\end{aligned}$$

Considering only the last term:

$$\begin{aligned}
\int_0^t |(\mathcal{G}(\Phi(v)))(\tau)| \mathrm{d}\tau &= \|\mathcal{G}(\Phi(v)) \cdot 1\|_{L^1_{[0,t]}}, \text{using Holder's inequality} \\
&\leq \|\mathcal{G}(\Phi(v))\|_{L^2_{[0,t]}} \|1\|_{L^2_{[0,t]}} \\
&\leq \sqrt{t} \left(\int_0^t |(\mathcal{G}(\Phi(v)))(\tau)|^2 \mathrm{d}\tau \right)^{\frac{1}{2}}, \\
&\text{taking the supremum and factoring out the terms of the integral,} \\
&\leq t \|\mathcal{G}\| \max_{\tau \in [0,t]} |(\Phi(v))(\tau)|, \text{ by (N4) and } t \leq a, \\
&\leq a \|\mathcal{G}\| \beta(1 + \max_{\tau \in [0,t]} |v(\tau)|)
\end{aligned}$$

Since $\max_{\tau\in[0,t]} |v(\tau)| > 0$, from the above two sets of inequalities:

$$\begin{aligned}\int_0^t |(F(v))(\tau)|\mathrm{d}\tau &\leq \|\kappa\|_{L^\infty(\mathbb{R}_+)} [\rho a + \int_0^a |\eta(\tau)|\mathrm{d}\tau + a\,\|\mathcal{G}\|\,\beta(1 + \max_{\tau\in[0,t]} |v(\tau)|)],\\ &\leq \|\kappa\|_{L^\infty(\mathbb{R}_+)} [\rho a + \int_0^a |\eta(\tau)|\mathrm{d}\tau + a\,\|\mathcal{G}\|\,\beta] \cdot (1 + \max_{\tau\in[0,t]} |v(\tau)|).\end{aligned}$$

The operator F satisfies **(H2)** with

$$c := \|\kappa\|_{L^\infty(\mathbb{R}_+)} [\rho a + \textstyle\int_0^a |\eta(\tau)|\mathrm{d}\tau + a\,\|\mathcal{G}\|\,\beta].$$

There exists a unique solution x to A.1 defined on a maximal interval $[0, t_{max})$. It remains to show that x does not have finite escape time, that is, x is bounded locally. Let $t_1 > 0$ be an arbitrary time. Integrating (3.25) for $t \in [0, t_1)$ yields:

$$x(t) = x(0) + \int_0^t [\kappa(\tau)(\rho - \eta(\tau) + (\mathcal{G}(\Phi(x)))(\tau))]\mathrm{d}\tau.$$

However, the bound on $\max_{\sigma\in[0,t]} |x(\sigma)|$ will be considered in place of the usual $|x(t)|$. This will be more useful since **(N4)** yields x back in this form, and the proof relies on an application of Gronwall's Lemma. Making an estimate using the same tools as seen previously in this proof:

$$\max_{\sigma\in[0,t]} |x(\sigma)| \leq |x(0)| + \|\kappa\|_{L^\infty(\mathbb{R}_+)} [\rho t + \int_0^t |\eta(\tau)|\mathrm{d}\tau + \int_0^t |(\mathcal{G}(\Phi(u)))(\tau)|\mathrm{d}\tau], \text{ for all } t \in [0, t_1). \tag{A.3}$$

Estimating the last term (and applying **(N4)** in the second last step) yields:

$$\begin{aligned}\int_0^t |(\mathcal{G}(\Phi(x)))(\tau)|\mathrm{d}\tau &\leq \sqrt{t}\left(\int_0^t |(\mathcal{G}(\Phi(x)))(\tau)|^2\mathrm{d}\tau\right)^{\frac{1}{2}},\\ &\leq \sqrt{t_1}\,\|\mathcal{G}\|\left(\int_0^t \max_{\sigma\in[0,\tau]} |(\Phi(x))(\sigma)|^2\mathrm{d}\tau\right)^{1/2}\\ &\leq \sqrt{t_1}\,\|\mathcal{G}\|\left(\int_0^{t_1} \max_{\sigma\in[0,\tau]} (1 + |x(\sigma)|)^2\mathrm{d}\tau\right)^{1/2}\\ &\leq \sqrt{2t_1}\,\|\mathcal{G}\|\left(\int_0^{t_1} \max_{\sigma\in[0,\tau]} (1 + |x(\sigma)|^2)\mathrm{d}\tau\right)^{1/2}.\end{aligned}$$

The last step used the inequality $2a^2+2b^2 \geq (a+b)^2+(a-b)^2 \geq (a+b)^2$. Next, let $\tilde{x}(t) := \max_{\sigma\in[0,t]} |x(\sigma)|$. Since t_1 is fixed, there exists constants β_1 and β_2 (simply by equating components) such that

$$\tilde{x}(t) \leq \beta_1 + \beta_2 \left(\int_0^t (1 + (\tilde{x}^2(\tau)))\mathrm{d}\tau \right)^{1/2}.$$

Thus,

$$\begin{aligned}
\tilde{x}^2(t) &\leq \left(\beta_1 + \beta_2 \left(\int_0^t (1 + \tilde{x}^2(\tau))\mathrm{d}\tau \right)^{1/2} \right) \\
&\leq 2\beta_1^2 + 2\beta_2^2 \left(\int_0^t (1 + \tilde{x}^2(\tau))\mathrm{d}\tau \right) \\
&\leq 2\beta_1^2 + 2\beta_2^2 t_1 + 2\beta_2^2 \int_0^t \tilde{x}^2(\tau)\mathrm{d}\tau, \text{ for all } t \in [0, t_1).
\end{aligned}$$

Applying Gronwall's Lemma:

$$\tilde{x}^2(t) \leq (2\beta_1^2 + 2\beta_2^2 t_1) \exp(2\beta_2^2 t_1), \text{ for all } t \in [0, t_1).$$

But since t_1 was chosen arbitrarily, this argument holds for $t_1 \in (0, \infty)$, so x is bounded locally. Hence x does not have finite escape time.

A.3 Leibniz's Rule for Convolution Differentiation

Here, Leibniz's integral rule will be applied to the differentiation of a convolution. Let g and h be functions defined on the right-half real line, and let $f(\tau, t) = g(\tau)h(t-\tau)$.

$$\begin{aligned}
&\frac{d}{dt}\left(g(t) \star h(t)\right) \\
=&\frac{d}{dt}\left(\int_0^t g(\tau)h(t-\tau)d\tau \right) \\
=&\frac{d}{dt}\left(\int_0^t f(\tau, t)d\tau \right)
\end{aligned}$$

Leibniz's rule states:

$$\frac{\partial}{\partial z}\int_{a(z)}^{b(z)} f(x,z)dx = \int_{a(z)}^{b(z)} \frac{\partial f}{\partial z}dx + f(b(z),z)\frac{\partial b}{\partial z} - f(a(z),z)\frac{\partial a}{\partial z},$$

so from above:

$$\begin{aligned}
&\frac{d}{dt}(g(t) \star h(t)) \\
=&f(t,t) + 0 + \int_0^t g(\tau)h'(t-\tau)d\tau \\
=&g(t)h(0) + g(t) \star h'(t) \\
=&g(t) \star h(0)\delta_0 + g(t) \star h'(t)
\end{aligned}$$

but since convolution is commutative:

$$\begin{aligned}
&\frac{d}{dt}(g(t) \star h(t)) \\
=&\frac{d}{dt}(h(t) \star g(t)) \\
=&h(t) \star g(0)\delta_0 + h(t) \star g'(t)
\end{aligned}$$

A.4 Left Half Complex Plane Poles → Exponentially Decaying Functions

A brief justification of the poles of a second-order transfer function having negative real part → exponentially decays is given here. This result can be readily extended to higher order systems. It can be verified that:

$$\hat{h}(s) = \frac{1}{ms^2 + cs + k}.$$

Note that the coefficients of the polynomial in the denominator of $\hat{h}(s)$ are real. The transfer function of ρ has the same denominator, so the exact same argument can be applied. This implies that the roots of $p(s) := ms^2 + cs + k$ are either real, or occur in complex conjugates. By the fundamental theorem of algebra, $\hat{h}(s)$ can be written as:

$$\hat{h}(s) = \frac{\frac{1}{m}}{(s-a_1)(s-a_2)},$$

where in general $a_1, a_2 \in \mathbb{C}$. Since $p(s)$ is a second degree real coefficient polynomial, either the roots are both strictly real, or are complex conjugates. Suppose all of a_1, a_2 are real. Then there exists a unique partial fraction decomposition, such that:

$$\hat{h}(s) = \frac{A_1}{s - a_1} + \frac{A_2}{s - a_2}$$

such that $A_1, A_2 \in \mathbb{R}$. By linearity of the Laplace transform, $h(t)$ is the sum of the inverse Laplace transforms of each of the terms above.

$$L^{-1}(\hat{h}(s)) = h(t) = A_1 e^{a_1 t} + A_2 e^{a_2 t}$$

Knowing that $a_1, a_2 < 0$ it is clear that h exponentially decays as $t \to \infty$. Consider the other case, where a_1, a_2 are complex conjugates. Hence, the polynomial $(s - a_1)(s - a_2) = (s^2 - (a_1 + a_2)s + a_1 a_2)$ would have real coefficients. Again, by partial fraction decomposition, there exists a unique $B_1, B_2 \in \mathbb{R}$ such that

$$\hat{h}(s) = \frac{B_1 s + B_2}{s^2 - (a_1 + a_2)s + a_1 a_2},$$

whose inverse Laplace transform would be $h(t) = f(t)e^{Re(a_1)t}$, where $f(t)$ is a bounded oscillatory function (a sum of sine and cosine functions). Again by the Hurwitz condition, $\mathrm{Re}(a_i) < 0$ for $i = 1, 2$, therefore h exponentially decays as $t \to \infty$. Therefore if the poles of $\hat{h}(s)$ are Hurwitz, then h decays exponentially and hence $h \in L^2_\alpha(\mathbb{R}_+)$. Because of the form of h, any linear combination of its derivatives must also be exponentially decaying.

Appendix B

MATLAB® Code

The code used to produce the simulations will be presented here. The following is the code used for the backlash model.

```
function [y,binc] = backlashfast(u1,u2,u3,curbinc,bfac)
%u1 = present u, u2 = u one time step ago,
%u3 = u one time step before u2

%Initial operator value.

y = bh(bfac,u1,curbinc);
if sign(u1-u2) ~= sign(u2-u3)
    binc = y;
else
    binc = curbinc;
end
%When u ceases to be monotone,
%the next subinterval in the partition
%begins.

end
```

```
function output = bh(h,v,w)
output = max(v-h,min(v+h,w));
%Defines the bh function needed to define the backlash operator.
end
```

The elastic-plastic operator is defined similarly.

```
%Defined structurally the same as the fast backlash operator.
function [y,einc,uinc] =...
 elasticplasticfast(u1,u2,u3,cureinc,curuinc,efac)

y = eh(efac,u1 - curuinc + cureinc);
if sign(u1-u2) ~= sign(u2-u3)
    einc = y;
    uinc = u1;
else
    einc = cureinc;
    uinc = curuinc;
end

function output = eh(h,u)
output = min(h,max(-h,u));
end
```

The Preisach model required several functions. The function *buildlinesegments* identified the locations of all the line segments that form the boundary. The function *findbound* found all the relevant points that make up the boundary from a given input.

```
function [v,boundaryout] =...
 preisachtestweight(u,usat,boundaryin,weight)

%v,boundaryout

%a is the distance from the bottom of the
%cell to where the boundary is
%b is 1 if a had to be modified
%(i.e. the rounding function put a and the
%boundary in two different cells)
%c is a fix in the case of boundary = usat, or -usat

%initialize plane

gridsize = 0.5;
%note, gridsize must divide usat
%(i.e. usat/gridsize must be a natural number)
relsize = round(usat/gridsize);
plane = zeros(relsize*2,relsize);
for i=1:1:relsize
```

```
    for j=1:1:i
    plane(i,j) = -1;
    plane(relsize*2-i+1,j) = 1;
    end
    plane(i,i) = -0.5;
    plane(relsize*2-i+1,i)=0.5;
end
if abs(u(end)) < usat

%initialize weighting
%if new corner emerges, or a corner is erased....
if size(boundaryin,2)>1
if sign(boundaryin(end) - boundaryin(end-1)) ~=...
 sign(u(end) - boundaryin(end)) || abs(u(end)) >= abs(boundaryin(end-1))
boundary = findbound(u,usat);
else
 boundary = [boundaryin(1:end-1),u(end)];
end
else
 boundary(1) = min(usat,max(-usat,u(end)));
 if size(u,2) > 1
 boundary(1) = min(usat,max(-usat,u(end-1)));
    end
    if sign(boundary(1))==...
      -sign(u(end)-boundary(1)) && abs(boundary(1))~=usat
        boundary(2) = u(end);
    end
end
lineseg = buildlinesegments(boundary);

a=0;
b=0;
c=0;
boundaryout = boundary;
%offset for boundary
if abs(boundary) == usat
    c = 1;
end

%Start editing the plane:
%cls for current line segment

corners = zeros(size(plane));

for cls = 0:1:size(lineseg,1) - 1
```

```
%LOCATE CORNERS
if lineseg(end-cls,3)/gridsize ~=...
 floor(lineseg(end-cls,3)/gridsize)
    locy = relsize - floor(lineseg(end-cls,4)/gridsize);
    locx = floor(lineseg(end-cls,3)/gridsize)+1;
    corners(locy,locx) = corners(locy,locx)  + 1;
end

end

for cls = 0:1:size(lineseg,1) - 1

    %find   the sign of y2-y1
incdec = sign(lineseg(end-cls,4)-lineseg(end-cls,2));

%if there is no change, then the boundary is complete
%(i.e. we've hit the
%0 slope part of the boundary, note that this might not always occur
if incdec == 0
    if a~=1 && a~=0
        if term == 1
            plane(starty-i+b,stopx) = 2*a - a^2;
        else
            plane(starty+i-b,stopx) = a^2 - 1;
        end
    end
    break
end

%
diffx = lineseg(end-cls,1)/gridsize -...
 floor(lineseg(end-cls,1)/gridsize);
b = 0;
%Consider two seperate cases,
%where xmin does not fall on an edge of the
%cell, and one that does
if diffx ==0
%xmin touches the edge of a cell
    a = (lineseg(end-cls,2))/gridsize - ...
    floor((lineseg(end-cls,2))/gridsize);
else
%xmin does not touch the edge of a cell
    a = -incdec*diffx + (lineseg(end-cls,2))/gridsize -...
        floor(lineseg(end-cls,2)/gridsize);
end
```

```
if a > 1;
    a = a-1;
    b = 1;
end

if a < 0;
    a = a + 1;
    b=1;
end

%y2-y1 < 0
if incdec == -1
    startx = floor(lineseg(end-cls,1)/gridsize) + 1;
    stopx = floor(lineseg(end-cls,3)/gridsize) + 1;
    starty = relsize - floor(lineseg(end-cls,2)/gridsize);
    stopy = relsize - floor(lineseg(end-cls,4)/gridsize);
   %Build the in between points to the corners
   for i = 1+ceil(diffx):1:stopx-startx
   plane(starty + i -1 - b+c,startx + i - 1) = a^2 - 1;
   plane(starty + i -b,startx + i -1) = 2*a-a^2;
    %Rewrite cells:
    if starty+i-1-b > relsize + 1
        for j = 1:1:starty+i-1-b - relsize
            plane(starty + i - 1 - b - j, startx + i - 1) = -1;
        end
    end

    if starty+i-1-b < relsize - 1
        for j = 1:1:relsize - (starty+i-1-b) - 1
            plane(starty + i - b + j, startx + i - 1) = 1;
        end
    end
   end
    %Corners: (can only handle 1 per cell, for now...)
   if lineseg(end-cls,3)/gridsize -...
    floor(lineseg(end-cls,3)/gridsize)~=...
           0 && lineseg(end-cls,4) - lineseg(end-cls-1,4) ~=0
       diffx1 = lineseg(end-cls,3)/gridsize -...
           floor(lineseg(end-cls,3)/gridsize);
       diffx2 = ceil(lineseg(end-cls,3)/gridsize) -...
           lineseg(end-cls,3)/gridsize;
       %oa and ob determine the cells in the same column
       %as the corner cell
       %that need to be changed
```

```
oa = 0; ob = 0;
   if ceil(lineseg(end-cls,4)/gridsize) -...
           lineseg(end-cls,4)/gridsize - diffx1 >= 0
    a1 = ceil(lineseg(end-cls,4)/gridsize) -...
        lineseg(end-cls,4)/gridsize - diffx1;
    a2 = ceil(lineseg(end-cls,4)/gridsize) -...
        lineseg(end-cls,4)/gridsize;
    b1 = a2;
       if ceil(lineseg(end-cls,4)/gridsize) -...
              lineseg(end-cls,4)/gridsize - diffx2 >= 0
         b2 = ceil(lineseg(end-cls,4)/gridsize) -...
             lineseg(end-cls,4)/gridsize - diffx2;
       else
         b2 = 0; ob = 1;
         diffx2 = b1;
       end
   else
       a1 = 0; oa = 1;
       a2 = ceil(lineseg(end-cls,4)/gridsize) -...
           lineseg(end-cls,4)/gridsize;
       diffx1 = a2;
       b1 = a2;
       if ceil(lineseg(end-cls,4)/gridsize) -...
              lineseg(end-cls,4)/gridsize - diffx2 >= 0
         b2 = ceil(lineseg(end-cls,4)/gridsize) -...
             lineseg(end-cls,4)/gridsize - diffx2;
       else
         b2 = 0; ob = 1;
         diffx2 = b1;
       end

   end

 negarea = (a1 + a2)/2*diffx1 + (b1 + b2)/2*diffx2;
plane(stopy,stopx) = 1 - 2*negarea;
if stopy ==1
plane(stopy, stopx) = (oa*(1 -(ceil(lineseg(end-cls,3)/gridsize) -...
    lineseg(end-cls,3)/gridsize) -diffx1)^2 + ob*(1-...
    (lineseg(end-cls,3)/gridsize -...
    floor(lineseg(end-cls,3)/gridsize)) - diffx2)^2) - 1;
else
plane(stopy-1,stopx)=(oa*(1-(ceil(lineseg(end-cls,3)/gridsize)-...
    lineseg(end-cls,3)/gridsize) -diffx1)^2 + ob*(1-...
    (lineseg(end-cls,3)/gridsize -...
    floor(lineseg(end-cls,3)/gridsize)) - diffx2)^2) - 1;
```

```
        end
    if stopy-1-b > relsize + 1
        for j = 1:1:stopy-1-b - relsize
            plane(stopy - j - 1, stopx) = -1;
        end
    end

    if stopy-1-b < relsize - 1
        for j = 1:1:relsize - (stopy-1-b) - 1
            plane(stopy + j, stopx) = 1;
        end
    end

   end

end

%y2-y1 > 0
if incdec == 1
    startx = floor(lineseg(end-cls,1)/gridsize) + 1;
    stopx = floor(lineseg(end-cls,3)/gridsize) + 1;
    starty = relsize - floor(lineseg(end-cls,2)/gridsize);
    stopy = relsize - floor(lineseg(end-cls,4)/gridsize);
    %Build the in between points to the corners
    for i = 1+ceil(diffx):1:stopx-startx
   plane(starty - i + b,startx + i - 1) = a^2-1;
   plane(starty + 1 - i + b, startx + i - 1) = 2*a - a^2;
   %Rewrite cells:
   if starty-i + b > relsize + 1
        for j = 1:1:starty-i+b-relsize
            plane(starty - i + b - j, startx + i - 1) = -1;
        end
    end

    if starty-i+b < relsize
        for j = 1:1:relsize-(starty-i+b)-1
            plane(starty - i + b + j + 1, startx + i - 1) = 1;
        end
    end
    end

    %Corners: (can only handle 1 per cell, for now...)
   if lineseg(end-cls,3)/gridsize -...
    floor(lineseg(end-cls,3)/gridsize)~=...
           0 && lineseg(end-cls,4) - lineseg(end-cls-1,4) ~=0
```

```
diffx1 = lineseg(end-cls,3)/gridsize -...
    floor(lineseg(end-cls,3)/gridsize);
diffx2 = ceil(lineseg(end-cls,3)/gridsize) -...
    lineseg(end-cls,3)/gridsize;
%oa and ob determine the cells
%in the same column as the corner cell
%that need to be changed
oa = 0; ob = 0;
 if lineseg(end-cls,4)/gridsize -...
     floor(lineseg(end-cls)/gridsize) - diffx1 >= 0
  a1 = lineseg(end-cls,4)/gridsize - diffx1 -...
     floor(lineseg(end-cls,4)/gridsize);
  a2 = lineseg(end-cls,4)/gridsize -...
     floor(lineseg(end-cls,4)/gridsize);
    b1 = a2;
     if lineseg(end-cls,4)/gridsize -...
      floor(lineseg(end-cls,4)/gridsize) - diffx2 >= 0
      b2 = lineseg(end-cls,4)/gridsize - diffx2 -...
      floor(lineseg(end-cls,4)/gridsize);
     else
      b2 = 0; ob = 1;
      diffx2 = b1;
     end
 else
  a1 = 0; oa = 1;
  a2 = lineseg(end-cls,4)/gridsize -...
  floor(lineseg(end-cls,4)/gridsize);
  diffx1 = a2;
  b1 = a2;
   if lineseg(end-cls,4)/gridsize -...
    floor(lineseg(end-cls,4)/gridsize) - diffx2 >= 0
    b2 = lineseg(end-cls,4)/gridsize - diffx2 -...
    floor(lineseg(end-cls,4)/gridsize);
   else
    b2 = 0; ob = 1;
    diffx2 = b1;
   end

   end

 posarea = (a1 + a2)/2*diffx1 + (b1 + b2)/2*diffx2;
 plane(stopy,stopx) = 2*posarea - 1;
if stopy == size(plane,1)
 plane(stopy,stopx) = 1-...
 (oa*(1-(ceil(lineseg(end-cls,3)/gridsize) -...
```

```
            lineseg(end-cls,3)/gridsize) -diffx1)^2 + ob*(1-...
            (lineseg(end-cls,3)/gridsize -...
            floor(lineseg(end-cls,3)/gridsize)) - diffx2)^2);
        else
         plane(stopy+1,stopx) = 1-...
         (oa*(1-(ceil(lineseg(end-cls,3)/gridsize)-...
            lineseg(end-cls,3)/gridsize) -diffx1)^2 + ob*(1-...
            (lineseg(end-cls,3)/gridsize -...
            floor(lineseg(end-cls,3)/gridsize)) - diffx2)^2);
        end
    if stopy-1-b > relsize + 1
         for j = 1:1:stopy-1-b - relsize
            plane(stopy - j, stopx) = -1;
         end
    end

    if stopy-1-b < relsize - 1
         for j = 1:1:relsize - (stopy-1-b) - 1
            plane(stopy + j + 1, stopx) = 1;
         end
    end

   end


end

term = incdec;
end

%Fix the borders

for i = 1:1:usat/gridsize
       if plane(i,i)<=-1
          plane(i,i) = -0.5;
       end
       if 0<=plane(i+1,i) && plane(i,i)~=-0.5
       plane(i,i) = plane(i,i) + 0.5;
           if i > 1
           plane(i-1,i) = 0;
           end
       end
       if corners(i,i)~=0 && plane(i,i) <=0
           plane(i,i) = plane(i,i)+ 0.5;
       end
```

```
      if plane(end-i+1,i) >=1
          plane(end-i+1,i) = 0.5;
      end
      if 0>= plane(end-i,i) && plane(end-i+1,i)~= 0.5
          plane(end-i+1,i) = plane(end-i+1,i) -0.5;
          if i > 1
              plane(end-i+2,i) = 0;
          end
      end
 v = sum(sum(plane.*weight));


end
else
        v = sum(sum(weight))*sign(u(end));
        boundary(1) = usat*sign(u(end));
        boundaryout = boundary;
end


function boundary = findbound(u,usat)
%Finds the information necessary for the Preisach boundary

[val,ind] = max(abs(u));
if val > usat
    boundary(1) = usat*sign(u(ind));
else
boundary(1) = sign(u(ind))*val;
end
minmax = sign(u(ind));
unew = u(ind:end);
k=2;
while max(size(unew))>1
if minmax == 1
[val,ind] = min(unew);
if abs(val) > usat
    boundary(k) = -usat;
else
    boundary(k) = val;
end
k=k+1;
unew = unew(ind:end);
minmax=minmax*-1;
end
```

```
if minmax== -1
[val,ind]=max(unew);
if abs(val) > usat
    boundary(k) = usat;
else
    boundary(k) = val;
end
k=k+1;
unew = unew(ind:end);
minmax=minmax*-1;
end
if size(unew,2) > 1
if unew(1) == unew(2)
    unew = unew(2:end);
    k = k-1;
end
end
end

    if size(boundary,2)>1
    if boundary(end)==boundary(end-1)
        boundary = boundary(1:end-1);
    end
    end
end

function lineseg = buildlinesegments(boundary)
%lineseg is a matrix carrying details about the line segments:
%column 1: xmin, column 2: y at xmin, column 3: xmax,
%column 4: y at xmax

%initialize the line segments:
lineseg = zeros(size(boundary,2),4);
lineseg(1,1) = 0;
lineseg(1,2) = 0;
lineseg(1,3) = 10;
lineseg(1,4) = 0;
%The first two lines don't satisfy
%the "-1", "+1" properties since they
%deal with the 0 boundary
lineseg(2,1) = 0;
lineseg(2,2) = boundary(1);
lineseg(2,3) = abs(boundary(1));
lineseg(2,4) = 0;
```

```
lineseg(1,1) = lineseg(2,3);
lineseg(1,2) = lineseg(2,4);

for i = 3:1:size(boundary,2)+1
   %Build line segment matrix according to boundary
   %See Drawings
   lineseg(i,1) = 0;
   lineseg(i,2) = boundary(i-1);
   if boundary(i-1)-boundary(i-2)>0
       %Increasing
   lineseg(i,3) = (lineseg(i-1,3) -...
    lineseg(i-1,4) + lineseg(i,2))/2;
   lineseg(i,4) = (lineseg(i-1,4) -...
    lineseg(i-1,3) + lineseg(i,2))/2;
   else
       %Decreasing
   lineseg(i,3) = (lineseg(i-1,4) +...
    lineseg(i-1,3) - lineseg(i,2))/2;
   lineseg(i,4) = (lineseg(i-1,4) +...
    lineseg(i-1,3) + lineseg(i,2))/2;
   end
   for j=i:-1:2
       lineseg(j-1,1)=lineseg(j,3);
       lineseg(j-1,2)=lineseg(j,4);
   end
end
check = 0;
i=1;
while check ~=1
   if lineseg(i,1) ==lineseg(i,3)
      lineseg = [lineseg(1:i-1,:);lineseg(i+1:end,:)];
      i = i-1;
   end
   if i == size(lineseg,1)
      check = 1;
   end
   i=i+1;
end
```

The procedure that ran the ode4 Runge-Kutta solver was identical for all three hysteresis operators. Only the code for the backlash operator is presented here. Running the code for thee other operators would simply require a change in each place the backlash function is called and the inputs to each function.

```
function [time,y] = ...
ode4backlashfast(Kp,Ki,M,sigma,h,timesteps,bfac,Xi,r)

y = zeros(1,timesteps);
y(1) = 0;
y(2) = 0;
u = zeros(1,timesteps);
u(1) = 0;
u(2) = 0;
e = zeros(1,timesteps);
e(1) = r(0) - y(1);
e(2) = r(h) - y(2);
v = zeros(1,timesteps);
time = 0:h:h*timesteps-h;
t = 0;
curbinc = Xi;
epsilon = 0.001;
cumerror = h*(e(1) + e(2))/2;
k1 = M*bh(bfac,Kp*r(0),Xi);
k2 = -sigma*(0.5*h*k1) + M*bh(bfac,Kp*(r(0.5*h) - 0.5*k1*h) +...
    Ki*(0.25*h*(r(0.5*h) + r(0) - 0.5*h*k1)),Xi);
k3 = -sigma*(0.5*h*k2) + M*bh(bfac,Kp*(r(0.5*h) - 0.5*k2*h) +...
    Ki*(0.25*h*(r(0.5*h) + r(0) - 0.5*h*k1)),Xi);
k4 = -sigma*(h*k3) + M*bh(bfac,Kp*(r(h) - h*k3) +...
    Ki*0.5*(r(0.5*h) + r(0) - h*k1),Xi);

for i=3:1:timesteps

        y(i) = y(i-1) + h*(k1+2*k2+2*k3+k4)/6;
    e(i) = r(t) - y(i);
    cumerror = cumerror + h*(exp(epsilon*t)*e(i) +...
        exp(epsilon*(t-h))*e(i-1))/2;
    u(i) = Kp*(e(i)) + Ki*exp(epsilon*-t)*cumerror;
    k1 = -sigma*y(i) +...
     M*backlashfast(u(i),u(i-1),u(i-2),curbinc,bfac);
    u(i) = Kp*(r(t+0.5*h) - y(i) - 0.5*k1*h) + ...
        Ki*exp(-epsilon*(t+0.5*h))*(cumerror + ...
        0.25*h*(exp(epsilon*(t+0.5*h))*(r(t+0.5*h) ...
        - y(i) -0.5*h*k1)+exp(epsilon*t)*(r(t) - y(i))));
   k2 = -sigma*(y(i) + 0.5*k1*h) +...
       M*backlashfast(u(i),u(i-1),u(i-2),curbinc,bfac);
    u(i) = Kp*(r(t+0.5*h) - y(i) - 0.5*k2*h) +...
        Ki*exp(-epsilon*(t+0.5*h))*(cumerror +...
        0.25*h*(exp(epsilon*...
        (t+0.5*h))*(r(t+0.5*h) - y(i)-...
```

```
        0.5*h*k1)+exp(epsilon*t)*(r(t) - y(i))));
    k3 = -sigma*(y(i) + 0.5*k2*h) +...
        M*backlashfast(u(i),u(i-1),u(i-2),curbinc,bfac);
    u(i) = Kp*(r(t+h) - y(i) - h*k3) +...
        Ki*exp(-epsilon*(t+h))*(cumerror +...
        0.5*h*(exp(epsilon*(t+h))*(r(t+h) - y(i) -h*k1)+...
        exp(epsilon*t)*(r(t) - y(i))));
    k4 = -sigma*(y(i) + k3*h) +...
     M*backlashfast(u(i),u(i-1),u(i-2),curbinc,bfac);


    %Rewrite u(i) to be what we expected it to be originally
    u(i) = Kp*e(i) + Ki*exp(epsilon*-t)*cumerror;


    [void,binc] = backlashfast(u(i),u(i-1),u(i-2),curbinc,bfac);
    curbinc = binc;
    v(i-1) = backlashfast(u(i),u(i-1),u(i-2),curbinc,bfac);
    t = t+h;
    %i
end
v(i) = backlashfast(u(i),u(i-1),u(i-2),curbinc,bfac);
y(end) = y(end-1) + h*(k1+2*k2+2*k3+k4)/6;
```

References

[1] K.K. Ahn and N.B. Kha. Modeling and control of shape memory alloy actuators using Preisach model, genetic algorithm and fuzzy logic. *Mechatronics*, 18:141–152, 2008. 23

[2] F. Bagagiolo. Dynamic programming for some optimal control problems with hysteresis. *Nonlinear Differential Equations and Applications NoDEA*, 9:149–174, 2002. 60

[3] F. Bagagiolo. Viscosity solutions for an optimal control problem with Preisach hysteresis nonlinearities. *ESAIM: Control, Optimization and Calculus of Variations*, 10:271–294, 2004. 60

[4] M. Brokate and J. Sprekels. *Phase transitions and hysteresis*. Springer-Verlag, 1994. 4, 8, 13, 18, 23, 24, 25

[5] G.S. Choi, Y.A. Lim, and G.H. Choi. Tracking position control of piezoelectric actuators for periodic reference inputs. *Mechatronics*, 12:669–684, 2002. 23

[6] M.L. Corradini, G. Orlando, and G. Parlangeli. A VSC (variable structure control) approach for the robust stabilization of nonlinear plants with uncertain nonsmooth actuator nonlinearities - a unified framework. *IEEE Transactions on Automatic Control*, 54:807 – 813, 2004.

[7] R. Curtain, H. Logemann, and O. Staffans. Stability results of Popov-type for infinite-dimensional systems with applications to integral control. *Proc. London Math. Soc.*, 86:779–816, 2003.

[8] R. Curtain and H. Zwart. *An Introduction to Infinite-Dimensional Linear Systems Theory*. Springer, 1995. 21, 22, 50, 51

[9] C.A. Desoer and M. Vidyasagar. *Feedback Systems: Input-Output Properties*. Academic Press, 1975. 21, 35, 36, 37, 51

[10] D. Flynn, H. McNamara, P. OKane, and A. Pokrovskii. Application of the Preisach model in soil-moisture hysteresis. *Preprint*.

[11] R. Gorbet. *Control of Hysteresis systems with Preisach Representations*. PhD thesis, University of Waterloo, 1997. 8

[12] R. Gorbet, K. Morris, and D. Wang. Passivity-based stability and control of hysteresis in smartactuators. *IEEE Transactions on Control Systems Technology*, 9:5–16, January 2001. 8

[13] A. Hatch, R. Smith, and T. De. Model development and control design for high speed atomic force microscopy. *SPIE Conference, San Diego*, 2004. 62

[14] C. Hu and X. Zhang. Closed-loop control system of piezoceramic actuators with improved Preisach model. *Proceedings of the 7th World Congress on Intelligent Control and Automation*, pages 7385 – 7388, 2008. 23, 62

[15] F. Ikhouane, V. Maosa, and J. Rodellar. Adaptive control of a hysteretic structural system. *Automatica*, 41:225–231, 2005. 62

[16] F. Ikhouane and J. Rodellar. A linear controller for hysteretic systems. *IEEE Transactions on automatic control*, 51:340–344, February 2006. 22

[17] R. V. Iyer, X. Tan, and P.S. Krishnaprasad. Approximate inversion of the Preisach hysteresis operator with application to control of smart actuators. *IEEE Transactions on automatic control*, 50:798–810, June 2005. 10, 62

[18] B. Jayawardhana, H. Logemann, and E. Ryan. PID control of second-order systems with hysteresis. *International Journal of Control*, 81:1331–1342, 2008. 4, 7, 20, 22, 38, 42, 52, 53, 57

[19] D.C. Jiles and D.L. Atherton. Theory of ferromagnetic hysteresis. *Journal of Magnetism and Magnetic Materials*, 61:48–60, 1986.

[20] H.C. Liaw, B. Shirinzadeh, and J. Smith. Sliding-mode enhanced adaptive motion tracking control of piezoelectric actuation systems for micro/nano manipulation. *IEEE Transactions on Control Systems Technology*, 16:826–833, July 2008. 61

[21] H. Logemann and A. Mawby. *Low-gain integral control of infinite-dimensional regular linear systems subject to input hysteresis*. Birkh 2001. 47

[22] H. Logemann and E. Ryan. Systems with hysteresis in the feedback loop: Existence, regularity and asymptotic behaviour of solutions. *ESAIM: Control, Optimisation and Calculus of Variations*, 9:169–196, 2003. 22

[23] H. Logemann, E. Ryan, and I. Shvartsman. Integral control of infinite-dimensional systems in the presence of hysteresis: an input-ouput approach. *ESAIM: Control, Optimisation and Calculus of Variations*, 13:458–483, 2007. 38, 42, 45, 46, 47

[24] H. Mabie and F. Ocvirk. *Mechanisms and Dynamics of Machinery*. John Wiley and Sons, third edition, 1975. viii, 1, 2

[25] I. Mayergoyz. *Mathematical Models of Hysteresis and their Applications*. Elsevier, 2003. 8, 67

[26] Kirsten Morris. *Introduction to Feedback Control*. Harcourt/Academic Press, 2001. 21, 35

[27] A. Naylor and G. Sell. *Linear operator theory in engineering and science*. Holt, Rinehart and Winston, Inc., 1971. 28

[28] JinHyoung Oh and Dennis Bernstein. Semilinear Duhem model for rate-independent and rate-dependent hysteresis. *IEEE: Transactions on Automatic Control*, 50:631–645, May 2005. 18

[29] JinHyoung Oh and Dennis Bernstein. Piecewise linear identification for the rate-independent and rate-dependent Duhem hysteresis models. *IEEE: Transactions on Automatic Control*, 52:576–582, March 2008. 18

[30] W. Panusittkorn and P. Ro. Modeling and control of a magnetostrictive tool servo system. *Journal of Dynamic Systems, Measurement and Control, Transactions of the ASME*, 130(3):031003, May 2008. 61

[31] R. Smith. Inverse compensation for hysteresis in magentostrictive transducers. *Mathematical and Computer Modelling*, 33:285–298, 2001. 60, 62

[32] R. Smith. *Smart Material Systems: Model Development*. SIAM, 2005. 1, 18

[33] R. Smith and M. Dapino. A homogenized energy model for the direct magnetomechanical effect. *IEEE Transactions on Magnetics*, pages 1944–1957, Aug 2006. viii, 16, 17

[34] R. Smith, S. Seelecke, M. Dapino, and Z. Ounaies. A unified model for hysteresis in ferroic materials. *Smart Structures and Materials*, 5049:88–99, 2003. 16

[35] G. Song, V. Chaudhry, and C. Batur. Precision tracking control of shape memory alloy actuators using neural networks and a sliding-mode based robust controller. *Smart Materials and Structures*, 12(2):223–231, April 2003. 61

[36] X. Tan and J. Baras. Modeling and control of hysteresis in magnetostrictive actuators. *Automatica*, 40:1469–1480, 2004. 10, 62

[37] X. Tan and J. Baras. Adaptive identification and control of hysteresis in smart materials. *IEEE Transactions on automatic control*, 50:827–839, June 2005. 62

[38] X. Tan, J. Baras, and P.S. Krishnaprasad. Control of hysteresis in smart actuators with applications to micro-positioning. *Systems and Control Letters*, 54:483–492, 2005.

[39] S. Valadkhan. Modeling of magnetostrictive materials. Master's thesis, University of Waterloo, 2004. 18, 65, 67

[40] S. Valadkhan. *Nanopositioning Control Using Magnetostrictive Materials*. PhD thesis, University of Waterloo, 2007. 8, 18

[41] S. Valadkhan, K. Morris, and A. Khajepour. Stability and robust control of hysteretic systems. *Robust and Nonlinear Control, to appear*, 2008. viii, 3, 8, 13, 20, 23, 24, 25, 27, 29, 30, 31, 32, 42

[42] S. Valadkhan, K. Morris, and A. Shum. Load-dependent hysteresis of magnetostrictive materials. *Proceedings of SPIE*, 2007. 17

[43] Q. Wang and C. Su. Robust adaptive control of a class of nonlinear systems including actuator hysteresis with Prandtl-Ishlinskii presentations. *Automatica*, 42:859–867, 2006. 62

[44] K. Yoshida. *Functional Analysis and its Application*. Springer-Verlag, 1971.

[45] J. Zhou, C. Wen, and Y. Zhang. Adaptive backstepping control of a class of uncertain nonlinear systems with unknown backlash-like hysteresis. *IEEE Transactions on automatic control*, 49:1751–1757, October 2004. 62

[46] K. Zhou, J. Doyle, and K. Glover. *Robust and Optimal Control*. Prentice-Hall, 1996.